MICRO-DEVICE FOR SELECTIVE ISOLATION AND CYTOLOGY OF CANCER CELLS

by

YUAN WAN

Presented to the Faculty of the Graduate School of

The University of Texas at Arlington in Partial Fulfillment

of the Requirements

for the Degree of

DOCTOR OF PHILOSOPHY

THE UNIVERSITY OF TEXAS AT ARLINGTON

MAY 2012

ACKNOWLEDGEMENTS

Firstly, I would thank my parents for all the support that consistently inspired me to move forward in life. I also would like to thank my wife, Xiangting Song, for her love and support and understanding. With gratitude, I thank my advisor Dr. Samir M. Iqbal for offering me the opportunity to work in collaborative research group. I have benefited from his guidance, support, and technical expertise. I am grateful to Dr. Young-tae Kim for his guidance. I also thank Dr. Robert Bachoo, Dr. Jian Yang, and Dr. Baohong Yuan for reviewing my dissertation and being on my defense examination committee. I would like to thank my co-workers Dr. Andrew Ellington, Dr. Yanling Liu, Peter Allen, Waseem Asghar, Motasim Bellah, Cehtan Bhuwania, Swati Goyal, Qingjiang Guo, Wei Han, Arif Iftakher, Azhar Ilyas, Melissa Johnson, Kaillash Karthikeyan, Na Li, Mohammud Noor, Priyanka Ramachandran, Hassan Shah, Ahmed Shahid, Deepika Tamuly, Jifu Tan, and Srikanth Vasudevan for their advice and stimulating discussion during my research. I also would like to thank my friends, Xiaofei Han, Rui Li, Shaoshu Sha, Jinhui Shen, Yichen Shuai, Qi Wang, Weiquan Yang, Zhong Zhang, Bin Zhou, and Lei Zhu. A special thank to staff of nanotechnology research and teaching facility for equipment training.

February 22, 2012

ABSTRACT

MICRO-DEVICE FOR SELECTIVE ISOLATION AND CYTOLOGY OF CANCER CELLS

YUAN WAN, PhD

The University of Texas at Arlington, 2012

Supervising Professor: Supervising Professor Samir M. Iqbal

Early detection and isolation of circulating tumor cells (CTCs) can enable early cancer diagnosis and more effective therapeutics. Aptamers have emerged as probe molecules that have binding affinities comparable to antibodies but specificities better than those of antibodies. Epidermal Growth Factor Receptor (EGFR) is the most frequently overexpressed receptor in all human malignancies. The expression levels of EGFR in cancer cells can be over 100 times higher than those in normal cells. It is an attractive target for cancer therapy and cancer cell isolation.

This dissertation focuses on two different areas: developing strategies for anti-EGFR aptamer based cancer cell isolation, and studying its growth inhibitory activity to cancer cells. First of all, surface-bound anti-EGFR aptamers were demonstrated to capture human Glioblastoma (hGBM) cells and enrich hGBM cells from cell mixture. The ensuing work showed that nanotextured surfaces, which mimic the nano-scale topography of basement membrane showed increased sensitivity of capture. Furthermore, aptamer functionalized glass beads device was designed, modeled and fabricated to improve cell isolation sensitivity and specificity respectively. On the other hand, anti-EGFR aptamers were used to intercept the receptor tyrosine kinase (RTK) signal, and therefore inhibi hGBM cells proliferation and migration in vitro.

In brief, the anti-EGFR aptamer can specifically recognize and capture EGFR overexpressing cancer cells, and it has significant inhibition effect on hGBM cells proliferation and migration in vitro. It can have important implications for chip-based cancer cell isolation and cancer therapy.

TABLE OF CONTENTS

LIST OF ILLUSTRATIONS

Figure Page

LIST OF TABLES

CHAPTER 1

INTRODUCTION

1.1 Review and Major Objectives

Cancer is a major health problem in the world nowadays. In the United States, about 25% deaths are due to cancer, and the associated treatment costs have been continuously high. The cancer prevention and early detection can significantly decrease mortality and improve patients' prognosis. Numerous approaches of early cancer detection have made; each with its own shortcomings. On the other hand, tumor associated specific biomarker detection is plagued by high rate of false results. Circulating tumor cells (CTCs) are cells that detach from a primary tumor and enter into peripheral blood or lymphatic vessels at very early stages of tumor development. It has been proven that CTCs play major role in the metastatic spread of carcinomas. They can be thus used not only for cancer diagnosis, but also for personalized medicine and therapy monitoring. Owing to extremely low number of CTCs in peripheral blood, it is a great technical challenge to enrich CTCs with high specificity. They have been several approaches reported for the isolation of CTCs, and the sorting methods based on affinity interactions show higher efficiency and specificity. However, antibodies which have been widely adapted in these approaches have various disadvantages. Therefore, it is necessary to develop a more efficient and specific sorting method or device for CTCs isolation. Aptamers have been shown to have better specificity and stability than those of antibodies, and their cell targeting and signaling pathway interception capabilities have started to emerge only recently. The aptamer application in cancer cell isolation and therapy is expected to change cancer epidemiology. This dissertation focuses on developing various aptamer-based cancer cell isolation methods. Design, model and fabricate microfluidic devices with emphasis on increasing sensitivity and selectively of CTC isolation; and characterize cancer cell signaling

pathway interception by aptamers.

1.2 Overview of Research Works

This dissertation describes that aptamer based cancer cell isolation methods, relevant microfluidic device, and cancer cell treatment with aptamer in vitro. The literature review covering the carcinogenesis and development, CTC properties, detection and isolation significance, EGFR, aptamer, current isolation methods and devices, and their limitations are presented in Chapter 2. Chapter 3 details how anti-EGFR aptamer can be used for cancer cell isolation. Other strategies which can significantly improve cancer cell isolation sensitivity and specificity, such as nanotextured surfaces and optimized shear stress for cell isolation, are elaborated in Chapters 4 and 5 respectively. Chapter 6 details the design, modeling, and fabrication of Hele-Shaw microfluidic device with aptamer functionalized glass beads. Chapter 7 covers the inhibition effects of anti-EGFR aptamer on cancer cell proliferation and migration in vitro. Following is the overview of each chapter and major findings.

1.2.1 Cancer Cell Sorting on Aptamer Functionalized Substrates

Anti-EGFR aptamer molecules were tested whether these can specifically interact and bind to living cells. Subsequently, mouse derived tumor cells and hGBM cells which both overexpress EGFR on cell surface were incubated with anti-EGFR aptamer functionalized glass substrates, and both of these were seen to be captured on the substrates. Meanwhile, the shapes and sizes of captured cells showed a distinct behavior when compared to those on mutant aptamer functionalized surface. Toward the application of aptamer functionalized substrates in isolating tumor cells, a cell mixture was used. The results showed the anti-EGFR aptamer substrates selectively isolated and enriched cancer cells on the substrates.

1.2.2 Nano-textured Substrates for Cancer Cell Isolation

It is well known that nano-scaled basement membrane can anchor down the cancer cells to its loose underneath connective tissue through cell adhesion molecules. We mimicked this natural structure, and transferred nano-texture to polydimethylsiloxane (PDMS) substrates.

The nano-textured substrates showed more effective area and less steric effects for higher number of aptamers immobilization, which favored the cell isolation. The nano-textured substrates significantly improved cancer cell isolation efficiency without significant decrease in specificity. Moreover, SEM analysis revealed that the topography of substrate resulted in differential cell spreading showing much more distinct behavior on nano-textured substrates.

1.2.3 Optimization of Shear Stress for Cancer Cell Isolation

The expression level of EGFR in cancer cell can be up to 100 times higher than that in normal cells. On the other hand, the binding force between EGFR and anti-EGFR patmer can be predicted. Therefore, the surface adhesion forces of normal and cancer cell are different. Further, optimized shear stress can be applied to keep cancer cells on surface while eluting physically adsorbed normal cells. A model has been developed to predict the adhesion probability of both cancer and normal cells under various flow rates, and the experiments validate the model. The results showed the cancer cell isolation specificity could be improved over 5 times by carefully adjusting the flow behavior through microfluidic channels.

1.2.4 Isolation of Cancer Cells Using Glass Beads Array

A Hele-Shaw microfluidic device with anti-EGFR aptamer functionalized glass beads was designed, modeled, and fabricated to efficiency isolate cancer cells. The glass beads captured cancer cells with high selectivity then cell-bound glass beads were removed from the device surface in suspension followed by the release of the cells from glass beads for subsequent analysis of cells. This approach ensures that the cells remain undisturbed during capture and isolation from sample, and are available for post-analysis in native state. Glass beads are bound to overexpressed EGFR on cancer cells walls through anti-EGFR aptamer. An antisense RNA molecule is used for separation of glass beads from the cancer cells.

1.2.5 Anti-EGFR Aptamers Inhibit Cancer Cell Proliferation and Migration

The level of EGFR overexpression on cell surface not only supports cell isolation but also aids receptor mediated targeted therapeutic approach. Compared with traditional

chemotherapies which lack specificity and efficacy, the interception of tumor signaling pathway is a nontoxic method with potentially higher therapeutic index. Anti-EGFR aptamer can completely inhibit RTK by competitive binding with epidermal growth factor (EGF). Cancer cells which were treated with anti-EGFR aptamers showed lower proliferation and inhibited migration in vitro.

CHAPTER 2

BACKGROUND AND LITERATURE REVIEW

2.1 Carcinogenesis and Development

Carcinogenesis is a process by which normal cells are transformed into cancer cells on cellular and genetic level. It can be induced by virus, chemical and physical factors (*1*). These factors changes normal behavior of cells, change the balance between proliferation and apoptosis, leading to cancer. After a series of mutations to certain classes of genes, a normal cell undergoes uncontrolled growth and disdifferentiation, thus transforming into a malignant cell (*2*). During the period, the activation of proto-oncogenes and deactivation of cancer suppressor genes are of importance in understanding the carcinogenesis. When tumor suppressor gene is mutated to cause a loss or reduction in its function, the cell can progress to cancer. On the contrary, upon activation, a proto-oncogene can become an oncogene due to mutation or increased expression. Abnormal function in either may induce cancer (*2*).

2.1.1 Oncovirus

In 1908, Ellerman and Bang were the first to report an infectious cause for leukaemia, and they transferred the disease from one to another by cell-free tissue filtrates (*3*). In the following century, numerous oncoviruses were discovered. Nowadays, it is recognized that oncovirus have direct association with oncogenesis. The carcinogenesis of oncovirus involves either integration of viral nucleic acid into host chromosome or activation of proto-oncogene in the genome (*4*).

2.1.2 Chemical Carcinogens

These can induce DNA-adduct (DNA covalently bonded to a chemical) formation and/or directly cause DNA fragmentation and sequence deletion, especially if tumor suppressor genes

are damaged (*5*). Without proper DNA repair the abnormal cell cannot be cleared. This can be the start of a mutation (*6*).

2.1.3 Physical Carcinogens

Ionizing radiation and ultraviolet radiation are main factors. Unlike chemical carcinogens, if radiation happens to strike a chromosome, it may damage the chromosome, and result in gene mutation. On the other hand it may trigger certain cell responses that can increase the likelihood of mutations (*7*).

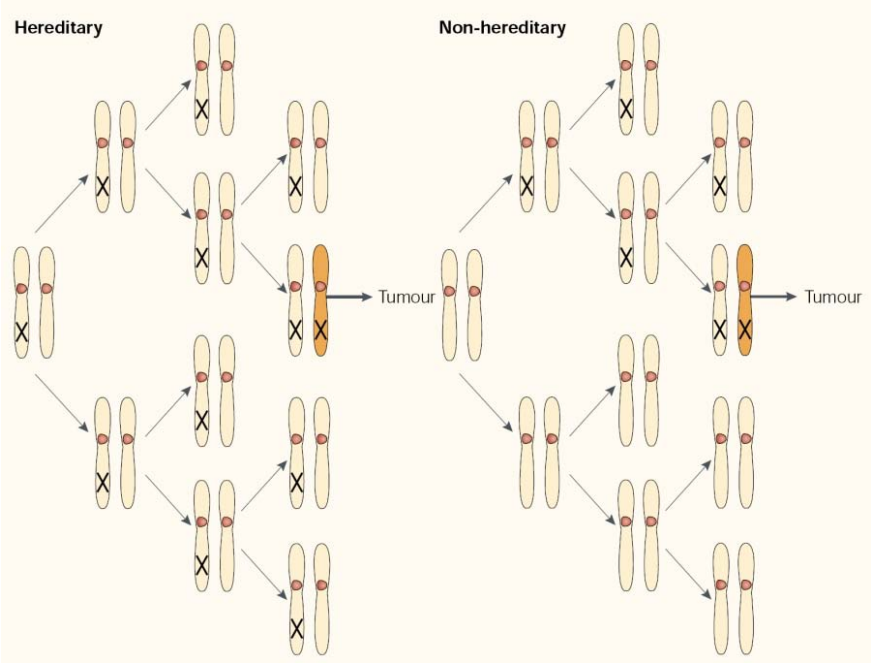

Figure 2.1 Two-Hit theory of Carcinogenesis (*8*). Used by permission.

In some rare circumstances, cancer cells can experience reversion and restore to normal state. However, in most cases, cancer cells loose ability of differentiation regulation, regress to a more embryonic unspecialized form, and show malignant proliferation (*10*). Further, cancer cell can move into tissue surrounding the tumor and vasculature, travel in the circulation to a distant site and form a secondary cellular colony. This process is called metastasis. It involves cancer cell malignant proliferation, cell-cell loose adhesive restraint, cancer cell motility, and intercellular adhesion molecule forfeit (*11*). Firstly, uncontrolled cell growth cause

cell number to significantly increase, thus cancer cell is inclined to extend to surrounding tissue. And when sufficient cancer cells loose some or all of molecules (such as E-cadherin and other epithelial markers) which mediate cell adhesion (cell-cell adhesion, and cell-extracellular matrix adhesion), the cancer cells are more likely to detach from its native tissue. Finally, studies have also demonstrated that abnormal gene expression (mutation, deletion or translocation) in human cancer and extrinsic factors in the tumor microenvironment can promote the motility of cancer cell (*12, 13*). The combined action of these three processes causes cancer cell invasion and metastasis. Before cancer cell migrate to other sites, it has to overcome two constraints. First, cancer cell has to adhere to extracellular matrix via appropriate integrins, which can allow cell to survive and proliferate. Otherwise, unattached cell not only stop growing but commit suicide (*14*). And cancer cell has to penetrate basement membranes which form a barrier that most normal cells cannot breach (*15*).

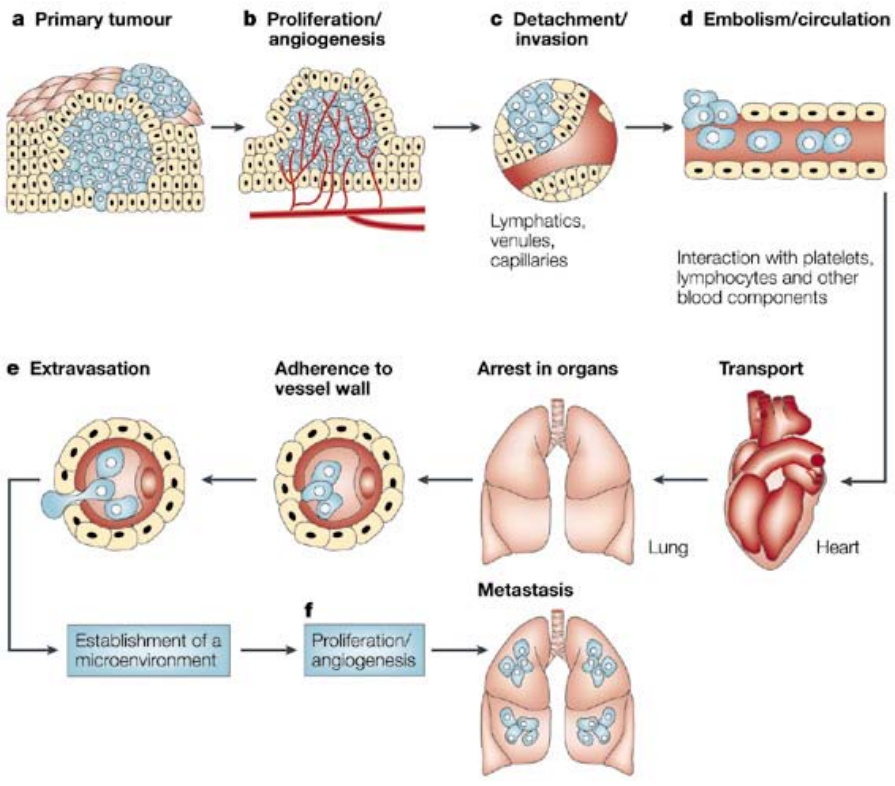

Figure 2.2 An overview of cancer metastasis (*9*). Used by permission.

2.2 Basement Membrane

Basement membrane is a thin sheet of fibers, which is 20-200 nm broad. It consists of fibrous collagen, hyaluronic acid, proteoglycans, laminnin, and fibronectin. Structurally, it is composed of basal lamina and reticular lamina. The later is attached to the former via type VII collagen fibers and fibrillin (*16*). The basal lamina also involves two layers, lamina lucida and lamina densa. The thickness of lamina lucida is around 35 to 40 nm. It is composed of laminin and relevant isomers, and lamina lucida participates in the formation of extracellular matrix and anchoring filament. Lamina densa is about 30 to 45 nm in thickness, and consists of type IV collagen fibers and laminin. It stabilizes the whole basement membrane (*17*). It has been demonstrated that basement membranes provide a mechanical support and divide tissue into compartments, but also can anchor down the epithelium to its loose connective tissue underneath via substrate adhesion molecules. For example, the activation of plasma membrane integrin receptors bind to ligands on the basement membrane, therefore it can modulate cell behavior; integrin receptors on basement membrane can mediate cell attachment, migration, and even differentiation (*18-20*). Normally, basement membrane acts as a mechanical barrier which prevents cancer cells from invading the surrounding tissues. Especially at the early stage, cancer cells can be limited to the epithelial layer by the basement membrane. However, The invasive potential is enhanced by activation of various metalloproteinases, which can dissolve basement membrane and other extracellular matrices (*21*), higher expression of integrins, and change in phenotype that facilitate their escape from the structural constraints. After penetrating the basement membrane, cancer cells can invade into surrounding tissue or spread to a distant site via bloodstream. Basement membranes possess a complex, 3D topography consisting of nanometer sized features (*22*). SEM micrographs have shown that basement membranes are comprised of nanometer size pores, ridges, and fibers (*23, 24*). It is worth noting that the nanostructured characteristics of the basement membrane can improve cell adhesion and growth, and this property is important for tissue engineering, and it might be useful for cell

culture or isolation.

2.3 Circulating Tumor Cells

After detaching from the primary tumor and breaching the basement membrane surrounding a blood vessel, cancer cells reach bloodstream that can carry these to distant sites. These cancer cells in peripheral blood are called circulating tumor cells. CTCs may cause subsequent growth of additional tumor in distant tissues. The presence of CTCs was found by Ashworth in 1869 (*25*).

The importance of cancer cells disseminated into bone marrow and peripheral blood has been proven. However, cancer cells in bone marrow are usually dormant, and they cannot be destroyed by immune system. Therefore, these cancer cells do not provide too much information for therapy and progression of disease (*26*). Contrarily, CTCs have high clinical diagnostic potential in oncology. Cancer cells may enter into the circulation through normal neighboring vessels, or via newly formed capillaries by angiogenesis. Therefore, CTCs can directly provide cancer progression information. They may represent the genetic and phenotypic composition of the primary tumor. In early stage, they can be used to predict patients' prognosis and detect the malignancy. Besides, they are also useful in personalized medicine, and to monitor the effectiveness of therapy (*27*). In breast cancer, patients who had fewer than 5 CTCs per 7.5 ml blood shown survival average of 7 months or more; patients with 5 or more CTCs per 7.5 ml blood had 2.7 survival months, the average overall survival times in these two groups was 10.1 month and 18 months respectively (*27*). Research results from other groups have also demonstrated the overall survival time can be prolonged if there are fewer number of CTCs in blood (*28-30*). In prostate cancer and in colorectal cancer, researchers have reached similar conclusions that fewer CTCs in bloodstream indicate better prognosis after surgery and/or additional chemotherapy (*31-35*). In brief, the detection of CTCs in the peripheral blood can be used for prognosis in breast, prostate and colorectal cancers, and the significance of CTCs is well-known now.

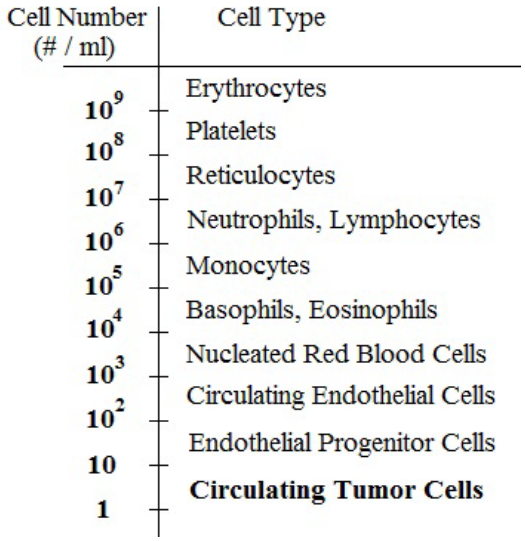

Figure 2.3 Cell number of various blood cells in whole blood versus CTCs.

2.4 Cell Detection and Isolation Techniques

The faithful of CTCs is a challenge. First, the survival time of CTCs in bloodstream is relatively short (*36*). The frequency of CTCs in 1 ml of whole blood is on the order of 1 to 10; meanwhile, in 1 ml whole blood, there are a few million white blood cells and a billion red blood cells (*37*). CTCs that are viable in circulation must be kept viable after isolation for subsequent molecular analysis. The available biological markers are also not sufficient. CTCs have large morphological variability, and show varying molecular functional characteristics. The isolation specificity of CTCs must be high (*32*). Lots of approaches relying on either the physical properties or immunochemical characteristics of CTCs have been adopted for detection and isolation; however, none of them constitute the optimal platform for CTCs detection and isolation. Their technical description, advantages and disadvantages are discussed below.

2.4.1 RT-PCR

Reverse transcription polymerase chain reaction can qualitatively and quantitatively analyze specific gene of CTCs. It is based on the design of primers which can recognize and amplify the target gene. RT-PCR can detect 1 CTC in at most 10 million normal cells (*38*). The limitations include amplification of nonspecific products, lacking of consistent protocol and

primer design, potential false-positive, lacking of specific biomarkers, and physical contamination (*39*).

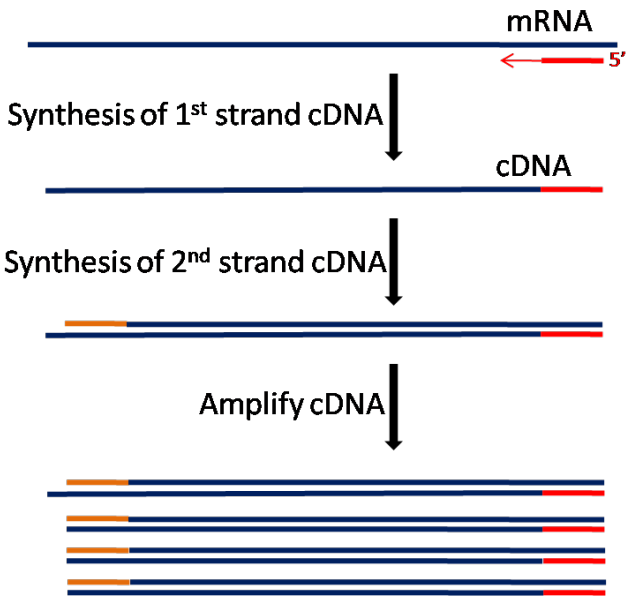

Figure 2.4 RT-PCR principle.

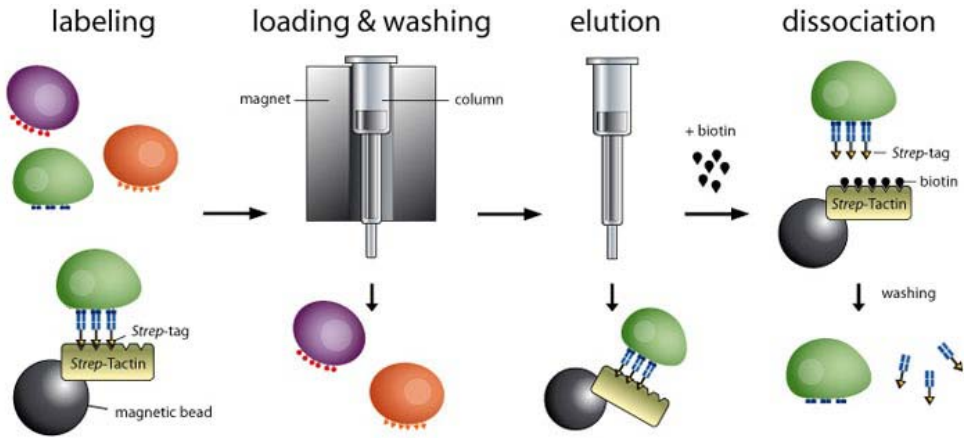

Figure 2.5 Principle of magnetic cell sorting.

2.4.2 Magnetic Cell Sorting

Magnetic nanoparticles coupled to antibodies which can specifically recognize cell relevant antigens are incubated with whole blood sample first, and then target CTCs those are bound to magnetic nanoparticles are captured on magnet. The enriched cell can be used for

subsequent nucleic acid amplification and protein isolation (*40, 41*). The separation and isolation protocol can be found elsewhere (*42, 43*). The advantages are visualization, quantification, and high specificity. However, this technique is expensive and time-consuming. Additionally, the variability of CTCs between patients and the nonstandardized methods and reagents make the detection trickier (*44, 45*).

2.4.3 Density Gradient Centrifugation

Difference in density between cancer cell and other normal cells have been use to separate CTCs from whole blood (*46-49*). Density gradients can be generated by placing layer after layer of gradient media. The heaviest layer goes to the bottom and the lightest layer floats to the top. The sensitivity and specificity of this method are pretty poor due to the very small number of CTCs in the circulation.

2.4.4 Immunohistochemistry

It relies on antibodies recognition of specific biomarkers. Currently, various biomarkers have been utilized in CTCs isolation, such as epithelial cell adhesion molecule (EpCAM) (*50*), CD45 (a tyrosine phosphatase) (*51*), rostatic acid phosphatase (PAP) (*52*), and so on. However, the reliability and specificity of immunohistochemistry is far from ideal; for examples, cells might not express or shown reduced expression of relevant markers. The sensitivity, reproducibility and limited quantitation are thus shortcomings of this approach. Additionally, the cost of antibodies is also very high.

2.4.5 Filtration

Isolation of CTCs by their increased size (> 8 μm), compared with white blood cells and red blood cells, has been widely used (*53-56*). However, no validation has been confirmed that CTCs are not smaller than 8 μm; for example, the size of malignant cells in small cell lung cancer might be smaller; cancer cells size in early stage of cell development might be also smaller. On the other hand, the size of white blood cell is not always smaller than 8 μm either; their sizes range from 7 to 20 μm. The diameter of Neutrophil is 10 to 12 μm; Basophil's size is

12 to 15 μm; size of human macrophage can reach 21 μm. So the isolation method based on CTC size is not dependable; thus the sensitivity and specificity are again source of concern.

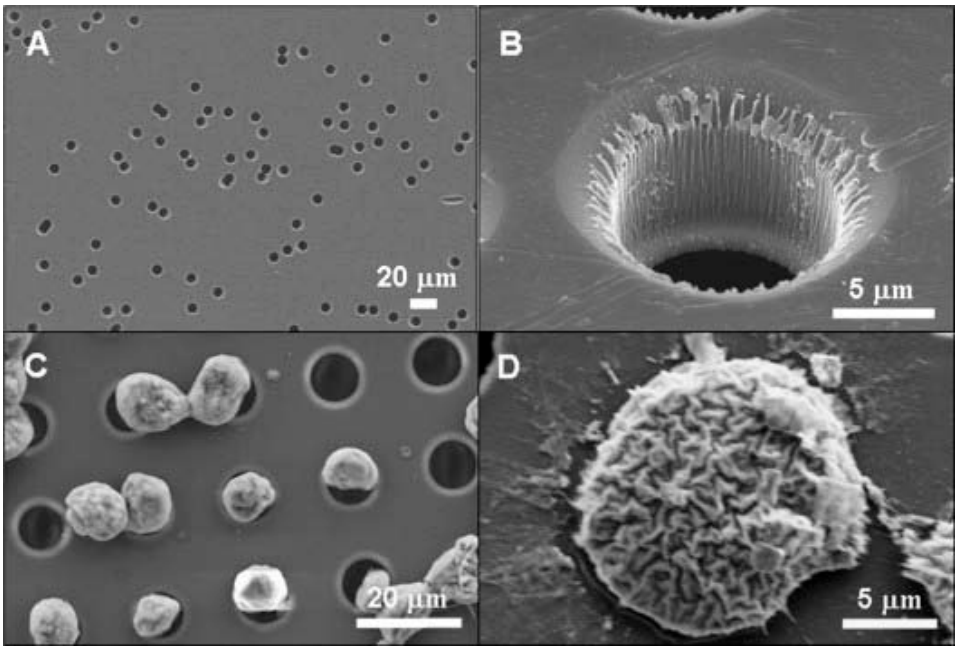

Figure 2.6 CTC enrichment by filtration (*56*). Used by permission.

2.4.6 Cytometric Methods

These methods include laser-scanning cytometry (*57*) and multiphoton intravital flow cytometry (*58*). Laser scanning cytometry require blood pretreatment; following lysis of whole-blood cells, CTCs should be labeled with antibodies. It is a time-consuming work. Multiphoton intravital flow cytometry requires no blood sample; before scanning, CTCs are marked with fluorescence labeled antibodies in vivo. In other words, it can only be used for CTCs detection and cell counting. These cytomitric methods require expensive flow cytometry and professional optical facilities.

2.4.7 Photoacoustic Flowmetry

It utilizes the broadband absorption spectrum of melanin to specifically detect melanoma cells (*59-61*). Although nanoparticles which can significantly improve detection sensitivity have been used for CTC detection, this technique has limited field of application, and

the facilities are also expensive.

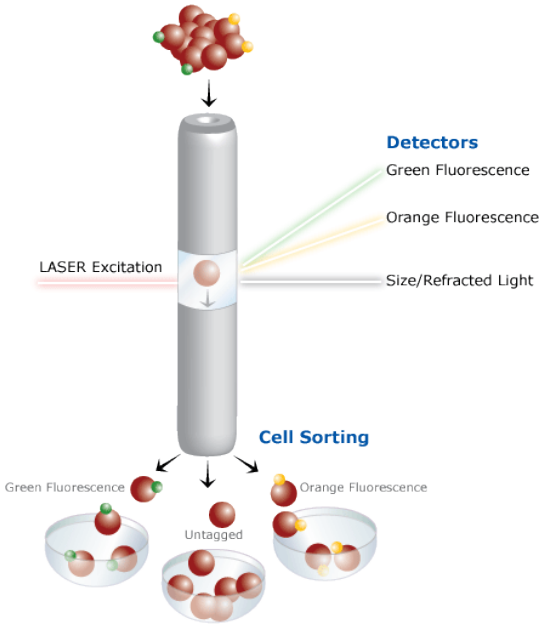

Figure 2.7 Flow Cytometry diagram.

2.4.8 Fiber-optic Array-scanning

It applies laser printing techniques to the cell detection field. It can swiftly detect fluorescence labeled cells on glass substrates; purification and enrichment steps are not required. However, the blood sample also requires lysis pretreatment. After scanning, cells might not be available for subsequent analysis (*62, 63*).

2.4.9 Microscale Optical Interactions

It uses a highly focused laser beam to provide an attractive force to physically hold and move cells (*64*). It is capable of carrying nanometer and micrometer sized dielectric objects. Cells can be moved along the gradient from the region of weak electric field to the region of strong one. Although current technique can satisfy high-throughput cell manipulation, it is impossible to handle the whole blood analysis, and the isolation efficiency is also poor (*65*).

2.4.10 Dielectrophoresis

Cell is a dielectric object which can be manipulated in a non-uniform electric field (*66-69*). The strength of the force depends on the medium and cell's electrical properties, on its

shape and size, as well as on the frequency of electric field. The dielectrophoretic characteristics of red blood cell, white blood cells and cancer cell are shown to be significantly different, and the difference is exploited to separate cancer cells from normal blood cells. It is reported that around 2 cancer cells can be separated from 10 million other cells in 5 ml of blood. The isolation process is fast and very sensitive; moreover this technique does not require cell to be charged or complicated pre-processing either. However, the major disadvantage is that the cells are localized at the electrodes after separation, and flushing needs to be performed to collect the isolated cells (*70*). To achieve the best isolation efficiency, the medium buffer and cells should be special selected. At last, the difference of dielectrophoretic characteristics among different cells is not always sufficient, which might cause lower specificity.

2.4.11 Microfluidic Devices

It combines immunohistochemistry and other isolation techniques, and miniaturizes the isolation on a small glass, wafer or polymer device. In 'CTC chip', an array of 78,000 microspots coated wih EpCAM antibodies was used to isolate CTCs from whole blood on wafer (*71*). Adams *et al*., immobilized EpCAM antibodies on poly(methyl methacrylate) (PMMA) channel surface for CTCs isolation from whole blood (*72*). Combination of E-seletin and EpCAM antibodies, which mimic the physiological environment, were immobilized on glass surface for CTCs isolation (*73*). Cytometry has also been miniaturized on a chip; it has been used for cell capture and separation (*74*). Magnetic cell sorting on PDMS device has been done by Deng and coworkers (*75*). There are a number of significant advantages. First, miniaturized device require less volume of analyte; the batch-fabrication is inexpensive; it enables the fabrication of highly integrated device for multiple analyses; reduced physical contamination; improved reaction speed and sensitivity; large scale equipment or facilities are not required (*76*). In short, microfluidic devices are a powerful and well-developed field that can be widely used in the cancer research today and in future. New class of highly-functional highly-integrated lab-on-a-chips is the future of biochemical analysis.

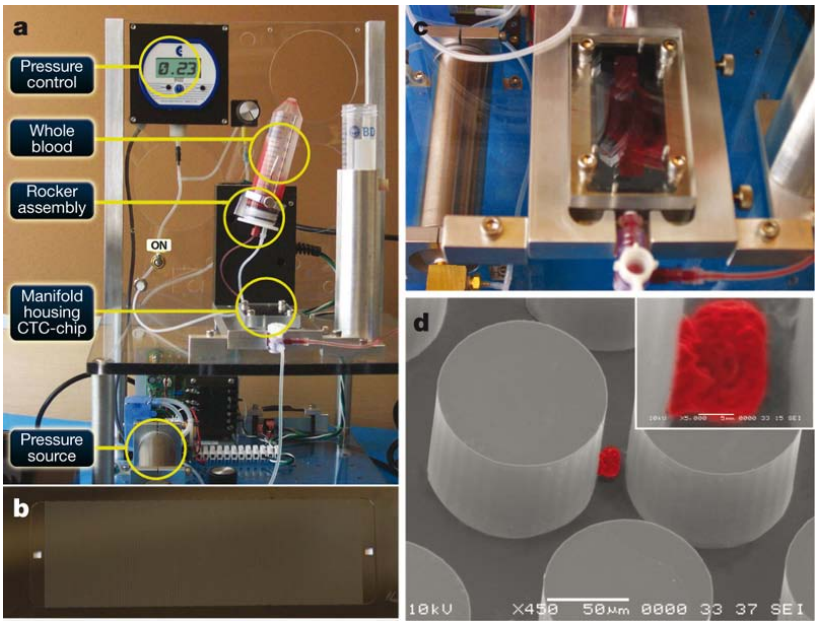

Figure 2.8 CTC Chip (*71*). Used by permission

2.5 Antibody versus Aptamer

In contrast to mechanical and electrical sorting techniques, detection and sorting based on affinity interactions is expected to yield higher efficiency and greater specificity (*77*). As mentioned before, most of affinity-based approaches rely on antibodies which are often subject to high levels of off-target cross-reactivity (*78*). Other disadvantages of antibodies involve: (i) they have limited shelf life and can easily undergo denaturation; (ii) strict physiological conditions are required for antibody-antigen binding; (iii) batch to batch variation; (iv) they require the use of animals for production; (v) kinetic parameters of antibody-antigen interactions cannot be altered; (vi) labeling cost may cause loss in function; (vii) heterogeneity of conjugation on device surface; (viii) cost (*79*). There is increasing recognition that aptamers may have great utility in cancer diagnosis and therapeutics. Aptamers have been shown to have affinities and specificities that are comparable with those of antibodies, but have more advantages. Aptamers lack the large hydrophobic cores of proteins and thus do not aggregate. They are stable at wide ranges of pH, temperature, and salt and ionic conditions, and they can be reversibly denatured. These can be chemically synthesized, so these are easier and more

economical to produce. Aptamers can be site-specifically labeled with functional groups or dye, and therefore these can be site-specifically immobilized. Selection conditions can be manipulated to obtain aptamers with properties desirable for in vitro assays (*80, 81*). Finally, because aptamers are much more hydrophilic than antibodies, they may provide surface passivation against nonspecific binding. Aptamers have been used in cell labeling studies (*82*), in activating cell signaling pathways (*83*), and in cell isolation and detection (*84*). In this work, anti-EGFR aptamer instead of antibody was used for cancer cell isolation and therapy. So, the next questions are: what is aptamer, and how to produce them?

2.6 Aptamer and SELEX

Aptamers are oligonucleotide or peptide molecules that bind to a specific target molecule. A part of mRNA, called riboswitch, can directly bind a small target molecule, and whose bindings of the target can affect the activity of gene. In 1990s, researchers developed selection technique, combining chemical synthesis to prepare aptamers in vitro (*85, 86*). It is called Systematic Evolution of Ligands by EXponential enrichment (SELEX). First, oligonucleotide library consisting of randomly generated sequence of fixed length is prepared. There are four nucleotides (A, T, C and G), therefore, the number of possible sequence in the library is 4^n. These sequences are exposed to the target ligand, and those that do not bind the target are removed. The sequences through primary sieving are further amplified by PCR. In the subsequent rounds of selection, their binding specificity and binding affinity are investigated for identify the tightest-binding sequences with high specificity (*87*). By 2001, an aptamer could be selected in vitro with significant reduction in the time it took for a selection experiment. Nowadays, the target ligand ccan be a protein, or a small organic compound, even a whole cell (*88*). The half-life of non-modified aptamers is very short (few minutes to few hours); contrarily, after 2'-fluorine-substituted pyrimidines modification, aptamers are available for days or even weeks. In this work, a modified anti-EGFR aptamer sequence was used. Peptide aptamers

aredifferent and are designed to interfere with proteins. Their selection process is different from oligonucleotide aptamers (*89*), and more details can be found elsewhere (*90*).

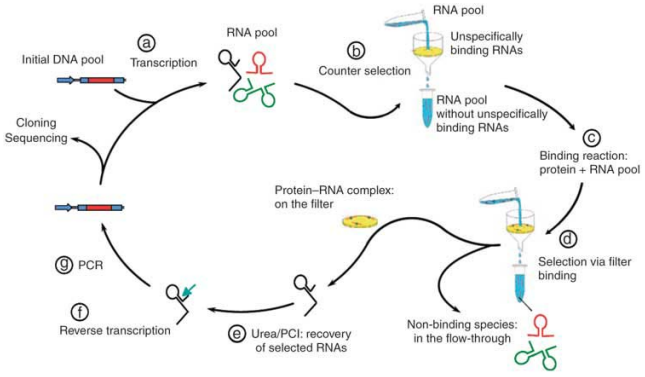

Figure 2.9 An overview of SELEX (*91*). Used by permission.

2.7 Epidermal Growth Factor

EGF is a growth factor which results in cellular proliferation, differentiation, and survival. In detail, its biological functions involve: stimulation of transport, activation of glycolysis, activation of the synthesis of extracellular macromolecules, activation of DNA, RNA and protein synthesis, and increased cell multiplication (*92*). Molecular weight of human EGF is 6045 kDa with 53 amino acid residues comprising each of the two polypeptides. It can specifically recognize EGFR on the cell surface, and the apparent dissociation constant is around $2 – 4 \times 10^{-10}$M. Non-covalent affinity can attract EGF to cell membrane when it gets close to EGFR, and the binding process initiates. In the beginning (around 1 hour), EGF is randomly distributed on EGFR sites, and the binding speed is very fast; however, the speed slows down due to high saturation of EGFR. Besides, higher concentration of EGF has faster binding speed. It has been demonstrated that the binding speed of 1 mM EGF can be 100 times higher than that for in 1 μM concentration (*93*). The binding activity decreases along with the decreasing EGF concentration. After EGF-EGFR complex formation, EGF can be internalized via receptor mediated endocytosis. Finally, EGF is degraded in lysosomes, and receptors can be sorted to the recycling endosome, from which they travel back to the cell surface.

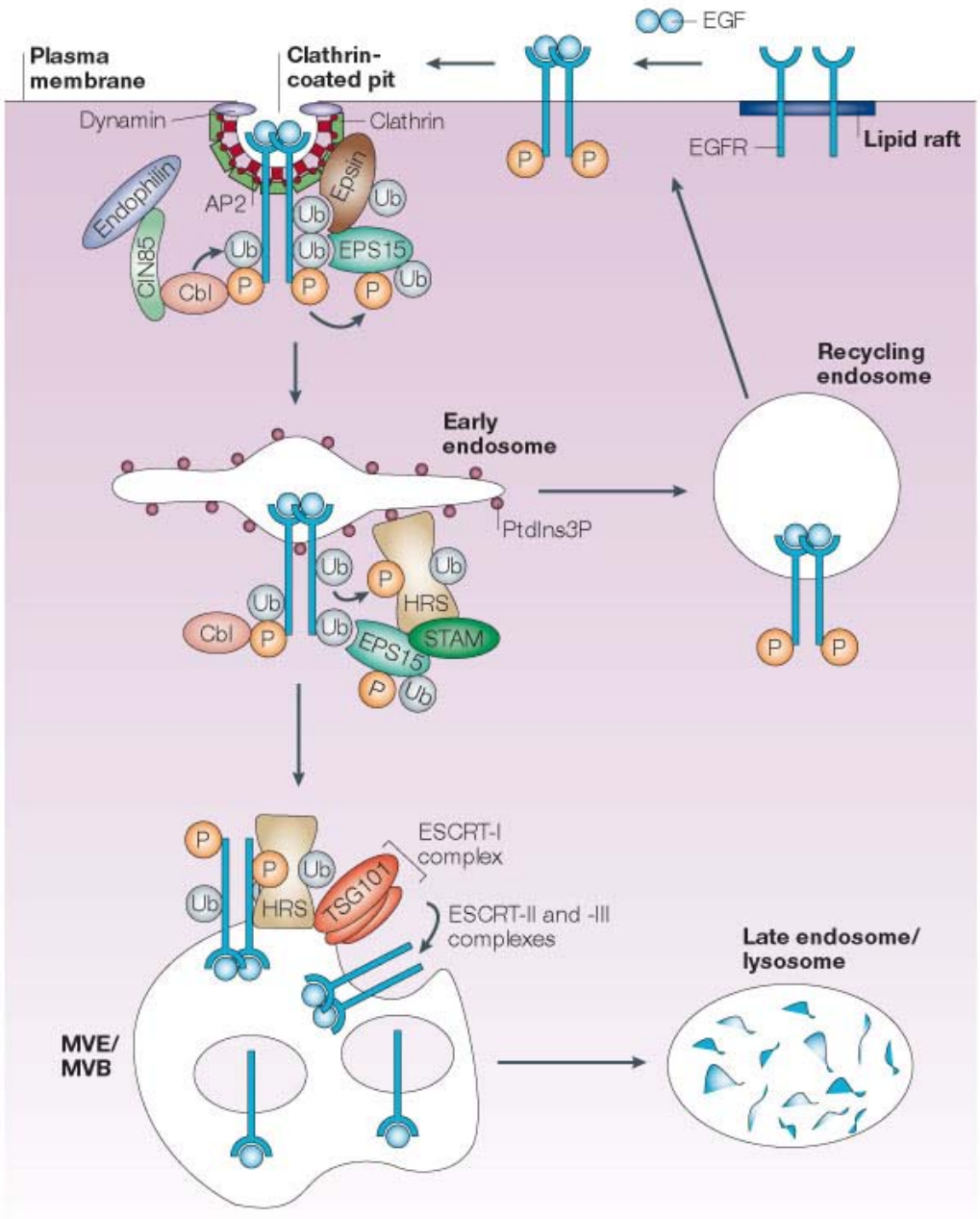

Figure 2.10 An overview of EGFR trafficking (*94*). Used by permission.

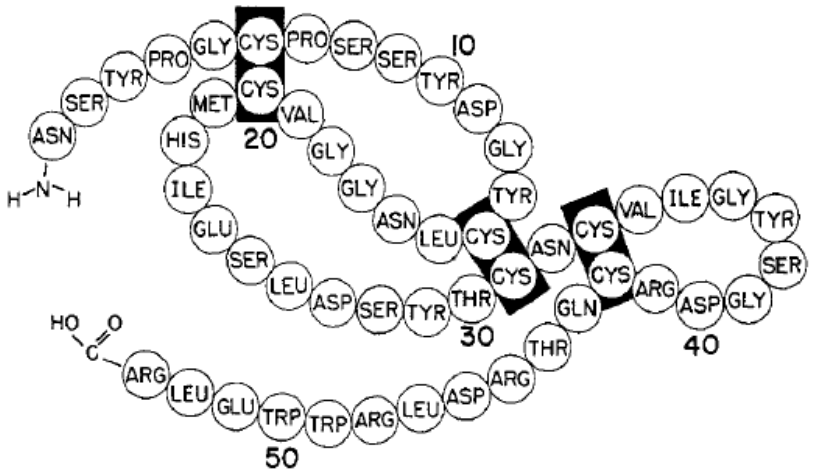

Figure 2.11 The amino acid sequence of EGF with placement of disulfite bonds (*95*). Used by Permission.

2.8 Epidermal Growth Factor Receptor

EGFR is encoded by *c-erbB1* proto-gene, and its molecular weight is around 170 kDa. EGFR is a transmembrane glycoprotein which can recognize and bind to the members of the EGF-family (EGF, TGF-α, etc.). EGFR has four functional domains: an extracellular ligand-binding domain; a transmembrane domain; an intracellular tyrosine kinase domain, and a C-terminal regulatory domain. The extracellular region can be further divided into four domains, I, II, III, and IV. Homologous domain I and III are cysteine-poor, and they provide binding sites for ligands. On the contrary, cysteine-rich domain II and IV determine the conformation of the external domain. The intracellular region contains an uninterrupted tyrosine kinase site and multiple autophosphorylation sites clustered at the C-terminal tail (*96*). When ligands selectively bind to EGFR extracellular domain, the receptor forms a dimer, and further triggers receptor autophosphorylation through tyrosine kinase activity. Autophosphorylation initiates the recruitment and phosphorylation of several intracellular substrates that promotes cell proliferation, angiogenesis, antiapoptosis and metastasis (*97, 98*).

Both normal cells and cancer cells can express EGFR on cell surface. EGFR is essential to cell normal functions, such as DNA synthesis, cell proliferation, migration, adhesion,

and so on. In normal cell, human fibroblast for example, about 40,000 to 100,000 EGFR can be expressed on cell membrane (*93*). In various cancer cells, such as breast cancer, cervical cancer, lung cancer, bladder cancer, ovarian cancer, and esophageal cancer can overexpress EGFR on cell surface (*99*). For instance, around 40 to 50% of glioblastoma overexpress EGFR (*100*), and this percentage can reach 80 to 100% in head and neck tumors (*101*). It has been demonstrated that overexpression of EGFR is implicated as an important factor in cell malignancy and poor prognosis. The expression level of EGFR in cancer cells can be 10 to 100 times higher than that in normal cells (*102*). Therefore, EGFR is an attractive target for cancer treatment (*103*). Currently, EGFR-targeting therapies involve antibodies that bind to the extracellular domain or small-molecule tyrosine kinase inhibitors that can inhibit the kinase activity of EGFR (*104*). It is noted that both treatments were originally developed to target wild type EGFR. Therefore the drug which targets the EGFR in patients may be limited by the emergence of drug-resistance mutations (*105*). Drug may not recognize the mutant extracellular domain, and also the kinase domain mutations may lead to drug resistance. In clinical therapy, it is necessary to isolate cancer cells and perform EGFR mutation analysis on DNA recovered from these cancer cells. The molecular analysis offers the possibility of monitoring changes in cancer cell genotypes during the course of therapy and provides personalized treatment.

At present, nine mutations altogether have been identified (Table 2.1). Five mutations happen in extracellular region (EGFRvI, EGFRvII, EGFRvIII, ΔEGFRvIII/ -13, and EGFR.TDM/2-7), and the rest appear in intracellular region (EGFRvIV, EGFRvV, EGFR.TDM/18-25, and EGFR.TDM/18-26). In EGFRvI an extensive N-terminal is truncated; EGFRvII loses 83 amino acids on domain IV (exons 14 and 15); Exons 2 to 7 is deleted in EGFRvIII; EGFRvIIIΔ1 2-13 further misses exons 12 and 13; EGFR.TDM/2-7 has tandem duplication of exons 2 to 7; exons 25 to 27 is missing in EGFRvIV; EGVRvV has incomplete C-terminal; EGFR.TDM/18-25 and EGFR.TDM/18-26 have tandem duplication of exons 18 to 25 and exons 18 to 26, respectively (*106*). In all these mutation, EGFRvIII (type III EGFR deletion-

mutant receptor) is the most common mutations. Its gene looses 801 base pairs, and the amino acids from 6 to 273 in extracellular domain are deleted correspondingly, which comprise exons 2 to 7. The molecular weight also decreases from 170 kDa for EGFR wild type to 145 kDa. Normally, a cascade of ligand-receptor reactions require ligand binding; however, EGFRvIII can continuously cause tyrosine kinase activation and receptor autophosphorylation, and further stimulate cell proliferation at low level without ligand binding. The mutations in kinase domain are on exon 18 through 21. On exon 18, 19 and 21, some gene mutation loci are also associated with drug sensitivity, and mutations on exon 20 are correlated to drug resistance.

Table 2.1 Structures of EGFRwt and nine mutations (Δ = deletion; TD = tandem duplication).

	Receptors	Ligand Dependence	Δ or TD	Protein Size (kDa)
Extracellular Domain	EGFRwt	+	None	170
	EGFRvI	-	N terminal truncation	145
	EGFRvII	+	Δ exons 14-15	150
	EGFRvIII	-	Δ exons 2-7	145
	EGFRvIII/Δ12-13	-	Δ exons 2-7 & Δ exons 12-13	125
	EGFR.TDM/2-7	+	TD exons 2-7	180
Intracellular Domain	EGFRvIV	+	Δ exons 25-27	167
	EGFRvV	+	C terminal truncation	105
	EGFR.TDM/18-25	-	TD exons 18-25	185
	EGFR.TDM/18-26	-	TD exons 18-26	190

2.9 EGFR Targeting for Cancer Therapy

EGFR targeting has been heavily pursued to define therapies for cancer treatment. There are three ways to achieve the goal: (i) durgs that bind to the extracellular domain; (ii)

small-molecule tyrosine kinase inhibitors that can inhibit the kinase activity of EGFR; (iii) ligand-binding cytotoxic agents which can specifically recognize cancer cells. The interception of tumor signaling pathway is a nontoxic method with higher therapeutic index in cancer treatment, compared with traditional chemotherapies which lack specificity and efficacy. Monoclonal antibodies, aptamers, enzyme inhibitors, small molecule drugs, immunotoxins, antisense oligonucleotides etc. have been applied in clinical therapy (*107, 108*). However, the issue is that indefinite proliferation is not limited to a single defect but a myriad of defects. It is difficult to effectively control all the signaling pathways.

In the first approach, drugs focus on inhibiting the binding of EGF to EGFR and to impede EGFR internalization, thereby interrupting the signaling. This signaling blocking can affect three major pathways, the RAS/ERK pathway, PI3 kinase/AKT pathway, and JAK/STAT pathway (*109*). Thereafter, DNA amplification, protein synthesis, cell growth and survival can be inhibited. However, the exclusive use of EGFR extracellular domain targeting drug may not obtain efficient therapy. For example, there is crosstalk between EGFR pathway and type 1 insulin-like growth factor receptor (IGF-1R) pathway. IGF-1R can activate PI3 kinase/AKT pathway in the absence of EGFR signaling. When ligands binds to IGF-1R, it initiates signals that stimulate cell proliferation and prevent apoptosis. Increased levels of IGF-1R have also been found in cancer cells. Moreover, the increased IGF-1R signaling often indicates the development of resistance to EGFR inhibitors (*110*).

The second strategy is RTK intrinsic tyrosine kinase activity inhibition. RTK is the primary mediator of the signaling network that transmits extracellular signals into the cell. Tyrosine kinases have been implicated in a variety of cancer indications, and EGFR also contains intracellular tyrosine kinase domain. When ligands bind to EGFR extracellular domain, it induces or stabilizes receptor dimerization leading to increased RTK activity, which leads to cell malignant transformation. Some protein tyrosine kinase inhibitors can selectively block receptor autophosphorylation and activation of downstream signal transducers; antisense RNA

or small interfering RNAs are aimed at the inhibition of RTK transcription and/or translation, which can block the expression of specific target proteins, such as EGFR (*111*).

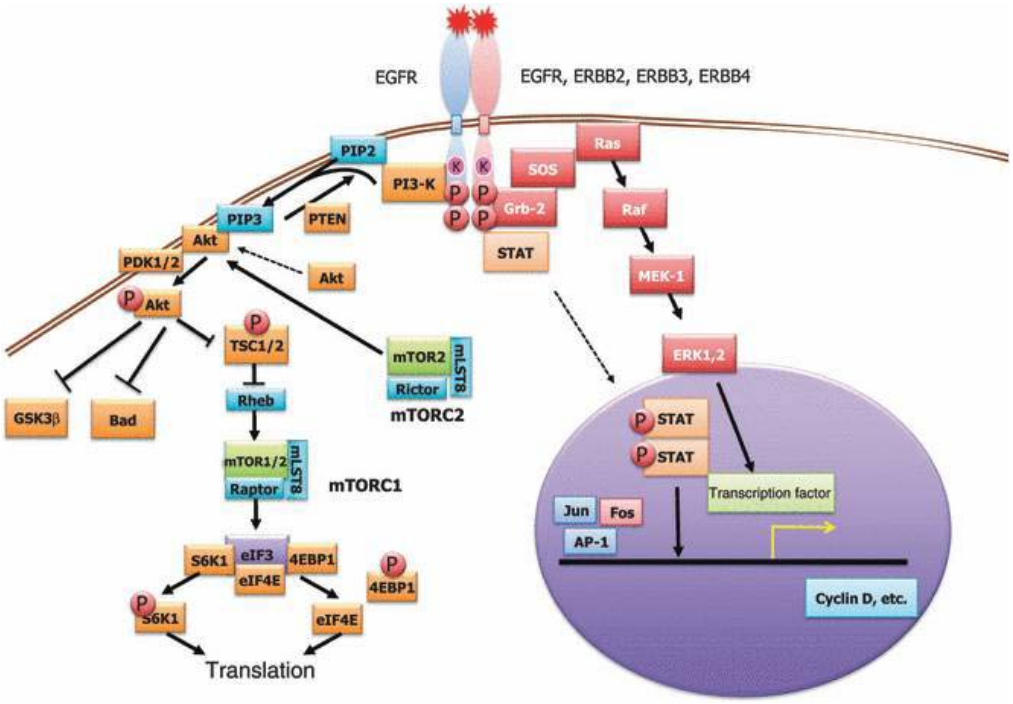

Figure 2.12 EGFR signaling pathway (*96*). Used by permission.

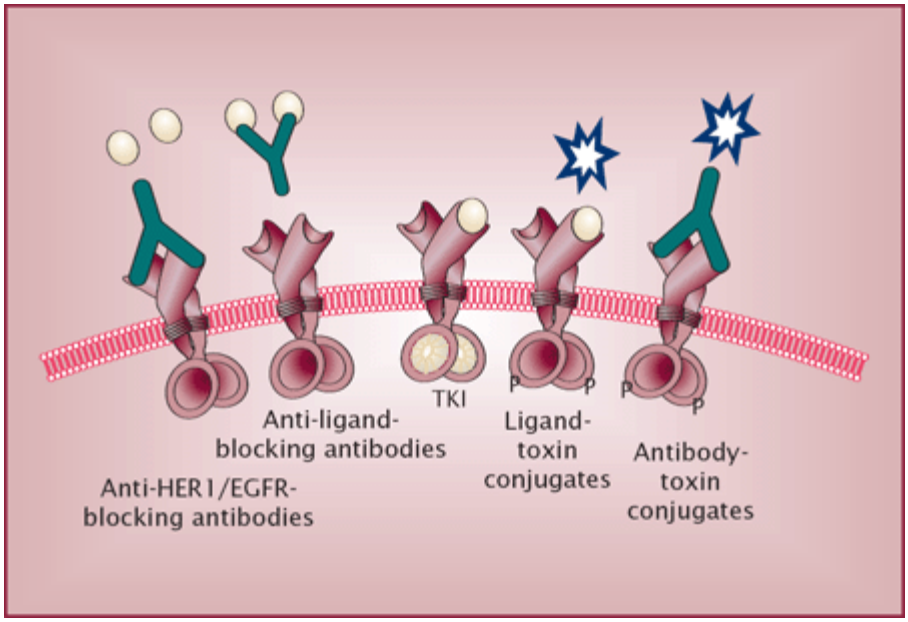

Figure 2.13 The interception of EGFR signaling pathway

The rest of EGFR targeting therapy strategy is using ligand-binding cytotoxic agents. They are conjugated to ligands which can bind to extracellular domain. After reaching the cell surface, they can internalize into an endosome and translocate to the cytosol where they inhibit DNA amplification, protein synthesis and further cause cell apoptosis. Although the expression level of EGFR on cancer cell surface support receptor-mediated targeted therapeutic approaches, using ligand-binding cytotoxic agents still can hurt normal cells which also express EGFR on cell membrane.

2.10 Oligonucleotide Immobilization

In this work, DNA was first attached on glass or PDMS surface as a hybridization probe for aptamer immobilization. The attachment method has been widely used in DNA microarray or DNA chip. Besides, there are numerous different methods can be applied in DNA arrays. Different attachment strategies are illustrated here.

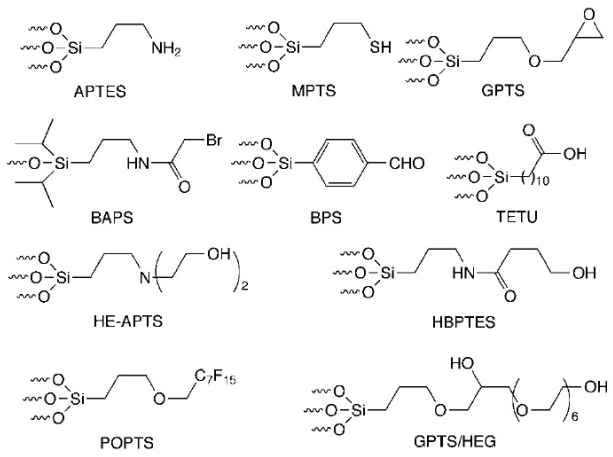

Figure 2.14 Different reagents used in oligonucleotide immobilization SiO_2 surface.

Before introducing the attachment methods, self-assembled monolayers (SAMs) have to be illustrated first. In SAMs, certain active groups are incorporated into oligonucleotides that can directly attach the molecule on the substrates. The organization of the organic constituents is specific based on affinities which the oligonucleotide has for the surface. For examples, (i) spontaneous adsorption of long-chian alkanoic acids is an acid-based raction, and the affinity is

the formation of a surface salt between the carboxylate anion and a surface metal cation (alkanoic acids on Al_2O_3 or on silver); (ii) the formation of Si-O-Si bonds can connect polysiloxane to surface silanol groups, and thus alkylchlorosilanes, alkylalkoxysilanes, and alkylaminosilanes can form SAMs on hydroxylated surface (SiO_2, Al_2O_3, etc.); (iii) surface active organosulfur compounds also can form monolayers on gold suface; (iv) alkyl chains can be covalently bound to a silicon substrate via C-Si bonds. (ii) and (iii) are frequently used (*112*).

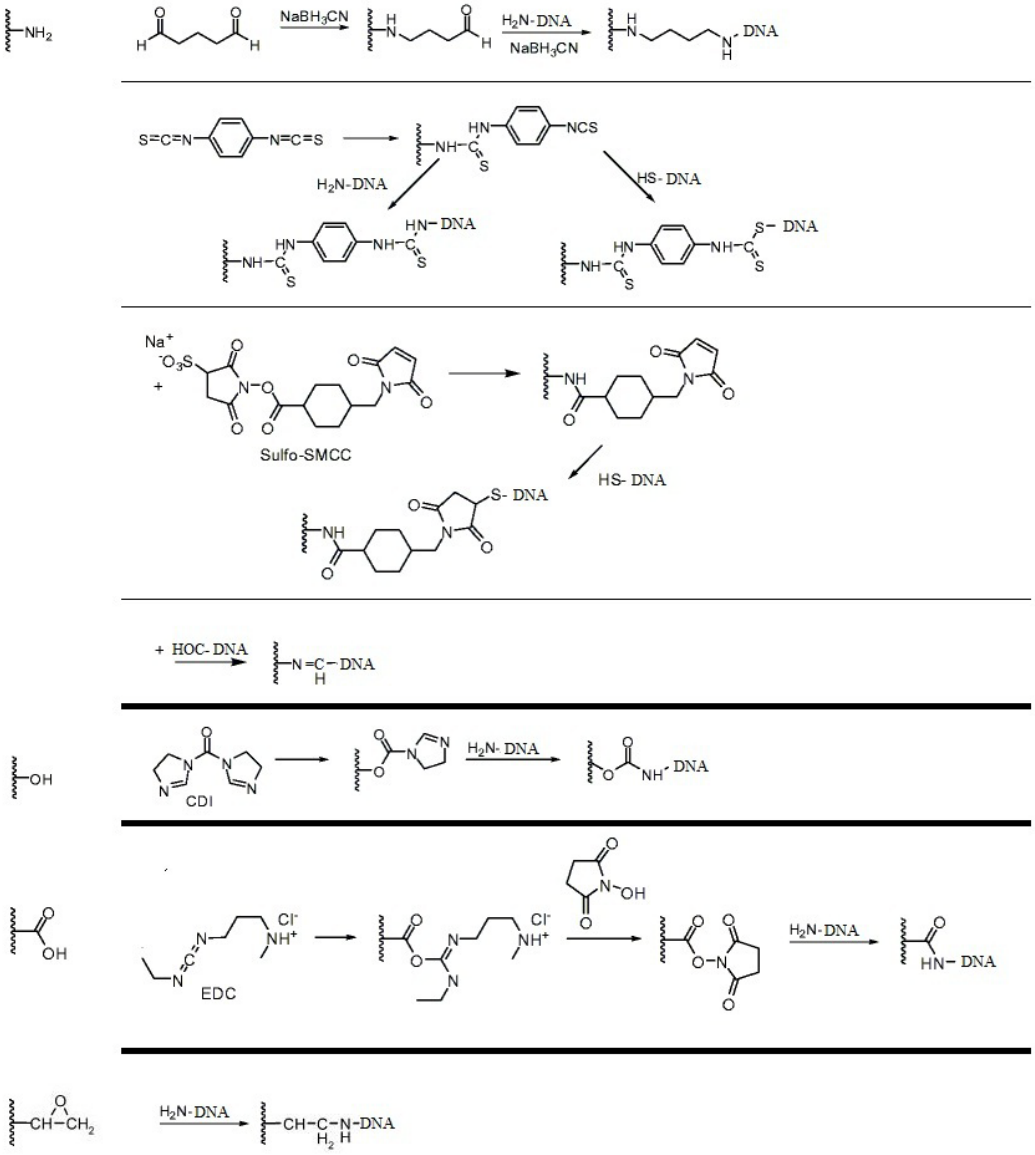

Figure 2.15 Common methods to immobilize DNA on silicon dioxide surface.

In method (ii), alkylalkoxysilanes and alkylaminosilanes are commonly used. Different silane reagents can make the surface carry various functional groups, such as –COOH, -NH_2, –Br, and so on (Figure 2.14). After silane modification, corresponding linker should be introduced on the surface for DNA attachment. More details can be found in Figure 2.15. The whole procedure requires multiple reactions. Moreover, the unreacted activated groups may cause DNA nonspecific absorption.

In method (iii), thiol modified DNA can attach on gold surface as sulfur compounds have a strong affinity to transition metals. In other words, the S-Au bond strength is very high. This DNA immobilization method is easy, and the manipulation is also simple. However, the thiol modified DNA requires deprotection with a special procedure before the DNA attachment. It also requires optimum buffer and pH value for the modification. It sometimes can bind the surface unspecifically. The interesting optical or electronic properties of gold nanoparticles, however, are not easily accessible after modification.

Other commonly used immobilization methods are: using streptavidin coating on substrates for biotin modified DNA immobilization; and methylcytidine modified DNA attached to surface carrying pyrrole groups (*113*).

There are two key parameters which directly affect final oligonucleotide immobilization: one is the number of sites per unit area for oligonucleotide immobilization; the other is the number of oligonucleotide per unit area. Normally, oligonucleotide cannot be attached to every site due to its larger size. Therefore, after oligonucleotide attachment, there is still abundance of unreacted sites. Take amino-modified DNA immobilization for example, the density of the anchored DNA can be approximately 1 per 4 or 5 nm^2 (*114*), and this value can give a better signal in detection process. A reduced distance between adjacent DNA probes can provide higher probe density; however, the negative charges from the tightly packed DNA probes on the surface can repel targets from inserting into the spaces between adjacent DNA probes and thus impede the target from hybridization (steric effect). On the other hand, presence of many

unreacted sites on the surface can cause nonspecific adhere of molecules to the surface. Steric effects and nonspecific absorption are major issues that should be addressed. The nonspecific absorption can be easily solved by deactivation of these sites with chemical reagents. Nano-textured surfaces are adopted to overcome steric effects. There are two advantages. First, larger surface area is available for immobilization. Thus, the total probe number would be far greater on 3D nano-textured surface. Second, on a 3D surface, the upper space between probes would be widened. In other words, the increase in probe density increases can be coupled with much more upper space for target hybridization.

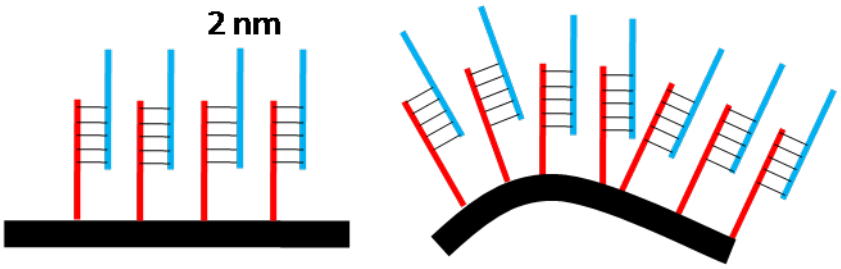

Figure 2.16 Steric Effect on planar surface.

2.11 Cells

2.11.1 Human Glioblastoma Cells

Human Glioblastoma Cells (hGBM) cells were used for experiments as these show overexpression of EGFR on cell membrane. It is necessary to illustrate the properties of GBM. GBM is one of the most common intracranial malignant tumors in humans and accounts for 20% of all intracranial tumors. Although the incidence is very low (5 cases per 100,000 people), most patients survives for only 12 to 15 months (*115*). No cause has been confirmed for GBM except the established risk factors: exposure to ionizing radiation. Malignant transformation in glioma results from the sequential accumulation of genetic aberrations, such as various deletions, amplifications and point mutations, which can further lead to the deregulation of growth-factor signaling pathways. The most common defects in signal transduction pathways include EGFR and platelet derived growth factor receptor (PDGFR). As mentioned before,

overexpression of EGFR on cell membrane occurs in 40 to 50% of patients. Additionally, at least three types of EGFR mutations have been found in high grade GBM: EGFR vI, EGFRvIII and EGFRvII. The first two types of mutation can constitutively autophosphorylate without extracellular ligand-binding. EGFRvIII is the most commonly found in GBM. Therefore, given the amplification and mutaionts in EGFR, RAS/ERK and PI3 kinase/AKT pathway are usually activated for cell survival, proliferation, invasion, angiogenesis, and inhibition of apoptosis. Particular interest has focused on RTK inhibition, and relevant antibodies have been used in therapy (*116*). Currently, imaging diagnosis is the major tool to find the lesions, and the definitive diagnosis requires a stereotactic biopsy or a craniotomy with tumor resection and pathologic confirmation. However, biopsy or subtotal tumor resection may result in incorrect tumor grading and intracranial spreading. Thus, it is important to develop a novel molecular diagnosis method.

2.11.2 Fibroblast

Fibroblasts can synthesize the collagen and compose the extracellular matrix. Fibroblasts appear to play an important role in wound healing. On culture dishes, fibroblasts are large, flat and spindle looking. In a crowd, these often locally align in parallel clusters. Compared to EGFR overexpression on tumor cells, fibroblasts also express it on cell membrane for sustaining their normal proliferation and migration. Fibroblasts were used as controls in the experiments. In some cases, if fibroblasts have inflammatory hyperplasia or reactive proliferation after injury, they also may lead to tumor. Furthermore, if the tumor is characterized by immature proliferating fibroblasts or undifferentiated anaplastic spindle cells, it might be a malignant tumor (*117*).

2.12 Cellular Experiments

2.12.1 Cell Culture

In cell culture, each cell line (a cell culture following its first passage, most cell lines are derived from cancers) has slightly different requirements. Satisfying these requirements can

keep cell genome stability. The longer a cell line is cultured in the dish, the greater the chance that it may have genotype changes. If it happens, some characteristics of the cell line may be damaged or changed. Therefore, numerous factors, such as culture time, culture medium, serum, temperature, pH value and antibiotics etc., should be carefully considered. Nevertheless, the continuous culture of cell line should be limited to 3 months, because the change in gene mutation will significantly increase during the long time period culture due to cell line cross-contamination and microbial contamination. Beyond the limit, fresh cells should be used for new cell line culture.

Table 2.2 Common cell fixation methods.

Fixative	Method
Acetone	-20°C, 5-10 min, no permeabilization
Methanol	-20°C, 5-10 min, no permeabilization
Ethanol	cooled 95% ethanol, 5% glacial acetic acid, 5-10 min
Methanol-Acetone	-20°C, 10 min, permeabilize with acetone for 1 min
Methanol-Acetone Mix	1:1 mixture, -20°C, 5-10 min
Methanol-Ethanol Mix	1:1 mixture, -20°C, 5-10 min
Formalin	10% neutral buffered formalin, 5-10 min, PBS rinsing, permeabilize with 0.5% Triton X-100 for 10 min
Paraformaldehyde-Triton	4% paraformaldehyde, 10-20 min, PBS rinsing, permeabilize with 0.5% Triton X-100 for 10 min
Paraformaldehyde-Methanol	4% paraformaldehyde, 10-20 min, PBS rinsing, permeabilize with -20°C methanol for 5-10 min

2.12.2 Cell Passage

Cell passaging is a technique that keeps cells alive and growing under cultured conditions for extend period of time. It involves transferring a small number of cells into a new culture medium. Normally, culture medium supports the exponential growth of cells by providing necessary nutrient. When nutrient exhaust, cells might die and/or have genetic and phenotypic changes. Therefore, when cells are confluent over 90%, they should be passed. The frequency of passaging depends on the growth rate of cell line and the density of seeding cells. For example, cells take less time to resume exponential growth with higher seeding density. In suspension culture, GBM culture for example, cells should be resuspended first, and then the diluted cell suspension transferred to a fresh culture dish. In adherent culture, fibroblasts culture

for example, cells should be detached from the surface and resuspended first, and the diluted sample should be used for a new culture.

2.12.3 Cell Fixation

Cell fixation is a chemical process by which biological tissues are preserved from autolysis or putrefaction. Moreover, cells must be fixed and permeabilized to ensure free access of the antibody to its antigen. Finally, fixative can increase cell mechanical strength and rigidity that facilitate subsequent experiments or analysis. Lots of fixation methods are available (Table 2.2); however in cellular experiments chemical fixation is commonly recommended. The fixatives involve organic solvents and cross-linking reagents. The solvents like alcohol and acetone remove lipids and dehydrate the cells, while precipitating the proteins on the cellular architecture. Paraformaldehyde forms intermolecular bridges, thus creating covalent chemical bonds between proteins and cytoskeleton. Cross-linkers preserve cell structure better than organic solvents, and provide additional rigidity, but may reduce the antigenicity of some cell components, and require the addition of permeabilization step, to allow access of the antibody to the target. Fixation denatures protein antigens; thereby antibodies prepared against denatured proteins may be more useful for cell staining. In this work, 4% paraformaldehyde-triton fixative was chosen. It can satisfy common histochemistry, immunochemistry, even PCR requirements. It is suitable for long term preservation and sample penetration. Glutaradehyde is another fixative, which has similar effects like paraformaldehyde. However, it is not suitable for fixing thicker tissue samples due to its larger molecular weight and slower diffusion rate.

2.12.4 Cell Staining

It is a tool that facilitates better visualization of cell and cell components under a microscope. Most stains can be used on fixed cells (in vitro), while few stains can be used on living cells (in vivo). In in vitro methods, fixation completely preserves the targets; and then a mild surfactant (sodium dodecyl sulfate, SDS) is used to dissolve the cell membrane allowing larger dye molecule or antibody access to the cell’s interior. Normally, first antibody is used for

target binding, and fluorescent labeled secondary antibody is used for binding to first antibody. In few cases, third antibody might be required. In vivo methods require dye molecules should be added to living cells. These dye molecules can bind to certain component or have specific chemical reactions within cells. For example, Bromodeoxyuridine (BrdU) staining is commonly used in the detection of proliferation of cells, which can replace thymidine during DNA replication. After cell fixation, antibodies specific for BrdU can be used to detect cell activity. In sum, although there are numerous stains and corresponding staining methods. It is important to carefully select stains and thoroughly rinse excess dye molecules. Common stains used in immunohistochemistry are listed in Table 2.3.

Table 2.3 Common stains used in immunohistochemistry.

Stains	Characteristics
Bismarck Brown	Colors acid mucins, yellow, can be used in vivo
Carmine	Colors glycogen, or animal starch, red
Coomassie Blue	Stains proteins, brilliant blue
Crystal Violet	Stains cell walls, purple
DAPI	Stains nuclear, ultraviolet light, can be used in vivo
Eosin	A counterstain to haematoxylin, pink or red
Ethidium Bromide	Illustrate the final stages of cell apoptosis, red-orange
Fuchsin	Stains collagen, smooth muscel or mitochondria, pink or red
Hematoxylin	Nuclear stain, bule-violet or brown
Hoechst Stains	Stain DNA in vivo, blue
Iodine	Starch indicator, dark blue
Malachite Green	A counterstain to safranin in Gimenez staining, blue-green
Methylene Blue	Stains nuclei, blue
Toluylene Red	Stains nuclei, red, can be used in vivo
Nile Blue	Stains nuclei, blue, can be used in vivo
Nile Red	Stains intracellular lipid globules, red, can be used in vivo
Osmium Tetroxide	Stains lipid, black
Rhodamine	A protein-specific fluorescent stain, red
Safranin	Stains nuclear or collagen, yellow

2.12.5 Cell Dehydration

Dehydration is an important process widely applied for water removal from cells by immersing them in a gradient concentration of solution. Because water still remains in cell after fixation, cellular structure may collapse when cell leaving aqua environment. Therefore, it is necessary to replace the water component first. Usually, gradient concentration of ethanol is

used for dehydration. It not only can replace water but also further can solidify cellular structure. After dehydration, volatile ethanol should be further substituted with isoamyl acetate which can sustain cellular original structure. It is noted that overquick dehydration treatment may lead to cell membrane significant shrink and cellular structure collapse. The dehydrated cells can be can be used for immunocytochemical analysis, or metal can be deposited on cell surface for SEM analysis.

2.13 Soft Lithography

Soft lithography utilizes a patterned elastomer as the stamp, mold or mask to generate micropatterns and microstructures (*118*). It has emerged to have many flavors like microcontact printing, replica molding, microtransfer molding, micromolding in capillaries, solven-assisted micromolding, phase-shift photolithography, cast molding, embossing molding, injection molding etc.. Although soft lithography has many applications, we used PDMS to fabricate microfluidic devices. The relevant properties of PDMS, its pros and cons, PDMS microstructure device assembly, surface activation, etc. will be introduced here. More on soft lithography can be found elsewhere (*119-121*).

2.13.1 PDMS

Many polymers can be used to make microfluidic system; however, PDMS is the most widely used silicone-based organic polymer consisting of inorganic siloxane backbone and organic methyl groups attached to silicon. It is supplied as a two-part kit: a liquid silicone rubber base and a curing agent. At room temperature, these are fluids, and have low glass transition temperatures. When mixed them together in certain ratios, these liquid materials from a solid, cross-linked elastomer via the hydrosilylation reaction between vinyl groups and hydrosilane groups. The advantages of PDMS involve: (i) it has a low interfacial free energy and good chemical stability in aqueous solution; (ii) it is permeable; (iii) it also has good thermal stability, and it can cure at various temperature (from 20 °C to 180 °C); (iv) it is optically transparent down to 280 nm wavelength of light; (v) it is durable; (vi) the interfacial properties of PDMS can

be changed by treating the surface with plasma or other chemicals; (vii) it is nontoxic and biocompatible; (viii) it can seal reversibly to itself and other materials via van der Waals forces, or it can irreversibly seal after plasma treatment by formation covalent bonds; (ix) it can be deformed reversibly, and so on. There are also some disadvantages that may limit its application. For example, (i) it shrinks upon curing, especially at higher temperatures; (ii) it gets swollen and dissolves in organic solvents (*122*); (iii) the elasticity and thermal expansion of PDMS make it difficult to get high accuracy; (iv) the aspect ratio of microstructure in PDMS is limited between 0.2 and 2.

2.13.2 Microfluidic System Preparation

Microfluidic systems have many benefits, including decreased cost; shorten analysis time; reduced consumption of reagents and analyte; little potential contamination; increased efficiency and portability; and so on. Moreover, in microfluidic systems, we can get laminar flows. Normally, a fluid with Reynold's number less than 2000 flow laminarly; above 2000, fluids flow turbulently. Therefore, in microfluidic systems, at few microns size of channel with low velocity, fluids can flow laminarly. This property can facilitate in many biological assays. The PDMS based fabrication procedure can be divided into four steps. First, the layout for the microfluidic system in a designing software, and translating the designed pattern to a mask. Using photolithography, the pattern is transferred to a negative photoresist. After development, the pattern stays on the wafer surface, and serves as a master or mold. A well mixed PDMS liquid solution is then cast on the master surface and cured till it become a solid. Finally, the solid PDMS can be peeled off from the master for microfluidic assembly. The whole process is illustrated in Figure 2.21. Sealing each part can finally assemble the microfluidic device. Sealing can be reversible or irreversible. PDMS can attach to a flat surface via van der Waals forces. This reversible sealing is watertight and fast. It is also easy to peel off PDMS. On the contrary, if PDMS is treated with oxygen plasma, it can form a tight, irreversible seal. The plasma introduces silanol groups at the expense of methyl groups. These silanol groups then condense

with other –OH or –COOH groups (Figure 2.22). In most of applications, PDMS is normally attached to glass and silicon dioxide surfaces for device assembly.

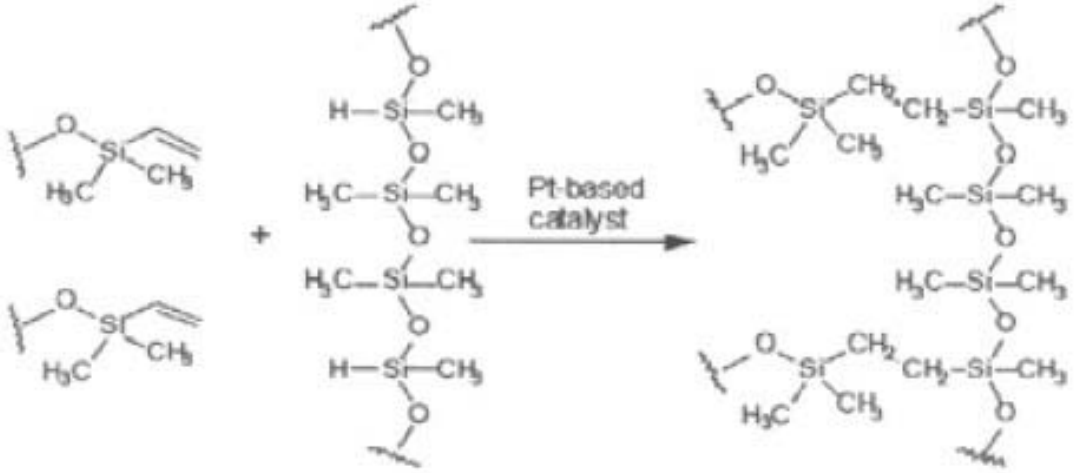

Figure 2.17 PDMS crosslinking

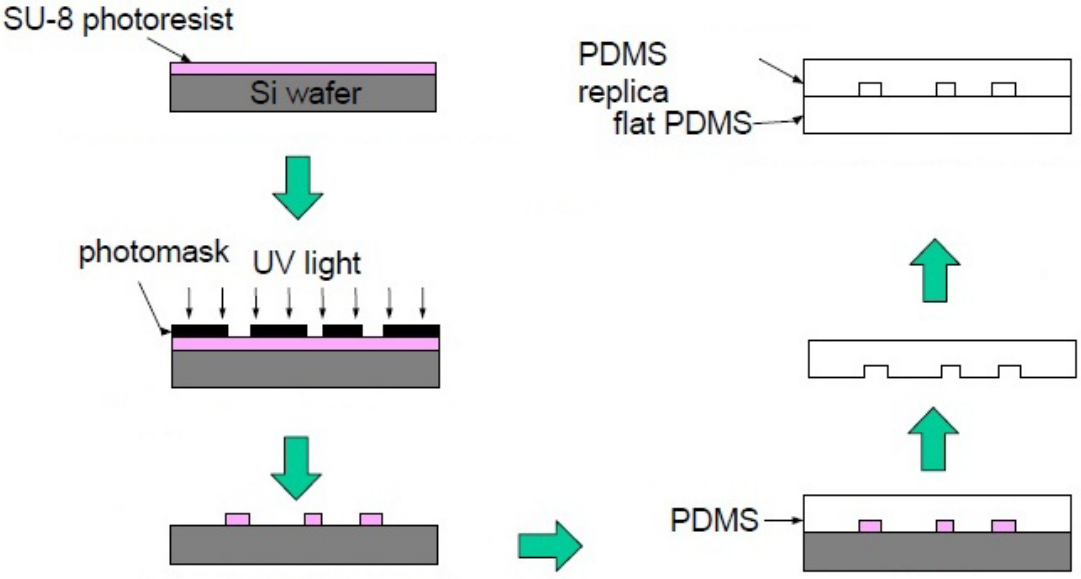

Figure 2.18 PDMS microfluidic device assembly

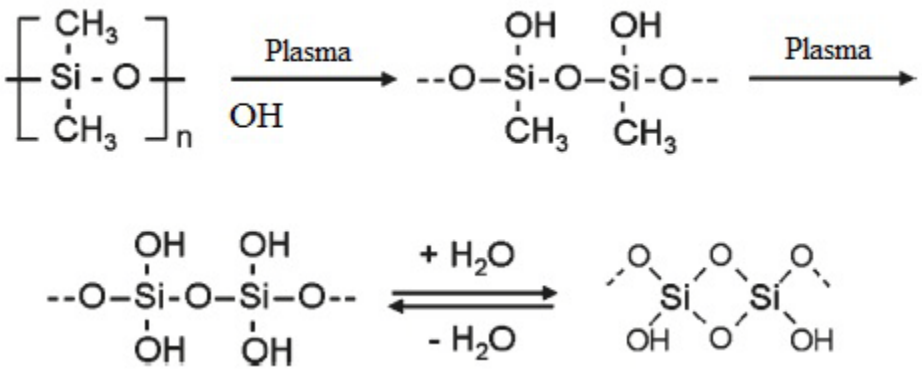

Figure 2.19 PDMS structure and surface properties after modification.

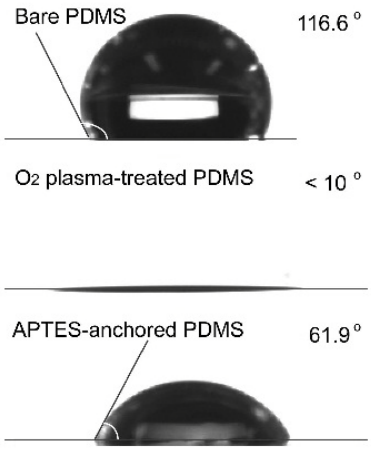

Figure 2.20 PDMS surface modification and the change of contact angle

2.13.3 PDMS Surface Properties

PDMS is very hydrophobic (contact angle is around 110°) due to two methyl groups on lateral chain (Figure 2.19). This property may sequester small hydrophobic molecules from media (*123*). On the other hand, PDMS curing cannot achieve 100% crosslinking, and 5% of the PDMS bulk remains uncrosslinked (*122*). In other words, few freely diffusive oligomers may leach from PDMS bulk into the culture media, and cause cytotoxicity or interference with cellular signaling pathways. Therefore, PDMS surface needs to be modified in order to achieve desirable functionality. Plasma treatment is the simplest and most common method used to change PDMS surface properties. The details of mechanism are well-known (*124*). Briefly, after

oxygen plasma treatment, two methyl groups are replaced by hydroxyl groups. The surface thus becomes hydrophilic, and the contact angle can decrease to as less as 10° (Figure 2.20). However, this hydrophilic property is reversible. PDMS recovers to hydrophobic nature due to the migration of unoxidized chains to the surface. Thus, the hydrophilic PDMS should be used for experiments immediately following oxidation (*125*). Alkyltrichlorosilanes or alkyltrialkoxysilanes are also commonly used chemicals for PDMS surface modification (*126*). These can form SAMs on plasma activated PDMS surface. Although the structure of SAMs is less ordered than SAMs of alkanethiolates on gold, they have been extensively used for surface modification. This kind of modification can reduce interfacial free energies and thus reduce physical adhesion; and it can be used for immobilization of oligonucleotides, peptides or proteins. In this work, plasma active PDMS surface was treated with aminopropyltriethoxysilane (APTES) which introduced amine groups on the surface, and the contact angle decreased to about 60°. Following the attachment method mentioned before, amine modified oligonucleotides were introduced on PDMS surface. In sum, plasma treatment and chemical modification can change PDMS surface properties, and due to its plasticity, PDMS can replace glass and play an important role in biochips, microfluidic devices, and other biological separation and analysis platforms. PDMS surface properties can also be altered by changing its surface structure. When PDMS surface containing micron, submicron and nano-composite structures, it becomes super-hydrophobic with contact angle higher than 160°. Therefore, the wettability of PDMS surface can be easily turned by controlling the size of micro- or nano-structures. On the other hand, if the super-hydrophobic surface is treated with plasma or silanes, it can change into super-hydrophilic one, which might be better for cellular experiments (*127, 128*).

CHAPTER 3

SURFACE-IMMOBILIZED APTAMERS FOR CANCER CELL ISOLATION AND MICROSCOPIC CYTOLOGY

Early detection of cancer cells and its metastasis not only can give a definite diagnosis but also can dramatically change therapy and prognosis. There are numerous detection methods reported for the detection and isolation of tumor cells. Comparing to mechanical and electrical sorting techniques, affinity interactions based isolation methods are expected to give higher efficiency and specificity. However, antibodies as a major tool are often subject to high levels of off-target cross-reactivity. The other major disadvantage of antibodies is heterogeneous surface character after its immobilization; the target binding domain of antibodies may towards the substrate during the conjugation process. Aptamers as a better alternative which own similar affinity and better specificity have been applied in cell labeling and in activating cell signal pathways (*82, 83, 129-132*). Only recently, aptamers have been used for cell sorting, detection and isolation (*84, 133-136*). In this chapter, we report results from anti-EGFR aptamer functionalized substrate to isolate EGFR overexpressing hGBM cells, as well as genetically engineered mouse glioma cells that photocopy human glioma. The approach shows a strong cytologic analysis modality to isolate and identify cancer cells. The data presented here provide a proof-of-principle approach for identifying and isolating uniquely malignant subpopulations of tumor cells with a high degree of sensitivity and specificity.

3.1 Materials and Methods

3.1.1 Aptamer Preparation

The anti-EGFR RNA aptamer was isolated by iteratively selecting binding species against purified human EGFR (R&D Systems) from a pool that spanned a 62-nucleotide random

region (*137*). The EGFR protein was purified from murine myeloma cells. It contained the extracellular domain of human EGFR (Leu^{25} – Ser^{645}) fused to the Fc domain of human IgG1 (Pro^{100} – Lys^{330}) via a peptide linker (IEGRMD). Anti-EGFR aptamer owning high binding affinity (K_d = 2.4 nmol/L) and nonfunctional mutant aptamer were extended with a capture sequence which did not disrupt aptamer structures. It can hybridize with DNA probes immobilized on substrate surface. The sequence for the extended anti-EGFR aptamer, mutant aptamer, and relevant DNA probes were shown in Table 3.1. The capture sequence is underlined. The anti-EGFR aptamer was prepared by transcribing a dsDNA template using Durascribe kits (Epicentre Biotechnologies). After PCR amplification, dsDNA products were precipitated with ethanol, and mixed with reaction buffer, DTT, ATP, GTP, 2' F-CTP, 2' F-UTP, and a mutant T7 polymerase for 10 hours at 37 °C. The 2-fluoro modification CTP and UTP is endonuclease-resistant, that can further increase the chemical stability of RNA. The DNA template was then degraded with DNase treatment for 30 minutes at 37 °C to completely remove DNA. An 8% denaturing PAGE was used to purify aptamer. The band for the aptamer was visualized by UV shadowing, and the aptamer was recovered via eluting in 0.3 mol/L solution acetate (pH 5.2) overnight at 37 °C and ethanol precipitation. The pellet was dissolved in DI water, and the concentration of aptamer was measured on a NanoDrop spectrophotometer (Thermo Scientific). The aptamer was modified by extending the DNA template at its 3' end with a 24-nucleotide sequence tag, and then hybridizing with DNA probes labeled with 6-FAM or an amine group at its 5' end.

3.1.2 Preparation of Anti-EGFR Aptamer/Antibody Functionalized Substrates

The attachment method can be found elsewhere (*138, 139*). 4 × 4 mm^2 glass pieces were cleaned with piranha solution (H_2O_2:H_2SO_4 = 1:3) at 90 °C for 10 minutes. After rinsing with DI water and drying in nitrogen flow, the glass substrates were immersed in a 19:1 (v/v) methanol/DI water solution containing 3% APTES for 30 minutes at room temperature. The silanized substrates were then sequentially rinsed with methanol and DI water and baked at 120

°C for 30 minutes. The substrates were then soaked in a dimethylformamide (DMF) solution containing 10% (v/v) pyridine and 1 mmol/L phenyldiisothiocyanate (PDITC) for 5 hours. Each substrate was then washed with DMF and 1,2-dichloroethane and dried with nitrogen. The amine modified DNA probes were prepared at 30 µmol/L concentration in DI water with 1% (v/v) N,N-diisopropylethylamine (DIPEA). A volume of 5 µL of DNA solution was placed on each substrate and allowed to incubate in a humidity chamber at 37 °C overnight. Methanol and diethyl pyrocarbonate (DEPC) treated DI water (0.02%, v/v) were used to rinse each substrate. The unreacted PDITC moieties on surface were deactivated by immersion in 50 mmol/L 6-amino-1-hexanol and 150 mmol/L DIPEA in DMF for 5 hours. Each substrate was then sequentially rinsed with DMF, methanol, and DEPC-treated DI water. The incubator was cleaned with RNase-free reagent and DEPC-treated DI water three times. A volume of 5 µl of anti-EGFR aptamer at 1µmol/L concentration was placed on each substrate in 1× annealing buffer [10 mmol/L Tris (pH 8.0), 1 mmol/L EDTA (pH 8.0), 100 mmol/L NaCl]. After 2 hours of hybridization at 37 °C, substrates were washed with 1× annealing buffer and DEPC-treated DI water for 5 minutes. The negative control devices were hybridized with mutant aptamer using the same protocol. The substrates were placed in 1 × PBS (pH 7.5) with 5 mmol/L $MgCl_2$ and kept at -20 °C for 1 week or used immediately. The EGFR antibody attachment was adapted from previous reports (*139, 140*). A 100 µg/mL EGFR antibody solution was placed on the glass substrates and incubated at 37 °C for 1 hour. Then, the substrates were blocked with bovine serum albumin (10 mg/mL) solution for 20 minutes, washed thoroughly with 1× PBS, and placed in 1× PBS solution.

3.1.3 Isolation and Characterization of EGFR-overexpressed Mouse Derived Tumor Cell

Embryonic (E13.5) neural stem cells (NSC) were isolated from Ink4a/Arf$^{-/-}$ embryo brain, maintained under standard neurosphere culture conditions, and infected with a retrovirus expressing the mutant EGFRvIII receptor (*141*). The Ink4a/Arf$^{-/-}$ EGFRIII NSCs were also stably

transduced with a lentivirus expressing monomeric-cherry (referred to as *m-cherry*) fluorescent protein for live cell imaging and identification.

Table 3.1 The respective sequence of anti-EGFR aptamer, mutant aptamer, and DNA probes.

Name	Sequence
Anti-EGFR Aptamer	5'-GGC GCU CCG ACC UUA GUC UCU GUG CCG CUA UAA UGC ACG GAU UUA AUC GCC GUA GAA AAG CAU GUC AAA GCC GGA ACC GUG UAG CAC AGC AGA GAA UUA AAU GCC CGC CAU GAC CAG-3'
Mutant Aptamer	5'-GGC GCU CCG ACC UUA GUC UCU GUU CCC ACA UCA UGC ACA AGG ACA AUU CUG UGC AUC CAA GGA GGA GUU CUC GGA ACC GUG UAG CAC AGC AGA GAA UUA AAU GCC CGC CAU GAC CAG-3'
DNA Probes	5'-amine-CTG GTC ATG GCG GGC ATT TAA TTC-3' 5'-6FAM-CTG GTC ATG GCG GGC ATT TAA TTC-3'

3.1.4 Isolation and Characterization of hGBM Cells

hGBM samples were obtained from consenting patients at the University of Texas Southwestern Medical Center (Dallas, TX) with the approval of the Institutional Review Board. On average, specimens > 50 mm^3 were placed into ice-cold HBSS medium immediately after surgery. Red blood cells were removed using lymphocyte-M (Cedarlane Labs). GBMs are highly cellular and molecularly heterogeneous tumors. Recent studies suggest that CD133, a membrane glycoprotein, may have an inexhaustible ability to self-renew, proliferate, and form a tumor when implanted into an immunocompromised host. Moreover, it also endows GBM cells with highly resistance of radiation and chemotherapy. In this study, $CD133^+$ cells we used were found to overexpress wild-type EGFR. The hGBM tumor tissue was gently dissociated with papain and dispase (both 2%), triturated, and then labeled with a CD133/2 (293C3)-PE antibody (Miltenyi Biotec) and sorted with FACSCalibur machine (BD Biosciences). Both $CD133^+$ and $CD133^-$ cells were suspended in a chemically defined serum-free DMEM/F-12 medium, consisting of 20 ng/mL of mouse EGF (PeproTech), 20 ng/mL of basic fibroblast growth factor (PeproTech), 1× B27 supplement (Invitrogen), 1× Insulin-Transferrin-Selenium-X (Invitrogen), and 100 units/mL penicillin-100 µg/mL streptomycin (HyClone), and plated at a density of 3 × 10^6 live cells/60-mm plate. Both $CD133^+$ and $CD133^-$ fractions underwent clonal expansion and formed orthotopic tumors (data not shown). For all the experiments, we used the $CD133^+$

fraction, referred to as hGBM cells. They were also stably transduced with a lentivirus expressing *m-cherry* fluorescent protein.

3.1.5 Meninge Derived Primary Fibroblast

Rat-derived primary meningeal fibroblasts were obstained from postnatal day 3 rat pups. Briefly, meninges were peeled from the cerebral cortices. They were dissociated with 0.5% collagenase for 30 minutes and 0.06% trypsin/EDTA for 20 minutes respectively before trituration, and then cells were plated in T-75 tissue culture flasks in DMEM/F-12 medium containing 10% fetal bovine serum and allowed to grow for 1 week to confluence.

3.1.6 Aptamer Binding to Cells

First, fibroblasts can tumor cells were seeded into separate PDMS wells (8-mm diameter) and cultured for 48 hours; thereby cells can firmly attach on Laminin treated glass surface. Equal amounts of aptamer (anti-EGFR aptamer or mutant aptamer) and DNA probe were annealed by heating samples to 70°C for 10 minutes and then slowly cooling down, and then annealed RNA/DNA was incubated with cells at 37°C for 30 minutes under 5% CO_2. After incubation, cells were washed with 1× PBS three times and stored in freshly sterilized 1× PBS for differential interference contrast (DIC) and fluorescence imaging. DIC data were used to image the cells, and fluorescence imaging was focused on aptamers. The fluorescence images were taken using appropriate filters. The excitation and emission wavelength of 6-FAM are 492 and 517 nm, respectively.

3.1.7 Tumor Cell Capture Using Anti-EGFR Aptamer/Antibody Substrates

Tumor cells were collected by centrifugation, and resuspended with 1× PBS (with 5 mmol/L $MgCl_2$). About 50 µL of cell suspension were placed on each substrate and allowed to incubate for 30, 60, or 90 minutes at 37°C (*82*). The whole substrates were washed with PBS on a shaker (Boekel Scientific) at 90 rpm for 6 to 10 minutes. In different trials, there was no difference seen in the results for the three different groups of 30, 60 and 90 minute incubation; however, the buffer evaporation was seen for longer incubation. Therefore in following trails,

aptamers were incubated cell for only 30 minutes. In tumor-specific isolation studies, hGBM cells were mixed with fibroblasts in a 1:1 ratio. Mutant aptamer-functionalized substrates were used as controls. The experiments of EGFR capture with antibodies followed exactly the same procedure.

3.1.8 Monitoring of Dynamic Interactions Between Tumor Cells and Anti-EGFR Aptamer

On a custom-designed platform the interaction between tumor cells and surface-grafted aptamers was monitored. Briefly, the substrates were placed on the platform, which maintained 5% CO_2 at 37°C and high humidity for live cell imaging (*142*). The interactions between cells and anti-EGFR aptamer surface were monitored using an inverted microscope. Images were taken every 30 seconds, and the interaction was recorded for 30 minutes. Tumor cells were also seeded on mutant aptamer functionalized surface, and the interaction was monitored in the same way.

3.1.9 Quantification and Statistical Analysis

For analysis, 5 representative images (of 25 total substrate areas) were randomly taken from each substrate. The images were analyzed with Image-Pro Plus software. The total number of captured cells and their relevant diameter on the surface were counted automatically; meanwhile the cell densities (number of cells per mm^2) were calculated. To show the diameter of tumor cells on aptamer grafted substrates, the data were sorted into six groups based on cell sized (from 20 μm to the miaximum; 5 μm interval), and relevant percentages were obtained.

3.2 Results and Discussion

3.2.1 Aptamer Binding to Mouse Derive Tumor Cells

The 6-FAM modified DNA probe were annealed with anti-EGFR aptamers, and specific binding to culture mouse-derived glioma cells and primary fibroblasts was observed (Figure 3.1); contrarily, mutant aptamer failed to recognize EGFR. After washing, strong green fluorescence was observed in mouse-derived tumor cell group (Figure 3.1B), and very weak fluorescence and be found on fibroblast surface. Neither anti-EGFR aptamer nor mutant

aptamer can be found on mouse derived glioma cells or primary fibroblasts. The fluorescence intensity data are shown in Figure 3.1C. Similar results were obtained for hGBM cells. This showed the specific binding of anti-EGFR aptamer with EGFR. The more EGFR on cell membrane, the stronger the fluorescence signals.

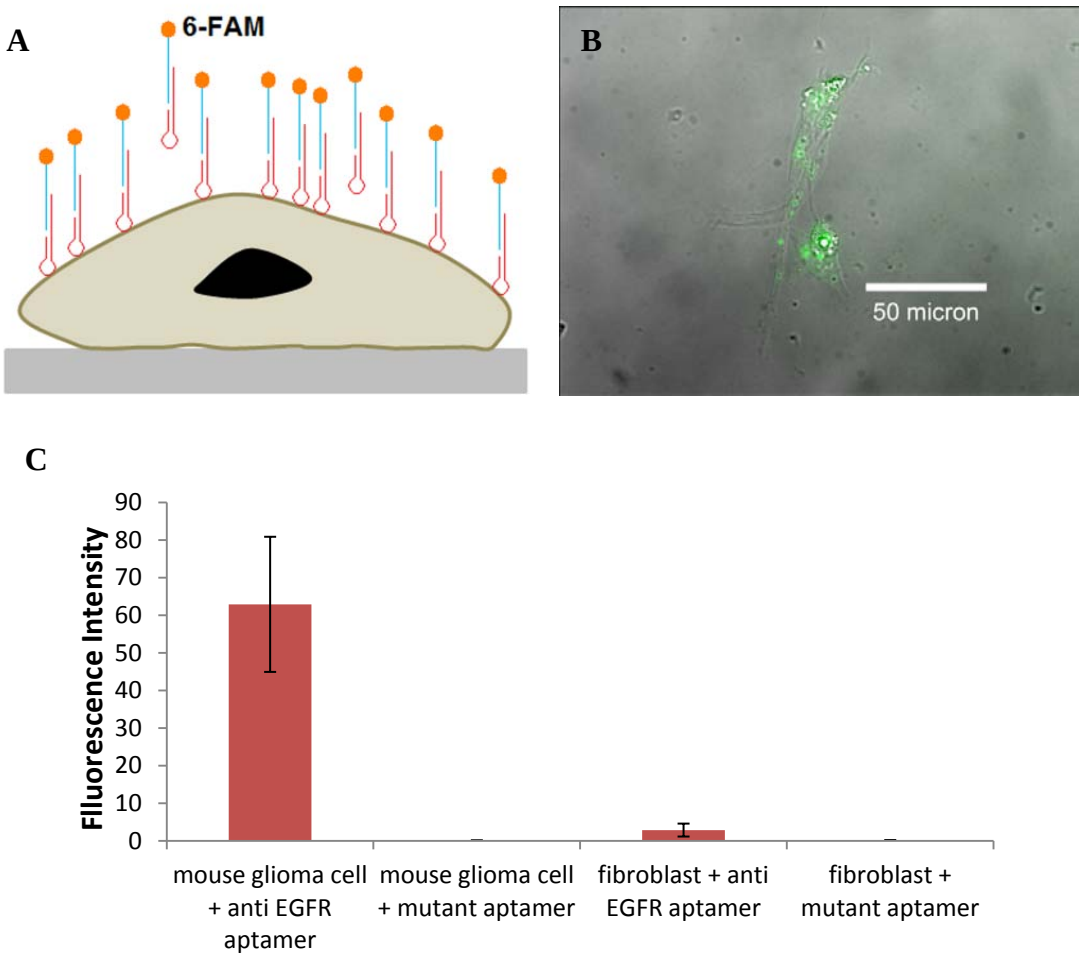

Figure 3.1 Anti-EGFR aptamer binding to the cultured mouse-derived tumor cell. A, schematic depicting mouse-derived cell bound with aptamer complex. B, overlaid fluorescent and DIC images. The green fluorescent shows the cell-bound aptamer molecules. C, average fluorescence intensity of each group.

3.2.2 Capture and Morphologic Characteristics o Mouse Derived Tumor Cells

PDITC activated surface can be used to immobilize any amine-modified molecules. After amine modified DNA probe immobilization, the unreacted PDITC moieties may occure the

nonspecific adsorption of aptamer. Thus, it is necessary to deactivate surplus PDITC end groups. The use of aptamer for the surface functionalization has many advantages: it shows a generalized approach to capture any functional nucleic acid, a distinct advantage relative to the use of proteins; it increases the distance between the substrate surface and the aptamer, alleviating the effects of steric and/or electrostatic hindrance that may come from surface tethering; and it increases the radius of gyration of the aptamer, thereby potentially increasing reactivity. This also resulted into very distinct behavior of cells when interacting with aptamers (discussed later). Figure 3.2 shows the flow chart of whole experiment: after aptamer immobilization cells were incubated with aptamers, and only EGFR overexpressing cells might be enriched on anti-EGFR aptamer functionalized surface.

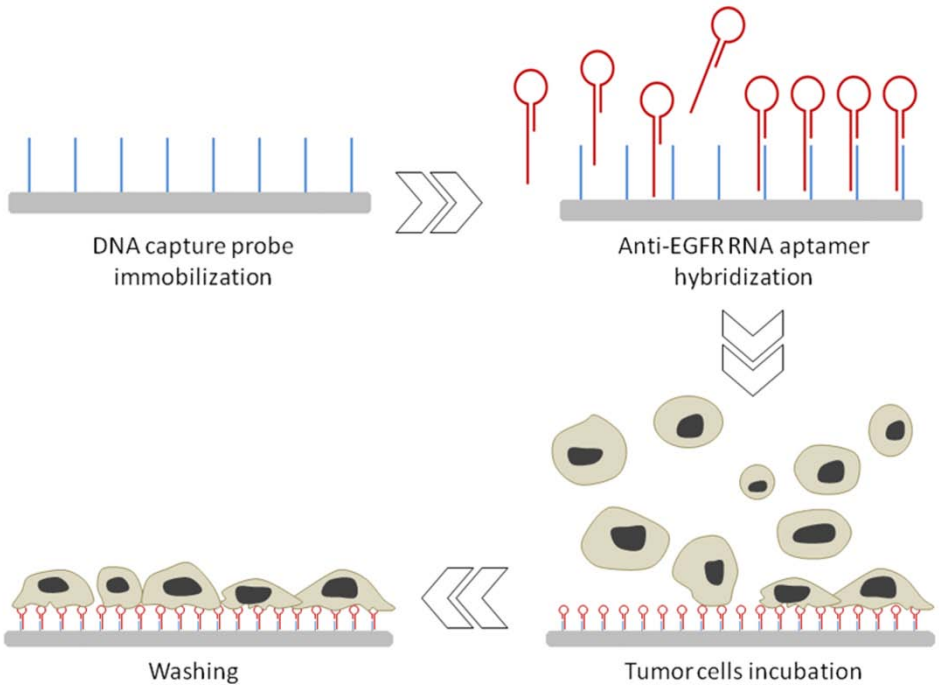

Figure 3.2 Schematics showing steps of experiments (not drawn to scale)

In the trials, a significantly higher number of cells were enriched on anti-EGFR aptamer functionalized surfaces (Figure. 3.3), and isolation efficiency (the ratio of captured cell number to the original number of cells on the surface) is 62%. On the contrary, fewer cells (average 7

cells/mm^2) were captured on mutant aptamer functionalized substrates. A passivation layer that minimizes non-specific adsorption can be generated by nucleic acids. The hydrophilic surface and electrostatic repulsion may prevent non-selective physical adsorption of the cells on mutant aptamer substrates (*143-145*). It is known that the density and amount of sialylation on cancer cells surface is higher than normal ones (*146-148*), and carboxyl groups from sialic acid often cause a net negative surface charge on cancer cells. The repulsion between negatively charged cells and the negative charges from the surface functionalized aptamer can be another putative reason for minimizing non-specific adsorption. On the other hand, EGFR overexpressing cancer cells can overcome these competing forces and selectively interact and bind to the anti-EGFR aptamers. The density and diameters of captured cells showed distinct behavior on the anti-EGFR and mutant aptamer substrates (Figure 3.3A and 3.3B). On 12 anti-EGFR aptamer substrates average 392 cancer cells per mm^2 were captured (SD: 143), with the size ranges depicted in the Figure 3.3B. About 70% of the captured cells had diameters above 30 μm, whereas the size of these cells in suspension ranged between 25-30 μm. This indicates that cancer cells were spreading on the anti-EGFR aptamer substrates. Nevertheless, anti-EGFR aptamer is an important analytical tool, serving as a novel and important phenomenon that can be a discriminating factor in cytological studies for the confirmation of captured tumor cells.

3.2.3 Capture of hGBM Cells

cells were also captured by the anti-EGFR aptamer functionalized substrates. Very few cells adhered to mutant aptamer functionalized substrates. Figure 3.4 shows the clear difference in the number and cell shapes of hGBM cells on anti-EGFR and mutant aptamer functionalized substrates. Along with difference in the numbers of captured cells, the shapes of the cells bound with aptamers and adsorbed on mutant aptamer surfaces were also quite different (discussed later). On average 117 hGBM cells were captured per mm^2 on anti-EGFR aptamer substrate (SD: 44), with isolation efficiency of 39%. On mutant aptamer functionalized substrate, average density of 4 cells per mm^2 was seen (SD: 3). Comparing to the mouse

derived tumor cells, fewer number of captured hGBM cells were captured on anti-EGFR aptamer functionalized surface. It can be explained in terms of overly high number of EGFR on mouse derived tumor cells membrane. The decreased density of captured hGBM cells was thus as expected.

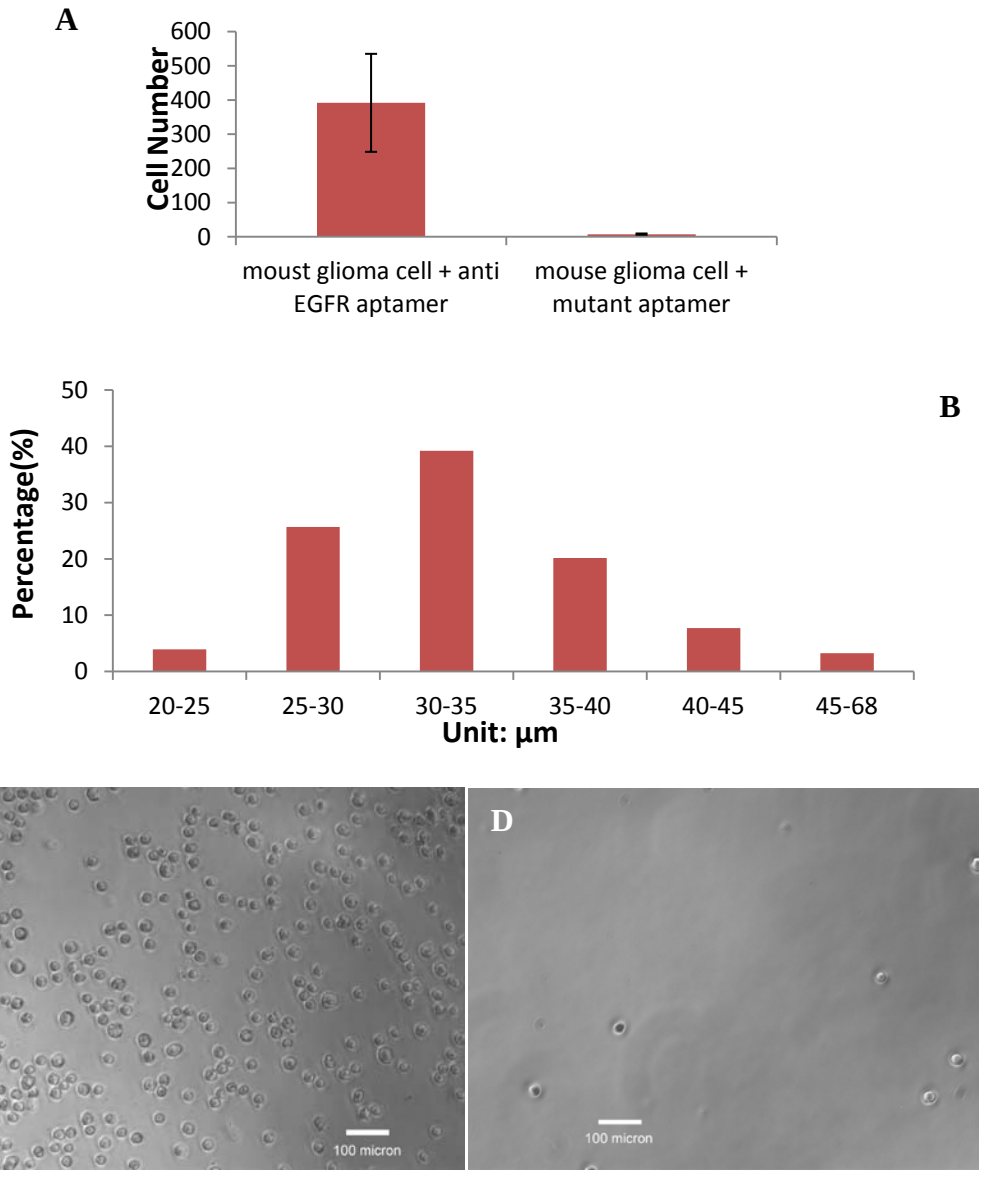

Figure 3.3 The density and size ranges of captured cells. A, average tumor cell density on anti-EGFR aptamer substrates (392 cells per mm^2, SD: 143) and on mutant aptamer substrates (7 cells per mm^2, SD: 3), *P < 0.01. B, distribution of the diameters of tumor cells. C and D, tumor cells enriched on mutant and anti-EGFR aptamer substrates respectively.

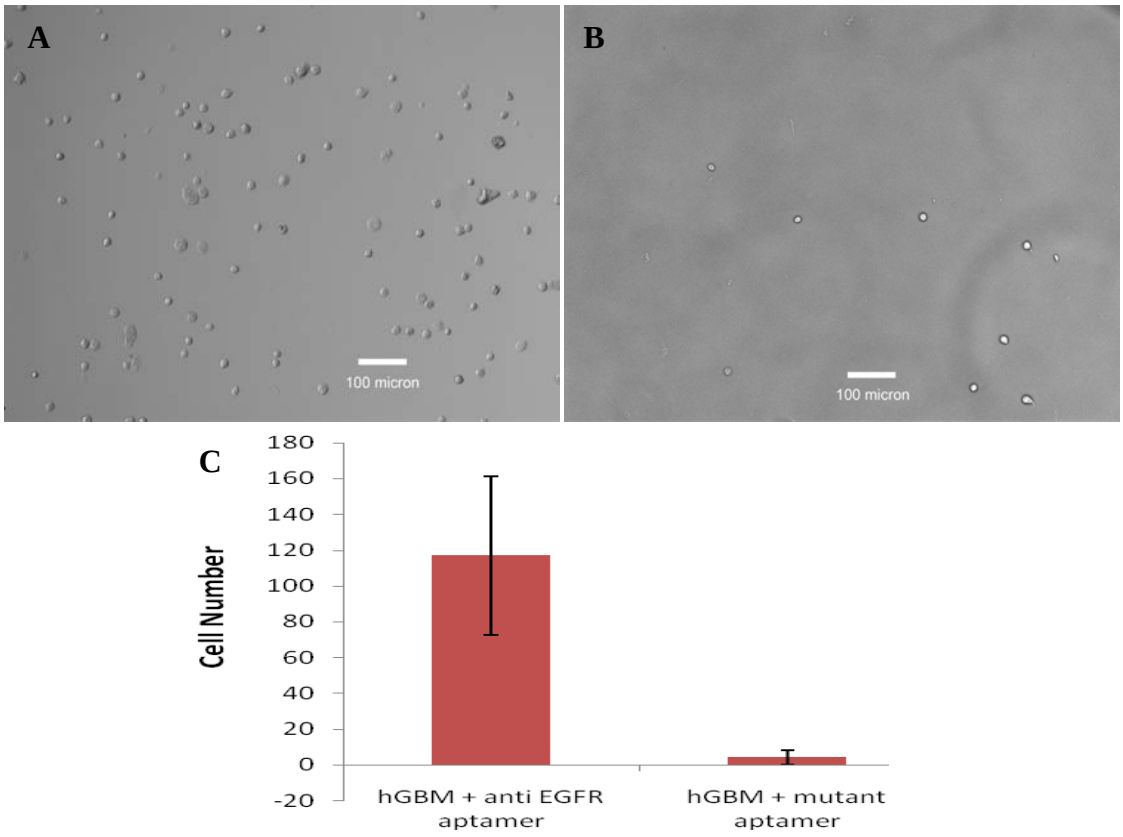

Figure 3.4 A and B, the hGBM cells on mutant and anti-EGFR aptamer functionalized surface. C, average hGBM cell density on anti-EGFR aptamer functionalized surface (117 cells per mm^2, SD: 44) and on mutant aptamer functionalized surface (13 cell per mm^2, SD:4), *P< 0.01.

3.2.4 Isolation of Cancer Cells from Cell Mixture

A cell mixture was used to study the cancer cell isolation efficiency from cell mixture and to study different cells respective behaviors on anti-EGFR aptamer functionalized surface. A mixture of hGBM and fibroblast cells was prepared in a ratio of 1:1, the average cell density on the surface after seeding was 303 cells per mm^2 (SD: 12). The substrates were incubated with cell mixture, washed and the results were imaged. In control group, only hGBM cells were incubated with anti-EGFR aptamer functionalized substrates. Both DIC and fluorescent images were taken (Figure 3.5A and 3.5B). Due to incomplete transfection, the *m-cherry* fluorescence expression in hGBM cells is not uniform. There were about 17% cells that did not show any fluorescence (189 out of 1133 cells from 12 substrates, Average: 16, SD: 5). In the mixture

group, about 28% cells (378 out of 1376 cells from 12 substrates, Average: 32, SD: 7) did not show fluorescence. The cells that did not give fluorescence signal included captured hGBM cells and non-specifically bound fibroblast. The difference of the two percentages, as a first order approximation, shows that on average about 10.8% captured cells was fibroblasts. Thus the anti-EGFR aptamer substrates can selectively isolate and enrich a 1:1 mixture suspension ratio of fibroblasts to cancer cells, to 1:8 on the surface. In EGFR antibody substrates control group, the ratio of captured fibroblasts to cancer cells was 1:3. The specificity of aptamer and antibody on cancer cell isolation was thus 95% and 69% respectively (Table 3.2). The results show anti-EGFR aptamer has higher specificity in cell enrichment. In practical application, in order to increase the isolation efficiency, a sample can be run for multiple times over the substrates. It may be important to note here that "mean capture yield" using Anti-EpCAM antibodies has been shown to be ~65% (*71*).

Table 3.2 Comparison between capture efficiency of anti-EGFR aptamer and EGFR Antibody

	EGFR antibody		Anti-EGFR aptamer	
	hGBM cells	Fibroblasts	hGBM cells	Fibroblasts
Captuerd	188	68	84	10
Uncaptured	30	150	134	208

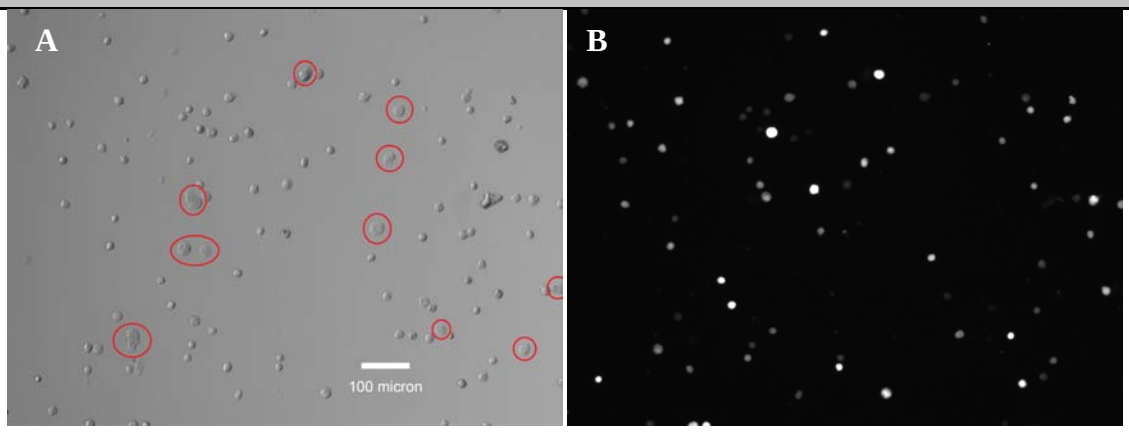

Figure 3.5 The hGBM cells and fibroblasts on the anti-EGFR aptamer functionalized surface. The circles in A indicate a few fibroblasts that were captured and cannot be seen in B.

3.2.5 Shape and Size of Cancer Cells on Functionalized Substrates

The cell shapes and sizes showed a distinct behavior: fibroblast altered their fusiform, stellar or irregular shape to spherical. Mouse derived tumor cells change from spherical in suspension to semi-elliptical and flat on the aptamer functionalized surfaces (Figure 3.6). The EGFR overexpressing tumor cells were re-shaping to cover as large of an area as possible. Figures 3.6A and 3.6C were taken at the beginning when mouse derived tumor cells were seeded on the anti-EGFR and mutant aptamer surfaces, and Figures 3.6B and 3.6D were taken at 30 minutes. Changes in cells shapes and flatness are evident in going from Figure 3.6A to 3.6B only. Many pseudopodia formed during the incubation period on anti-EGFR aptamer substrates. In contrast, going from figure 3.6C to 3.6D, the cells had almost no change in their shape during the 30 minutes. The behaviors of cancer cells on anti-EGFR aptamer functionalized surfaces can be used as an additional method to support histological findings and further identify tumor cells based on their physical behaviors. The findings are especially important given that enrichment of rare CTCs may be difficult for virtually any lab-on-chip device. The use of aptamers leads both to high passivation and the presentation of unique physical morphologies, and thus may be a novel first level detection step in point-of-care examination of CTCs.

3.3 Conclusion

It has been demonstrated that anti-EGFR aptamer functionalized substrates can specifically recognize, capture and isolate EGFR overexpressing cancer cells including human and murine GBM cells. It also specifically isolated hGBM cells from a mixture of fibroblasts. The isolation efficiency depended on strong binding between aptamer and the amount of EGFR expression on the cell membrane. The change in cell shape and cellular activity can serve as a novel way of identifying tumor cells. The substrates can also be used for identification and isolation of CTCs from peripheral blood, dramatically changing intervention and prognosis of metastasis.

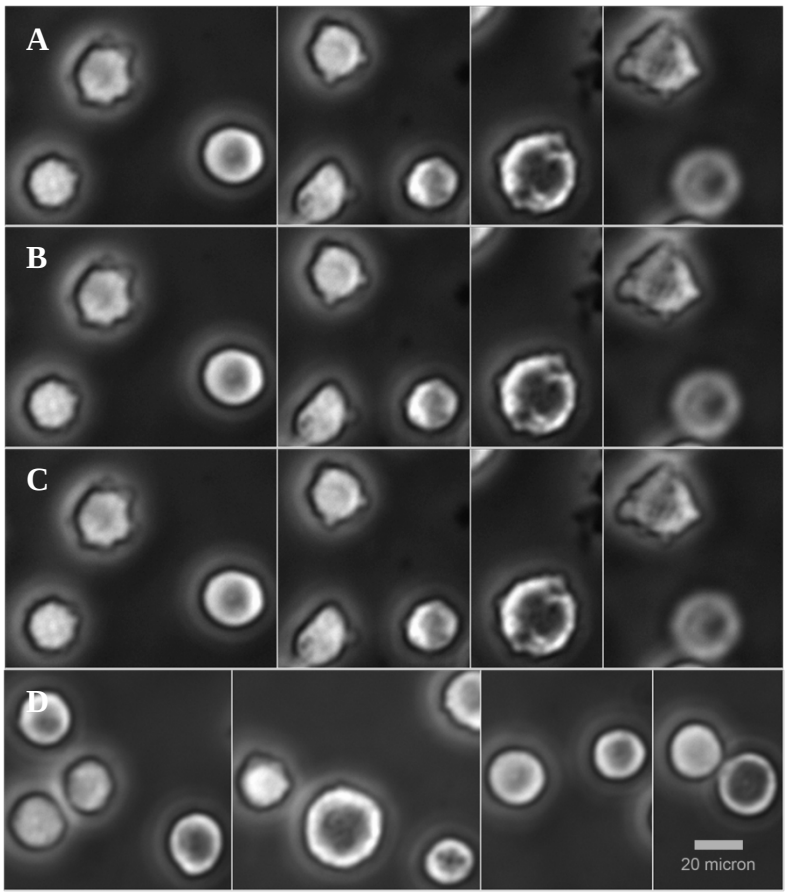

Figure 3.6 The changes in shapes of mouse-derive tumor cells. A and C, taken 3 min after cell seeding on anti-EGFR and mutant aptamer substrates. B and D, taken 30 min later on anti-EGFR and mutant aptamer substrates. A and B, changes of cell shapes on the anti-EGFR aptamer functionalized surface. C and D, no changes in cell shapes on mutant aptamer functionalized surface.

CHAPTER 4

NANOTEXTURED SUBSTRATES WITH IMMOBILIZED APTAMERS FOR CANCER CELL ISOLATION AND CYTOLOGY

Anti-EGFR aptamer can specifically recognize, capture and isolate EGFR overexpressing hGBM cells from a mixture of fibroblasts (*149*). Although the isolation specificity can reach 95%, its isolation sensitivity is poor. Higher isolation specificity can facilitate subsequent molecular analysis; however, blind emphasis on specificity usually results in false negative in cancer cell detection and isolation. Especially in the cancer early stage the number of cancer cells is rare, which might be missed easily. False negative results may disturb diagnosis and further delay the therapy. In this situation, higher isolation specificity is not a priority work anymore. In other words, the specificity optimization work can get ahead only after collecting enough cancer cells.

Basement membrane can anchor cancer cell to its loose, underlying connective tissue through cell adhesion molecules before cancer cell breaking through it and entering into the blood vessel (*150*). Its natural nanostructured characteristics therefore can improve cancer cell adhesion and local growth. Cancer cells attach on basement membrane for normal proliferation till they completely destroy the structure with various metalloproteinases (*21, 151-153*). On the other hand, in tissue engineering, researchers have tried to mimic the nanoscale topography of native tissues to increase cell proliferation on scaffolds (*154, 155*). The advantages of 3D scaffold include: (i) it provides larger surface area for cell attachment; (ii) it facilitate nutriment-waste exchange; (iii) it offers similar environment for cell proliferation, and so on (*156*). The results show that nanostructured scaffold can specifically and significantly improve the densities of certain cells.

Here, 3D nanotextured PDMS substrates were prepared and functionalized with anti-EGFR aptamers for cell isolation. It not only provides native structure for cancer cell attachment but also offers more available aptamers for cell binding. The data presented here provide a solid proof that nanotextured substrates can significantly improve cancer cell isolation sensitivity without a significant decrease in specificity. The findings may be helpful in PDMS-based cell culture and in developing novel cytologic tools for CTCs detection.

4.1 Materials and Methods

4.1.1 Aptamer Preparation

details can be found in chapter 3.1.1.

4.1.2 Preparation of Nanotextured PDMS Substrates

Half a gram of poly (D, L-lactide-co-glycolide) (PLGA) (50/50 w/w; MW: 12-16.5 × 10^3; Polysciences, Inc., Warrington, PA) was dissolved in 8 mL chloroform at 55°C for 40 minutes (*122, 157*). The solution was cast into a glass petri dish, and the dish was placed in a vacuum chamber (15 in Hg) for 2 days at room temperature till the chloroform complete evaporation. 10 N NaOH was used to etch the solid PLGA at room temperature for 1 hour to generate nanostructured surface and were further rinsed with DI water to remove residual NaOH. SYLGARD 184 silicon elastomer (Dow Corning, Midland, MI) was mixed (10:1 w/w) with a curing agent. The mixture was placed in a vacuum chamber to remove all air bubbles and then cast onto the PLGA surface. After 48 hour curing at room temperature, PDMS was peeled from the PLGA and immersed in DI water at 37 °C overnight to remove any residual PLGA. As mentioned before, organic solvents can cause PDMS bulk to dissolve and swell, and the solubility parameter of PDMS is 7.3 $cal^{1/2}cm^{-3/2}$. Theoretically, solvent which has similar solubility parameters can cause PDMS to swell more (*122*). Therefore, normal used solvents such as methanol or acetone which solubility parameters are 12.7 and 9.9 $cal^{1/2}cm^{-3/2}$ respectively may not good for the following chemical modification on PDMS surface. Methanol and acetonitrile (14.5 and 11.9 $cal^{1/2}cm^{-3/2}$ respectively) which have less swelling ratios (1.02 and 1.01

respectively) were used for aptamer immobilization on PDMS surface. Furthermore, although methanol and acetonitrile can dissolve PDMS, it requires extremely long time to dissolve it completely. Thus, the swelling and dissolving of PDMS in processes of silanization and isothiocyanate molecule incubations were insignificant.

4.1.3 Scanning Electron and Atomic Force Microscopy Characterization

SEM was used to qualitatively evaluate PDMS surface topography. PDMS samples were sputter-coated with 50nm gold layer at room temperature. Surface topography was further evaluated quantitatively by using AFM. The changes in surface area and root mean square surface roughness were measured. Height images of PDMS samples were captured in the ambient air at a tapping frequency of 300 kHz. The analyzed field measured 3 × 3μm at a scan rate of 1 Hz with 256 scanning lines.

4.1.4 Attachment of Anti-EGFR Aptamer on PDMS and Glass Substrates

The method of aptamer immobilization on glass surface can be found in chapter 3.2. The 5 × 5 mm^2 PDMS substrates were cleaned with UV-ozone plasma for 30 minutes. After rinsing with DI water and drying in a nitrogen flow, the PDMS substrates were immersed in 2% APTES in methanol for 30 minutes at room temperature. Then the substrates were rinsed sequentially with methanol and DI water. The amino groups on PDMS were converted to the isothiocyanate groups by introducing a 0.5% (v/v) thiophosgene solution in acetonitrile for 20 minutes at 40°C. The substrates were then rinsed with DI water and dried with nitrogen flow. DNA probes were prepared at 30 μM concentration in 5 mM Tris buffer with 50 mM NaCl. A volue of 5 μL of DNA solution was placed on each substrate, and it was allowed to incubate in a humidified chamber at 37°C overnight. Each substrate was then washed with DI water to move the residual DNA. Salmon sperm DNA was used for prehybridization to reduce RNA physical adsorption. A volume of 5 μL anti-EGFR aptamer at 1 μM concentration was placed on each substrate in 1× annealing buffer. After 1 hour of hybridization at 37 °C, the substrates were rinsed with 1× annealing buffer and DI water for 5 minutes. The mutant aptamer functionalized

PDMS substrates were prepared in the same way. All substrates were place in 1× PBS with 5 mM $MgCl_2$, and were used immediately.

4.1.5 Contact Angle Measurements

Contact angles were measured on isothiocyanate groups of modified PDMS (withi/without nanotexturing), unmodified PDMS (withi/without nanotexturing), and glass (withi/without isothiocyanate group modification). A droplet of DI water was placed on the surface of the substrate at room temperature, and after 30 seconds the contact angle was measured using a contact angle goniometer. On average, 5 measurements were calculated for each run.

4.1.6 Fluorescence Measurements of Fluorescamine

The density of surface grafted amine groups from APTES was measured by fluorogenic derivatization reaction with fluorescamine which can react with amine groups and give fluorescence signal (*158-160*). A mixture of 900 µL of 0.1% (w/v) fluorescamine dissolved in acetone, 150 µL of 0.1 M borate buffer, and 1.91 ml DI water was made. After APTES modification, glass, PDMS, and nanotextured PDMS samples were immersed into the fluorescamine mixture solution for minutes at room temperature. All samples were rinsed with acetone to remove the excessive reagents. The fluorescence measurements were taken at 390 nm wavelength. The fluorescence intensities were analyzed with *ImageJ* software.

4.1.7 Human Glioblastoma and Meninge Derived Primary Fibroblast Cell Culture

The respective culture methods of two types of cells follow the formal protocol.

4.1.8 Tumor Cell Capture on Substrates

The methods also follow the formal protocol described in Chapter 3.

4.2 Results and Discussion

4.2.1 Surface Topography of Nanotextured Substrates

After NaOH etching, the average surface roughness of PLGA was quantitatively analyzed with AFM (Figure 4.1 A and 4.1B). The surface roughness increased from 22 nm on

untreated PLGA to 310 nm on nanotextured PLGA. The photomicrographs of PDMS cast on nanotextured PLGA substrate are shown in Figure 4.1 C and 4.1D. Before and after chemical modification, the roughness of nanotextured PDMS are 347 nm and 289 nm respectively.

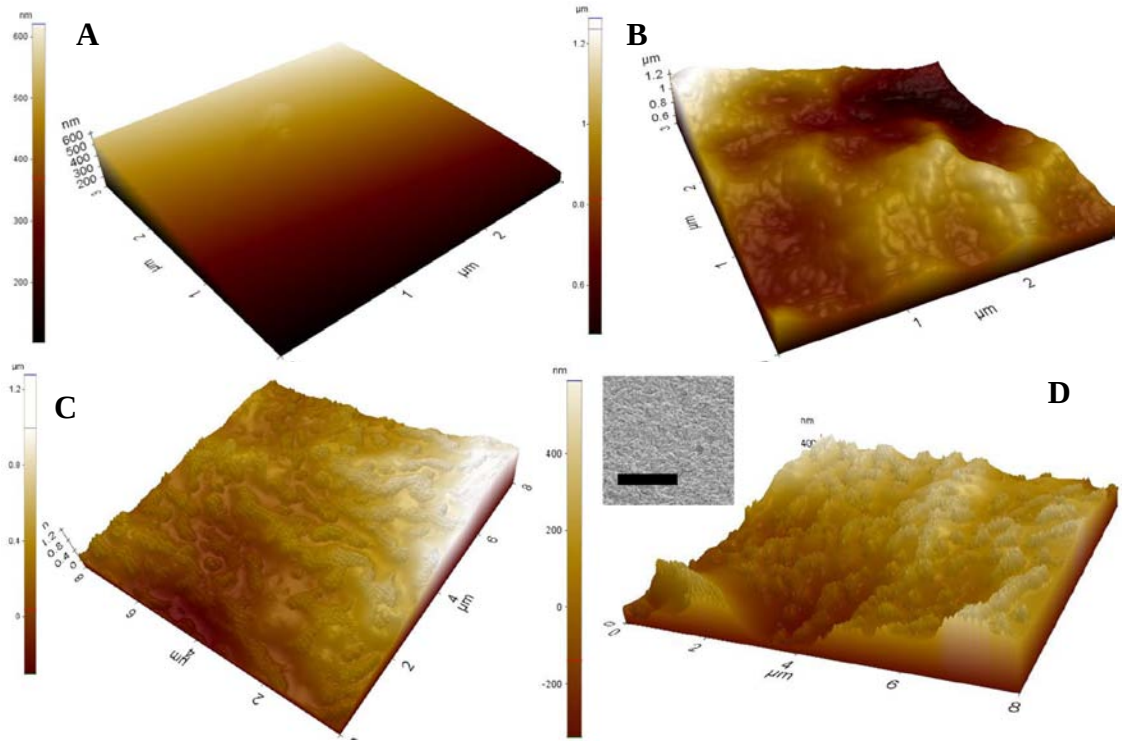

Figure 4.1 Images of the surface roughness of PLGA and PDMS cast on NaOH etched PLGA. AFM photomicrographs show (A) untreated PLGA, (B) PLGA after 10 N NaOH etching, (C) nanotexured PDMS, and (D) nanotextured PDMS surface after chemical modification. The inset in D shows a SEM image of nanotextured PDMS surface. Scale bar = 100 µm in inset.

Table 4.1 Contact angels measurement after chemical modification for each of the substrates.

	Contact Angle ± SD, Degrees	
Substrate Type	Base Substrate	After PDITC Treatment
Glass	46±1	51±1
PDMS	115±2	59±2
Nanotextured PDMS	144±4	46±3

4.2.2 Contact Angle Measurement

It normally used to analyze the hydrophobicity of a surface (*161*). The contact angles of each substrate was measured, and the average contact angle (n=10) and standard deviation were recorded. The results are listed in Table 4.1. PDMS is hydrophobic material. It has methyl groups on both sides of the backbone. Therefore the average contact angle on smooth PDMS surface is around 115°. As mentioned before, the roughness of a surface can significantly affect the contact angle (*162*). Due to the increased surface roughness, the nanotextured PDMS substrate had the largest contact angle which reaches 144° (*163*). Because the etching of NaOH created an anisotropic surface on PLGA, which, in turn, produced the same effect on PDMS when it was cast on PLGA, the strong anisotropy of the nanotextured PDMS surface caused larger standard deviation of contact angle on nanotextured PDMS if comparing it with the other two groups (*164, 165*). After APTES and isothiocyanate modification, all three types of substrates had hydrophilic surfaces. The change on glass surface in not obvious; the contact angle slightly increased from 46° to 51°. However, on nanotextured PDMS substrate the contact angle decreased to the lowest number from 144° to 46°. The contact angle of smooth PDMS only decreased from 115° to 59°. This phenomenon also attribute to its surface topography. In other works, after chemical modification, nanotextured PDMS is more hydrophilic than smooth PDMS. On the other hand, the change of contact angle of nanotextured PDMS also confirms that there are nanoscaled structures existing on its surface. The aptamer immobilization would further decrease the contact angle and make these substrates more hydrophilic. The hydrophilic surface can prevent protein and cell physical adsorption, which is good to cancer cell isolation specificity. It is noted that PDMS should be treated with UV-ozone plasma in order to replace methyl groups with hydroxyl ones before further chemical modification (*166, 167*). However, the residual methyl groups in PDMS can move towards to the surface; moreover, the hydroxyl groups would gradually change back to methyl groups in short period. Both of them not only contribute to the hydrophobicity of PDMS but also may disturb APTES modification. Thus, it was

important to perform the subsequent chemical treatment relatively quickly after UV-ozone treatment. In addition, the long UV-ozone treatment (> 90 minutes) can make the PDMS stiffer and can create lots of tiny cracks on the surface (*168-170*). Therefore, in these experiments, all PDMS surfaces were treated with UV-ozone for just 30 minuts to minimize such textural aberrations.

4.2.3 Fluorescence Measurements

Proper oxidization of the PDMS surface can significantly increase the number of hydroxyl groups which can further increase the number of available amine groups from APTES, and finally can improve the total number of immobilized aptamers. The relative number of amine groups can be determined by comparing the relative fluorescence intensities given from fluorescamine which only transmit into fluorescent derivatives by reacting with amine groups. The more amount of available amine groups on the surface, the stronger the fluorescent signals. The average fluorescence intensities of three types of samples are provided in Table 4.2. Nanotextured PDMS had the highest intensity (83.9 ± 14.1 arbitrary units). First, the nanotextured surface owns larger effective surface area; and two methyl groups on one Si can be replaced with hydroxyl groups. Consequently, comparing with the number of hydroxyl groups on plain PDMS or glass surface, a significantly higher number of hydroxyl groups can be generated on nanotextured PDMS surface. Thus, more amino groups can be introduced on the surface after silanization, and the density of amine groups can reach 4×10^{-8} mol/cm^2 (*171*). The other advantage of nanotextured PDMS is that it can reduce the steric effect on planar surface. The distance can be reduced between the immobilized ends of the DNA probes due to the free ends having more room on a curvaceous surface, and thus it requires a smaller footprint for the same radius of gyration. Thus, the probe density would be far greater on curvaceous surface. In sum, a reduced distance between adjacent probes and a larger effective area provide very high aptamer packing density on nanotextured PDMS surface. Higher density of aptamer itself can increase the binding chance between anti-EGFR aptamer and EGFR

expressed on cancer cell membrane.

Table 4.2 Fluorescence intensity data for glass, PDMS and nanotextured PDMS after APTES and fluorescamine modification

Substrate Type	Fluorescence Intensity: Mean ± SD, AU
Glass	4.7 ± 1.5
PDMS	52.7 ± 6.3
Nanotextured PDMS	83.9 ± 14.1

4.2.4 Isolation of hGBM Cells

The average density of cells on glass, PDMS, and nanotextured PDMS after seeding was 400 ± 43 per mm^2. After washing, fluorescent images of cells on 10 substrates of each type were taken. The quantitative analysis results are provided in Table 4.3; the captured cell images are shown in Figure 4.2 A to 4.2 F; and the average cell density on each type of substrate is illustrated in Figure 4.2G From the results, it is easy to find that anti-EGFR aptamer functionalized nanotextured PDMS can enrich the highest number of hGBM cells on the surface, and the amount of cell is almost twice as many as cell number on anti-EGFR aptamer functionalized glass surface. There are four major factors influenced the cell capture: (i) the available number of anti-EGFR aptamer molecules on the substrate, (ii) the EGFR density on the cell membrane, (iii) the affinity between EGFR and the anti-EGFR aptamer, and (iv) the surface quality of the substrate. To one cell, factor (ii) and (iii) are fixed. We deduce that the available number of aptamer molecules is a direct function. Cell isolation efficacy can be improved by increasing the affinity between surface bound aptamer and the EGFR on cell membrane. The more aptamers on the surface, the more chance the EGFR binding to them, and therefore the higher affinity forming. Fluorescamine analysis demonstrated that the nanotextured PDMS could provide more hydroxyl groups after oxidization for further APTES modification, and ultimately resulting in increased numbers of available anti-EGFR aptamer molecules. Additionally, the nanotextured surface mimicked the native structure of basement

membrane, further facilitating cell attachment. Therefore the number of captured cell on the nanotextured PDMS surface was higher than the numbers in the other two groups. A flat PDMS surface also can be immobilized more aptamers. However, the reform of silicon-oxygen-silicon bonds pulls the hydrophobic methyl groups to the surface; and cell-adhesive layer is not easy to form. These two factors prohibit the formation of a stable cell adhesive layer. Therefore, cancer cells can be easily removed from the surface in washing procedure. These two factors also exist in nanotextured PDMS substrate; however, the nanotexturing itself provides a tradeoff by improving cell attachment. On the other hand, nonspecific cancer cell adhesion on nanotextured surface also increases. In mutant aptamer groups, the number of cells on nanotextured PDMS was almost 12 times higher than the cell number on glass. Obviously, the higher physical absorption decreases isolation specificity because nanotextured PDMS can not only provide more sits for protein adsorption but also offer more focal contact adhesion sites, which are normally used by cells to attach to the surface. Thereby, in practical application, the selection of materials and surface topography depends on the competing goals of isolation sensitivity and specificity. Figure 4.3 reveals the captured cell shape on PDMS, nanotextured PDMS, and glass surface. After 30 minutes incubation, hGBM cells formed pseudopods and become flatter, indicating that cells could firmly attach to nanotextured PDMS surface. In contrast, this phenomenon was not observed on PDMS surface. On PDMS surface, cell has a globular shape from strong repulsion. Although cell on glass surface could form pseudopods and had semielliptical shape, whole cell did not spread as well as they did on nanotextured PDMS surface. The results indicate different topography of substrates can result in differential cell spreading and much more distinct behavior. It also may serve as a novel and important cytologic behavior that help distinguish between cancer cells and other normal cells.

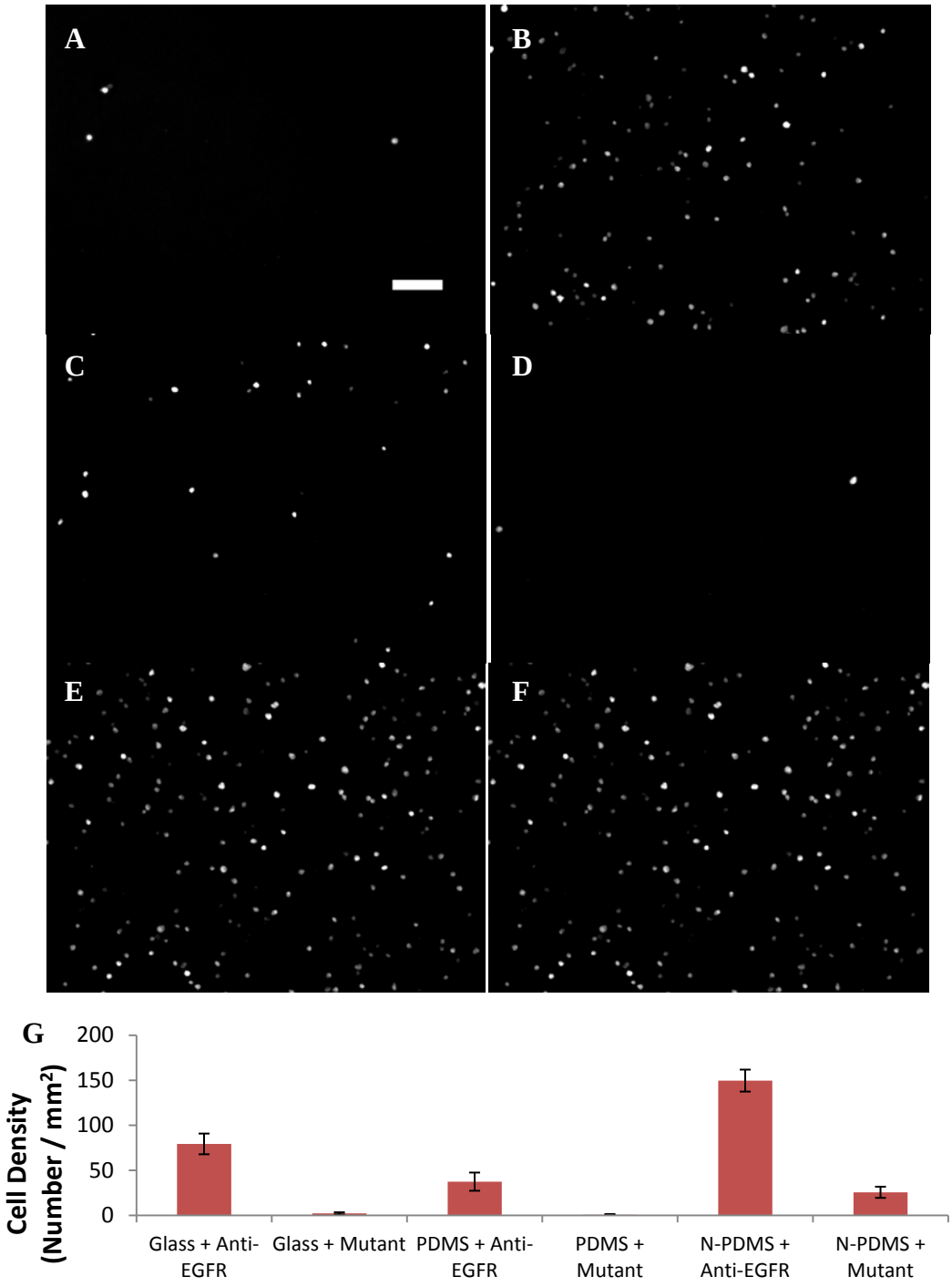

Figure 4.2 Cells captured on anti-EGFR functionalized (A) glass, (C) PDMS, and (E) nanotextured PDMS surface; Cells captured on mutant aptamer functionalized (B) glass, (D) PDMS, and (F) nanotextured PDMS surface. (G), showing the average cell density on each type of substrate. Scale bar =100 µm.

Table 4.3 The actual numbers of cancer cells captured on anti-EGFR or mutant aptamer functionalized glass, PDMS, and nanotextured PDMS surface.

	Anti-EGFR Aptamer (per mm^2)	Mutant Aptamer (per mm^2)
Glass	79.3 ± 11.5	2.2 ± 1.2
PDMS	37.4 ±10.1	0.6 ± 0.8
Nanotextured PDMS	149.6 ± 12.2	25.6 ± 6.2

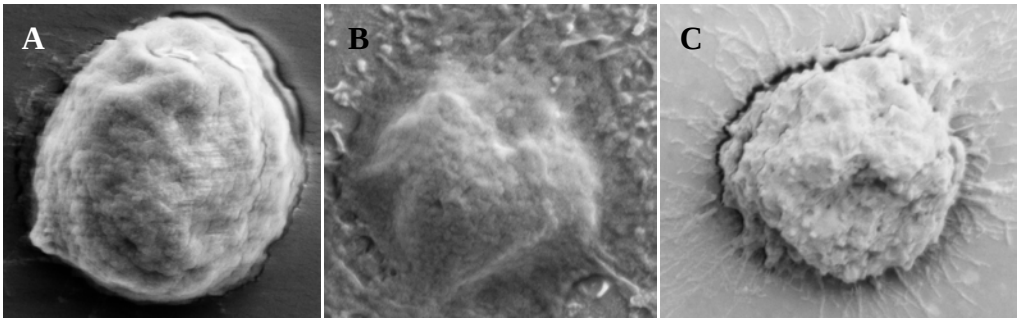

Figure 4.3 SEM photomicrographs of captured hGBM cells on (A) PDMS, (B) nanotextured PDMS, and (C) glass surface. Scale bar =1 μm.

4.2.5 Isolation of hGBM Cells from Cell Mixture

hGBM cells and fibroblast were mixed at a ratio of 1:1. The average density of plated cells on the surface was 332.3 ± 23.6 cells per mm^2. After incubation and washing, both DIC and fluorescent images were obtained. Approximately 18.4 ± 9.1 % hGBM cells from 10 substrates did not have any fluorescence due to incompletely *m-Cherry* fluorescent protein transfection. In mixture group, around 31% of cells from 10 substrates (846 of 2729 cells in the mixture groups; 58.8 ± 21.4 cells per mm^2) did not show any fluorescent signals, which includes nonfluorescent hGBM cells and nonspecifically bound fibroblast cells (2307.6 hGBM cells and 431.4 fibroblasts). Therefore, on average 15.4% of the captured cells were fibroblasts. The aptamer functionalized nanotextured PDMS was capable of selectively isolating and enrich a 1:1 mixture suspension of fibroblasts and hGBM cells to 1:5.5 on the surface. The result

indicates that the increased number of fibroblasts could be attributable to the nanotexturing and the higher number of available aptamers on the surface. Compared with 1:8 enrichment efficiency (on glass), this result indicate that nanotextured PDMS substrate still could specifically capture hGBM cells from the cell mixture. The increased sensitivity decreases its specificity, but the tradeoff is the advantage of isolating as many of the small number of cancer cells as possible.

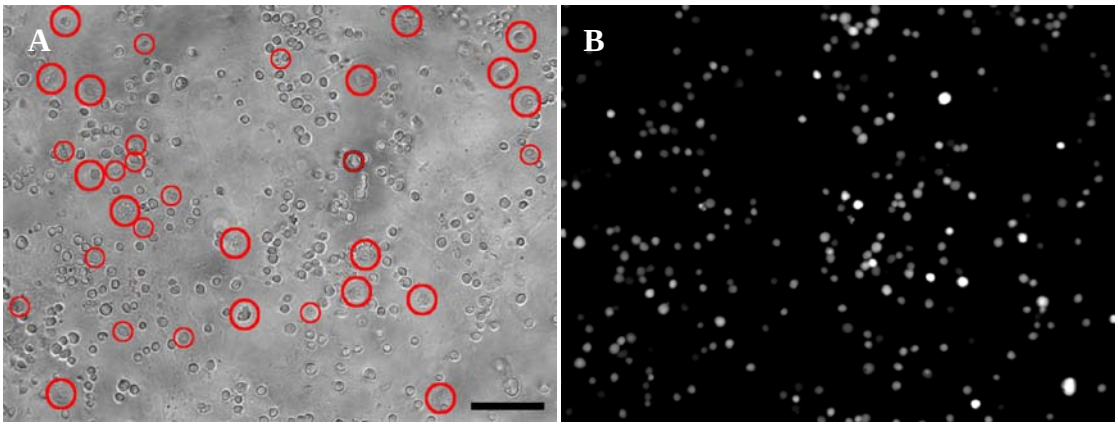

Figure 4.4 hGBM cells and fibroblasts are observed on nanotextured PDMS surface. The red circles in A indicate a few fibroblasts that were captured and cannot be seen in B. Scale bar = 100 µm.

4.3 Conclusion

This study demonstrated that anti-EGFR aptamer functionalized nanotextured PDMS substrates can capture more hGBM cells compared with traditional smooth glass substrates; moreover, the nanotextured surface which mimic the basement membrane can significantly improve cancer cells isolation sensitivity without a significant decrease in specificity. This can have important implications for PDMS-based cancer cell culture and isolation.

CHAPTER 5

VELOCITY EFFECT ON APTAMER-BASED CIRCULATING TUMOR CELL ISOLATION IN MICROFLUIDIC DEVICE

The expression levels of EGFR in cancer cells can be over 100 times higher than those in normal cells (*172, 173*), thus it is an attractive target for cancer therapy . In other words, on anti-EGFR aptamer functionalized surface cancer cells have significant higher adhesive force compared with normal cells'; therefore with optimized pattern design and fluid flow parameters, CTCs can be isolated from whole blood in antibody functionalized microfluidic device (*71, 72*). Moreover, the affinity interactions based cell sorting methods can yield higher efficiency and greater specificity (*77*). As we mentioned in Chapter 3 and 4, hGBM cells can be specifically enriched from a mixture of hGBM and fibroblast cells. However, the selection of washing speed for eluting normal cells and non-specifically bound tumor cells is subjective. In former works, washing speed was roughly optimized by experimental experience. Because the adhesive force of cancer cells is significantly different from normal cells', certain shear stress which falls in between two different adhesive forces can be used to separate cancer cells from the cell mixture. If the sizes of normal cells are relatively homogeneous, there can be a specific washing speed to elute most of them. However, it is known that the WBCs have various sizes, with diameters ranging between 8 – 20 μm (*174*). The variations in size indirectly result in the differential adhesive force. In other words, without reasonable washing speed large number of WBCs can still remain on the surface and may further disturb the tumor cell isolation and subsequent analysis. On the contrary, if cancer cells could be enriched with a suitable flow rate, the ratio of cancer cells during capture process can be significantly increased. Although the

eluting speeds can be calculated based on the established models, the value might not adapt to the dimensions of microfluidic devices (*175-177*). Therefore it is necessary to investigate the flow velocity effect on selective capture efficiency between cancer and normal cells in microfluidic devices. Here, we first use a model to roughly estimate the adhesion probabilities of hGBM cells and WBCs, and then use a straight channel with 25 μm height to optimize the cell suspension flow rate. The results show that 1.5 – 2 mm/s might be optimum flow rate that could be used for separating hGBM cell from WBCs.

5.1 Materials and Methods

5.1.1 Computational Model of Cell Capture

Numerical simulations have been used to study the binding probabilities of nanoparticles and cells (*177-179*). The magnitude of the cell adhesive force is the major study objective; therefore cells were treated as rigid spherical objects. The parameters used in calculation are listed in Table 5.1.

Table 5.1 Parameters of cancer and normal cells used in simulation

	Diameter (μm)	Bond Length (nm)	Viscosity (pa s)	Receptor Density (#/m^2)
hGBM Cells	10	10	1e-3	1e15
WBCs	10	10	1e-3	1e14

The microchannel was designed with 25 μm height and 1 mm width, where the flow was laminar. Newtonian flow was assumed for the fluid. Derived from Navier-Stokes equations, the fully developed velocity profile is given as:

$$V_x = \frac{\Delta p h^2}{8\mu L}\left(1 - \frac{4y^2}{h^2}\right) \qquad (1)$$

Where Δp is pressure difference, h is channel height, L is channel length, μ is viscosity of the fluid. A schematic velocity profile of the microchannel and hydrodynamic force applied to cells under shear flow is shown in Figure 5.1. The cells were adhered to the bottom of the

microchannel. Hydrodynamic forces, especially the drag force $F = 6\pi al\mu SF^S$ and torque $M = 4\pi a^3 \mu ST^S$, which would rotate and dislodge the cells, are required to remove cells, where *a* is the radius of the cell, l is the separation distance to the wall, and μ is the viscosity of the fluid, S is the shear rate at the wall, F^s and T^s are shape dependent coefficients. Thus, the binding probability of the cell is given by:

$$\frac{P_a}{m_r m_l K_a^0} = A_c \exp[-\frac{\lambda}{k_B T}\frac{F_{dis}}{m_r A_c}] \qquad (2)$$

where m_r, and m_l are the receptor and ligand density respectively; K_a^0 is the association constant at zero load of the ligand-receptor pair; A_c is contact area; λ is the characteristic length of the ligand-receptor bonds; k_B is the Boltzmann constant; F_{dis} is dislodging force acting per unit ligand-receptor pair; and *T* is the temperature.

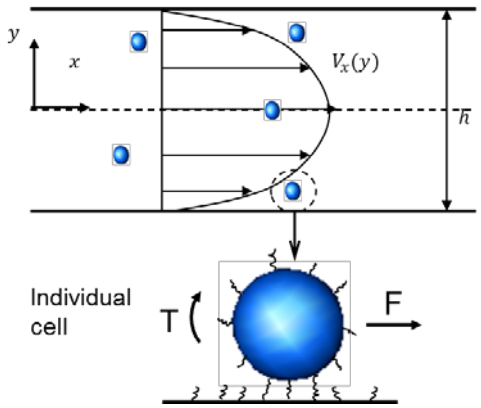

Figure 5.1 Schematic illustration of rectangular flow velocity profile and hydrodynamic force applied to cells under shear flow.

5.1.2 Aptamer Preparation

The details can be found in chapter 3.1.1.

5.1.3 Microfluidic Channel Preparation

The channel was designed in AutoCAD. 25 μm thickness of SU8-25 photoresist was spin-coated on wafer surface. The coated substrate was pre-baked at 65 °C for 3 min, and then

soft-baked at 95 °C for 7 min. After lithography exposure, it was post bake at 65 °C for 1 min, and then soft-baked at 95 °C for 3 min. Finally the master was gently rinsed with developer and isopropanol. PDMS devices were fabricated by casting PDMS solution on the master, and curing on the hot plate at 150 °C for 5 min. Polymerized PDMS was gently peeled off the master. Sample reservoirs were prepared by punching 2 mm diameter holes with a steel rod.

5.1.4 Attachment of Anti-EGFR Aptamer on Glass Substrates

The details can be found in chapter 3.1.2.

5.1.5 Human Glioblastoma Cell Culture

The details can be found in chapter 3.1.4.

5.1.6 Bovine Mononuclear Cells Preparation

Ten milliliter of bovine whole blood was mixed with 1.25 ml OptiPrep (Axis-Shield, Norway), and 0.5 ml Tricine Buffered Saline (TBS) was carefully loaded on the top. The mixture was spun down at 2000× g for 15 min. Mononuclear cells (i.e., WBCs) were collected from the top layer and resuspended in PBS. Mononuclear cells were washed three times with PBS to completely remove blood platelets. Cells were counted and the density was recorded.

5.1.7 Cells Capture with Microfluidic Device

After measuring cell density, cell suspension was injected into the aptamer functionalized channel with different velocities: 0.5, 1, 1.5, and 2 mm/s (WBCs) and 1, 2, 4, and 6 mm/s (hGBM cells) for 10 mins, and then 1× PBS was used to wash off the nonspecifically bound cells. Images were taken with Leica DM Inverted microscope.

5.2 Results and Discussion

5.2.1 Computation Results for Cell Capture Efficiency

The average diameter of hGBM cells and lymphocytes were 12.2 μm (S.D.: 2.3) and 7.5 μm (S.D.: 0.6), respectively. From equation (2), the adhesion probability at different flow rates for WBCs and hGBM cells is plotted in Figure 5.2. The simulation results provide a guide for the choice of proper flow rate for the experiment setup. The adhesion probability of both WBCs and

hGBM cells decreases as the flow rate increases. When the flow rate is 1 mm/s, 68% of the hGBM cells are adhered to the surface compared to less than 2% of the WBCs.

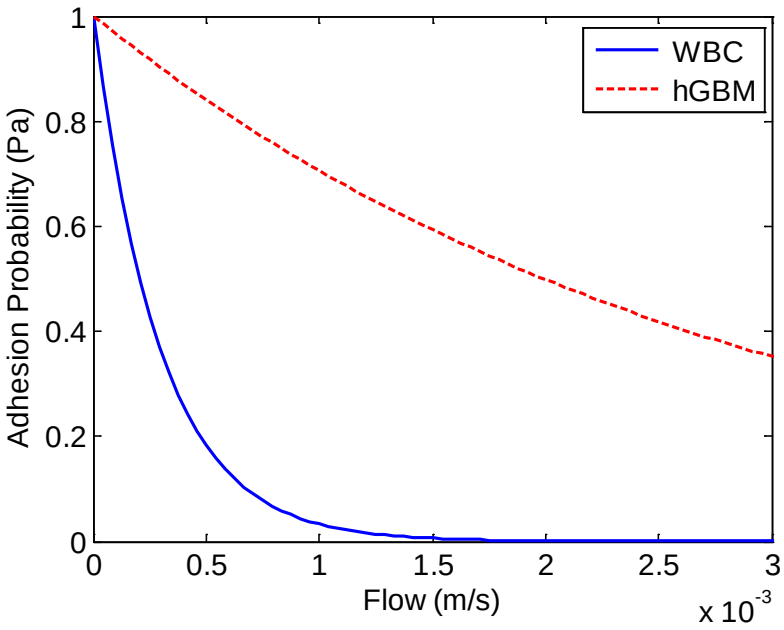

Figure 5.2 Adhesion probability of 7.5 µm diameter WBCs (blue solid line) and 12.2 µm diameter hGBM cells (red dashed line) on the anti-EGFR aptamer functionalized surface at different flow rates.

5.2.2 Experimental Velocity Effect on Cell Capture

As we mentioned before, the concentration of immobilized aptamers can affect the cell isolation efficacy (*84, 180*). More cells can be enriched on the surface if higher concentration of aptamers were used during immobilization; and the best molecule density is around 10^{12} molecules/cm^2 (*181, 182*). This density can offer better presentation of the aptamer to hGBM cells or WBCs. On the other hand, EGFR density on hGBM cell membrane is around 1 receptor per 100 nm^2. The number of aptamers in the same area on the substrate is around 20 – 25. Although the receptor and aptamer has one-to-one binding, more aptamers undoubtedly can increase the odds of binding. In other words, with an optimal density of surface-bound aptamers, it is only the EGFR density on cell surface that is the most important factor. The capture percentage was defined as the ratio of the number of captured cells to the total number

of cell flowing through the whole channel. Bovine mononuclear cells were studied first. The capture percentages at 0.5, 1, 1.5, and 2 mm/s flow rate were 53.6% (S.D.: 10.1%), 15.4% (S.D.: 6.5%), 1.4% (S.D.: 1.8%) and 0.6 (S.D.: 1.1%) respectively (Figure 5.3). Although the capture efficiency at 0.5 mm/s was much higher than the predicted value (approximately 35%), the overall decreasing trend of the adhesion probability with increased flow velocity agrees qualitatively well with the measured data. The difference in adhesion probability values between theory and experiments might due to the ideal setup used in the model, which assumed a uniform channel height, smooth surface, rigid cell, specific ligand-receptor binding, non-collision between cells, etc. Based on Bell's model, the single aptamer-EGFR binding force is around 8×10^{-6} dynes, and if the mononuclear cells firmly attach to the surface the total binding force is around 0.06 dynes. The force is calculated by multiplying the contact area, the receptor density and the single aptamer-EGFR binding force, assuming the cell radius to be 5 μm and maximum contact area of πr^2. If accelerated flow was not applied to elute attached cells, the washing speed could be calculated by Stokes' Law, and it should reach 17 m/s to wash off the attached cells. However, from our observations, captured mononuclear cell can be eluted at 10 cm/s. Due to the less EGFR density and cell properties, mononuclear cells cannot become flat to bind firmly and completely to the aptamer functionalized surface (*149*). Compared to the heights of captured hGBM cells which are less than 6 μm (measured with Zeiss LSM510 confocal microscope), the heights of attached mononuclear cells do not decrease significantly. The other reason might be some receptors may not bind with aptamers correctly or not bind at all. The situation also exists in hGBM cells (discussed later).

The capture percentage of hGBM cells at 1, 2, 4 and 6 mm/s were 70.4% (S.D.: 15.7%, Relative S.D.: 22.3%), 48.5% (S.D.: 12.9%, Relative S.D.: 26.7%), 28.3% (S.D.: 9.4%, Relative S.D.: 33%) and 15.4% (S.D.: 4.8%, Relative S.D.: 31.4%) respectively. In this case the capture efficiency was less than the predicted one at each velocity. The probable reason is that not all EGFRs bind to aptamers. However, if we examine the maximal values of capture percentage, it

seems those values were close to the predicted ones. The adhesion probability is the probability of the cells keeping adhered without being washed away at a given shear rate. In this simulation, the margination process before binding is not considered. However, in the experiment, the cells do marginate toward the bottom of the microchannel. The percentage of the cells attached at the surface is the total number of adhered cells divided by total cells flushed in the test, which leads to a large deviation. For higher flow rate, the number of cells attached on the surface decreases significantly, which leads to a smaller deviation. The total binding force is around 0.63 dynes if hGBM cells completely and firmly attach to the aptamer functionalized surface. The higher binding force indicates the hGBM cells can more firmly attach to the surface, and the decreased cell height further helps them from being washed off under high flow velocity. In our experiments, we find the hGBM cell density at the rear end to be slightly higher than that at the front part. This difference in density can be attributed to the relatively high flow rate that drove more hGBM cells to the lateral part before these came in contact with surface.

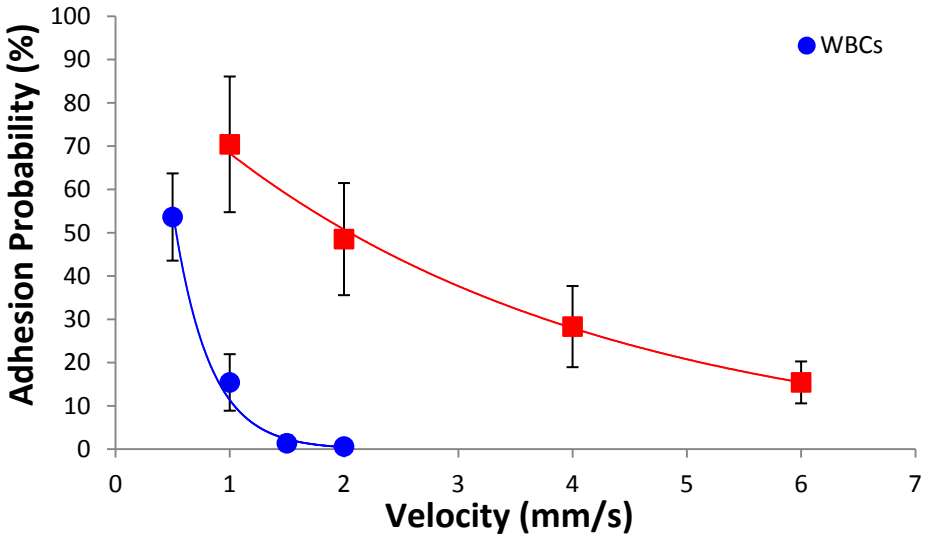

Figure 5.3 The experimental results of WBCs (dots, blue line) and hGBM cells (squares, red line) captured on anti-EGFR aptamer functionalized surface under different velocities.

Based on the above results, a 2 mm/s flow rate was investigated to effectively separate the cell mixture of hGBM cells and mononuclear cells in a ratio of 1:1. After separation and data calibration (around 11.2% hGBM cells did not show any fluorescence), the results showed surface-bound aptamers could selectively isolate and enrich a 1:1 mixture suspension ratio of mononuclear cells to hGBM cells, to 1:42.7 on the surface. The results show that the aptamer functionalized microfluidic channel can significantly improve the tumor cell isolation efficiency by optimizing flow velocity.

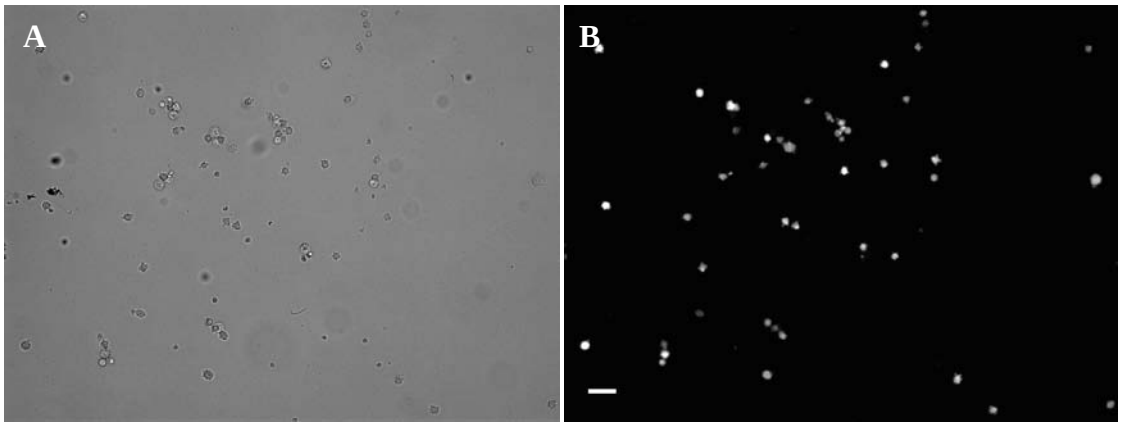

Figure 5.4 The experimental results of WBCs and hGBM cells captured on anti-EGFR aptamer functionalized surface from a 1:1 mixture. The red circles indicate a few WBCs were captured and cannot be seen in fluorescent image.

5.3 Conclusion

We found in channel with 25 μm heights, 2 mm/s flow rate could significantly facilitate cell mixture separation from 1:1 to 1:42.7. The analysis provides important insights into design of microfluidic devices that use surface-tethered probes to capture cells. This can be useful towards improving efficiency of lab on chip approaches aimed at CTC isolation from peripheral blood.

CHAPTER 6

ISOLATION OF CANCER CELLS USING APTAMER FUNCTIONALIZED GLASS BEAD ARRAY

Releasing captured tumor cells from sensor surface for subsequent molecular analysis or cell culture is an important and challenging work. In microfluidic device, cells would be eluted from the surface by reasonable flow rate. However, as we mentioned before, the washing speed should reach 17 m/s to wash off the attached cells if accelerated flow was not applied to elute attached cells. It is noted that cell structure of tumor cells is fragile. The extremely high shear stress generated from high flow rate has the potential to harm the completeness of cell structure. In addition, the spreading and flatness of captured cells on the surface require extremely high threshold of detachment force (*183-185*). Therefore, the strong adhesion forces between cells and antibody functionalized surface should be overcame first; and then under reasonable flow rate captured cells can be carefully collected. Currently, there are three major strategies can be applied in cell detachment in microfluidic devices. Proteolytic enzyme degradation method is commonly used, which directly destroy the antibody-receptor adhesion by degrading antibodies and/or cell receptors (*72*). It requires additional enzyme incubation and deactivation; moreover, it disregards the risk of receptor degradation that might affect subsequent molecular analysis. Electrochemical desorption utilizes reductive potential to disrupt the underlying thiollayer which connect antibody molecules on gold mieroelectrodes and results in release of captured cells (*186*). This technique demands either elaborate fabrication of sensors or hydrophilic hydrogel coating. In thermodynamic releasing method, a thermo-responsive copolymer which can show a transition between a cell-adhesive and a cell-repellent state at different temperature was used to push attached cell from the surface by cooling down

its critical solution temperature (*183*). This technique still needs complex sensor design, fabrication and copolymer reasonable combination. In this chapter, we are introducing a novel approach for cell isolation and collection using glass bead (GB) arrays and then simple and straight-forward detachment of cancer cells from GBs. Anti-EGFR aptamer functionalized GBs were loaded into micro-pits within a microfluidic device to form an array for capturing EGFR overexpressing tumor cells when they passed through the device. Captured cells can be easily harvested by collecting the removable GBs, and they were further released from beads surface through simple hybridization between aptamer and release oligonucleotide. This low-cost device may provide a potential platform for CTC isolation, and it can be integrated with other devices for subsequent molecular analysis.

6.1 Materials and Methods

6.1.1 Aptamer Preparation

The details can be found in chapter 3.1.1. The release RNA agent sequence is (5'-CCG UGC AUU AUA GCG GCA CAG AGA CUA AGG UCG GAG CGC CGA GGG AAG GAA GUA AG-3'). The complementary parts of release RNA agent are framed.

6.1.2 Aptamer Functionalized Glass Beads Preparation

More details can be found in chapter 3.1.2.

6.1.3 Human Glioblastoma Cells Culture

More details can be found in chapter 3.1.7.

6.1.4 Computational Analysis and Fabrication of Microfluidic Device

A Hele-Shaw microfluidic device was modeled and fabricated for cancer cell isolation (*71*). The distance between individual GBs and fluid flow behavior were simulated first. A view of the simulated microfluidic device is shown in Figure 6.1. The dimensions were chosen as 900 × 346 × 60 μm for simulation. GBs of 50 μm diameter were distributed in an array at the bottom plane of the device in an equilateral triangle fashion. To find the optimum distance between individual GBs for cell capture, the GBs center-to-center distance varies from 70 to 100 μm. The

left and right boundaries of the domain were assumed to have an inlet velocity to satisfy a whole device flow rate of 1 ml/h and an open boundary, respectively. The boundaries at two sides were assumed to be symmetrical, thus the modeled domain represented a portion of the actual device. The top and bottom surface walls were modeled as non-slip boundaries. A total of around 20,000 polygons were used in the finite element mesh.

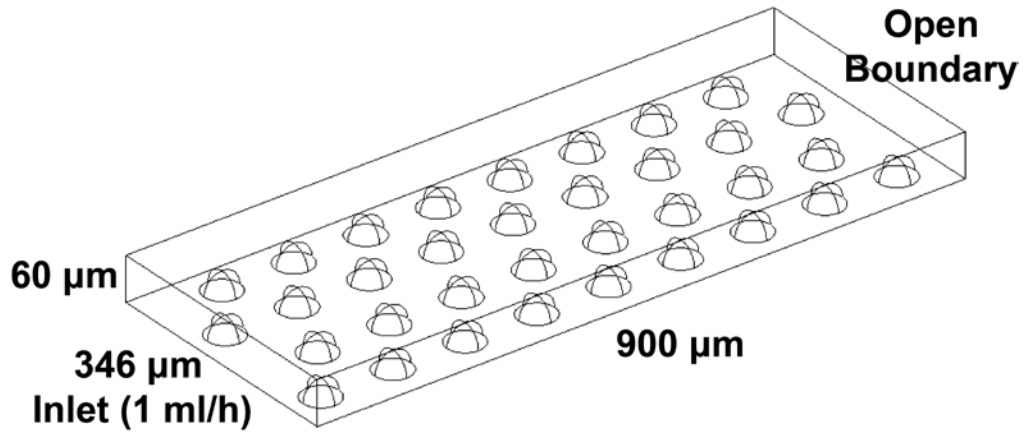

Figure 6.1. The numerical model of a GB array channel with dimensions. The GB loaded channel is used to analyze velocity pattern, shear stress, stream lines, trajectory and cell adhesion probability. The flow rate is set to 1 ml/h at the inlet and the other side is open boundary.

The microfluidic device was fabricated using soft lithography (*187*). In short, SU8 photoresist was used to generate desired pattern as a master mold (Figure 6.2). More details of photolithography and soft photolithography procedures can be found in chapter 5.2. Two types of devices were fabricated. One was just a flow through channel with 60 µm height, used to estimate and measure competition between forces of shear-stress and binding between EGFR and anti-EGFR aptamer. The other device was Hele-Shaw structure with pit array. The pits were filled with aptamer functionalized GBs.

6.1.5 Shear-stress Studies

Shear stress in Hele-Shaw device can be calculated using the equation derived by Usami *et al (188)*. PDMS chamber of 60 µm height was used for flow experiments. The PDMS chamber was treated with plasma and then immediately bonded to anti-EGFR or mutant

aptamer functionalized glass surface. The hGBM cells were injected at 30 × 10^4 cells per ml density into the device with a syringe pump at 1 ml/h for 30 min, and then PBS was used to elute nonspecifically bound cells at the same flow rate for 10 min. Pictures were taken, and captured cells were manually counted at selected points along the flow axis.

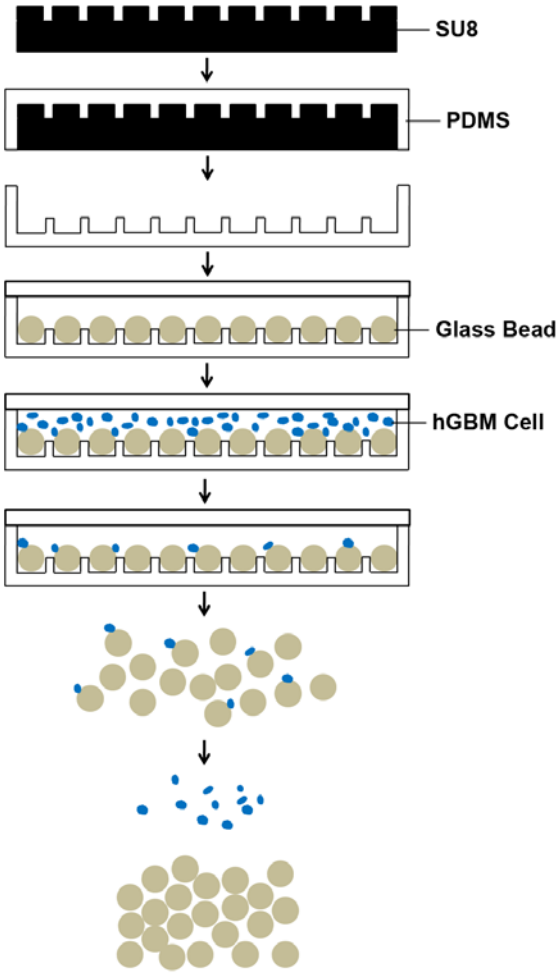

Figure 6.2 Schematics showing steps of fabrication and experiments. GBs are loaded into pits. Cancer cells are captured by aptamer functionalized GBs, and are finally released from the GB surface after GBs are collected from the device.

6.1.6 Glass Bead Aarry Hele-Shaw Device and Cell Capture

The fabrication and experiment flow chart is shown in Figure 6.2. The PDMS chamber was treated with oxygen plasma which made the PDMS surface hydrophilic. Anti-EGFR

aptamer functionalized GBs were suspended in pure ethanol, and then were added into the chamber. GBs automatically fell into pits with proper shaking. Flat PDMS cover was bonded to Hele-Shaw device at last. PBS was used to perfuse the whole chamber to completely remove ethanol. A 100 cells per ml spiked hGBM cell suspension was flown through the GB array at flow rate of 1 ml/h for 1 h, and then PBS was used to elute nonspecifically bound cells at same flow rate for 10 min. Captured cells were counted.

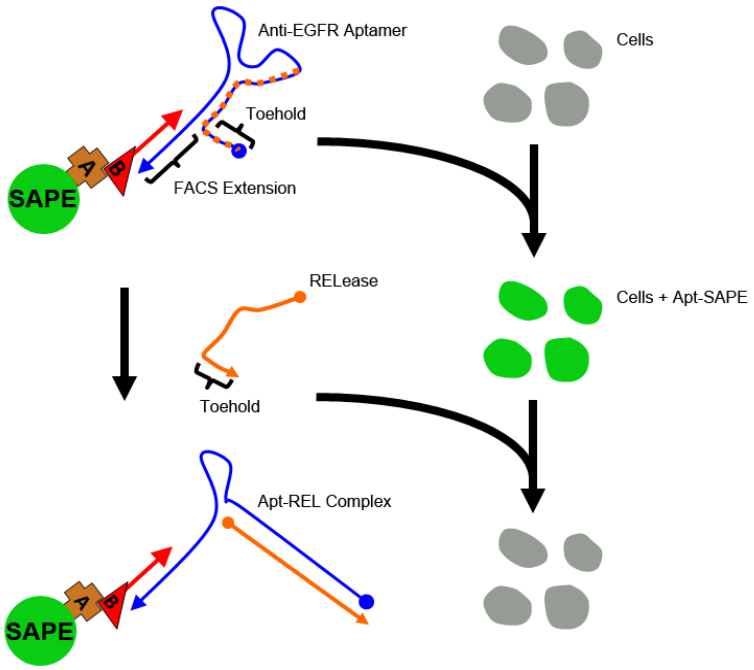

Figure 6.3 Schematics showing steps of anti-EGFR aptamer binding and release from cell surface. Fluorescence labeled anti-EGFR aptamer and A431 cells are incubated first. After washing, cells carry fluorescence due to anti-EGFR aptamer specific binding. When release RNA agent is added it competitively hybridizes with anti-EGFR aptamer, opens up its hairpin structure and anti-EGFR aptamers can be released from cell surface.

6.1.7 Flow Cytometry of Aptamer and Release RNA Agent

Anti-EGFR aptamer was annealed with biotin modified capture probe DNA in BND buffer (10 mM $MgCl_2$ in PBS) for 4 min at 80 °C then cooled to 4 °C at a slow ramp of 0.1 °C per second. This aptamer-DNA-biotin construct was then incubated for 10 min with streptavidin-phycoerythrin (SAPE, Invitrogen). A431 cells were harvested with trypsin. The cells were washed, resuspended in PBS and incubated at 4 °C for 30 min with the aptamer-DNA-biotin-

SAPE construct (Figure 6.3). Controls included A431 cells only; the DNA-biotin-SAPE construc only (no aptamer); A431 cells incubated with mutant aptamer-DNA-biotin-SAPE. The two cell samples incubated with aptamers were washed to remove free aptamer then treated with 2 equivalents of the release RNA molecules and allowed to incubate for 30 min at 4 °C or 37 °C respectively. All samples were then washed of any free aptamer, suspended in PBS and analyzed on a FACSCalibur flow cytometer (BD Biosciences).

6.1.8 hGBM Cell Capture and Detachment from Glass Beads

Anti-EGFR aptamer functionalized GBs were divided into two groups (15 mg each). hGBM cells were harvested with trypsin-EDTA and 0.2% collagenase, resuspended in PBS, and 2 ml (24×10^4 cells per ml) cell suspension were seeded on 15 mg GBs. After 30 min incubation at 37 °C, release RNA agent (which could hybridize with anti-EGFR aptamer) was added into the first group, and the mixture was incubated for another 30 min. At the end, GBs from two groups were softly resuspended by shaking solution with 20 µl micropipette; supernatant fluid was removed after GBs' precipitation; and GBs were resuspended in PBS, The cells which remained adherent to GBs were manually counted.

6.2 Results and Discussion

6.2.1 Computational Analysis

Figure 6.4 shows the velocity field obtained from numerical simulations. Figure 6.4A shows a non-uniformly distributed fluid flow and velocity between GBs. The fluid in the device was squeezed into the gaps among GBs due to the existence of GBs. The stream lines are shown in Figure 6.4B. The flow field near the GBs ix examined in detail in Figure 6.5. In the flow direction, the streamlines were distorted due to the GBs, as shown in Figure 6.5A. Such distorted flow pattern is favorable for cell capture because the flow would move the cell around in the suspension, thus increasing the probability of contact between cells and anti-EGFR aptamers functionalized GBs. Considering the velocity pattern in the direction perpendicular to flow, as shown in Figure 6.5B, cells would move up to the top and them move down to the

bottom when encountering GBs. Such velocity pattern is expected to increase the hydrodynamic efficiency of the device in capturing cells. Figure 6.6 shows the shear stress in the flow direction. At the top of the GB, the shear stress reaches its maximum value. The larger shear stress would stretch and rotate the cells; therefore cells would roll downwards and adhere to the lower part of the GB. When the distance between individual GB decreased from 50 to 20 μm, the shear stress increased from 0.237 to 0.303 Pa. In order to quantify capture efficiency, 2000 cells with randomly distributed initial positions were simulated for injection at the inlet of microfluidic device with various GB distance configurations. The cells were subjected to both bulk fluid flow and Brownian motion. Periodic boundary conditions were applied at the inlet and outlet. Trajectories of a few cells in the device are shown in Figure 6.7A. Figure 6.7B show the binding efficiency, which is defined as the ratio of the number of cells bound with GBs over the total number of cells released, as a function of time for devices with GB separation distance from 20 to 50 μm. The binding efficiency increased very fast in the first 0.3 sec and quickly reached equilibrium. This indicated that most captured cells were located in flow streamlines adjacent to the GBs, and Brownian motion did not significantly influence cell capture. The binding efficiency also increased from 1% to 4% as the distance decreased from 50 to 20 μm. This was due to the packing of many more GBs in the device at 20 μm distance and the more available surface for contact and binding.

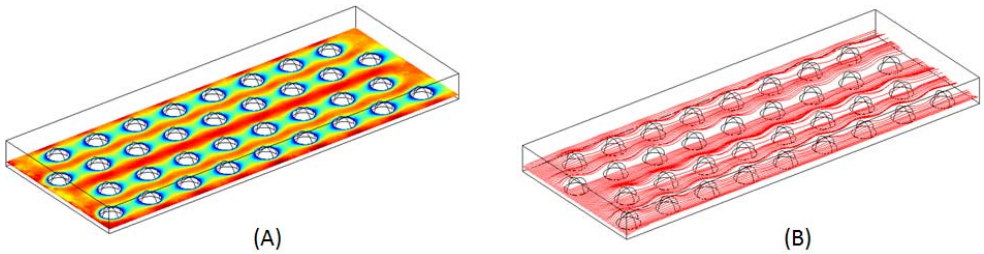

Figure 6.4 Velocity field in the device at 10μm height: A, velocity pattern; B, stream lines for the velocity field. The flwo rate is set as 1 ml/h.

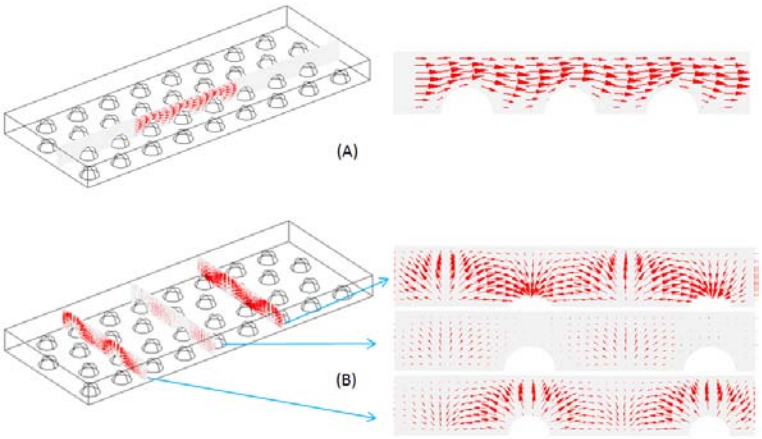

Figure 6.5 Velocity field in the device: A, velocity pattern along the inlet flow; B, velocity pattern perpendicular to the flow, the positions of the three slices are 15 µm before the central plane of beads, the central plane, and 15 µm after the central plane of beads, respectively.

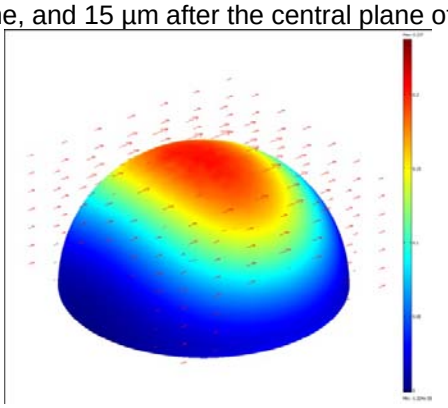

Figure 6.6 Shear stress on the surface of a glass bead. The maximum shear stress appears on the top of the bead and gradually decreases from top to bottom.

6.2.2 Shear-stress Studies Using Linear-shear Hele-Shaw Chamber

A Hele-Shaw cell capture microfluidic device was fabricated and cancer cell capture experiments were performed. The results showed the capture of cells on the surface and the density of captured cells increased as the shear stress decreased. The optimum shear stress not only significantly improved the isolation specificity but also ensured maximum cell capture. The average size of hGBM cells was 12.2 µm (S.D.: 2.3). The density of EGFR on hGBM cell membrane was around 1 EGFR per 100 nm^2 as estimated from the surface area of the cell and the total amount of EGFR. Bell's model can be used for predicting the binding force between anti-EGFR aptamer and EGFR, and the binding process can be considered to be

instantaneous. The binding force is around 8×10^{-6} dynes. EGFR density on hGBM cell is around $1 \times 10^{15}/m^2$, which can be over 100 times higher than those in normal cells (such as WBCs); therefore the total binding force for 12 µm hGBM cell and 10 µm normal cell are around 0.63 and 0.16 dynes, respectively. Such difference can be used for cancer cell isolation from the cell mixture under suitable shear stresses (*189*). Since the adhesion force of hGBM cells was thrice than that of normal cells, the nonspecific adhesion of normal cells would be minimized if the shear stress could be kept higher than 0.16 dynes. Hele-Shaw design utilizes the increasing channel width along the axis to induce linearly decreasing shear stress. Here, when the flow rate was set as 1 ml/h, at 40 mm position along the flow axis the shear stress was close to 0.2 dynes which was still higher than adhesion force of normal cell (Figure 6.8A). The isolation specificity and efficiency can be adjusted by changing the flow rate becomes higher or lower. In practical applications, it depends on the competing goals of isolation efficiency and specificity. The captured cells were manually counted every 5 mm along the flow axis from the inlet. The corresponding shear stress value and average cell densities measured on two different aptamer functionalized glass substrates are shown in Figure 6.8B. The results show that the density of cells (cells per mm^2) significantly increases when the shear stress decreases along the axis, and the maximum density is achieved at 40 mm position. Mean values of cell numbers at each point and corresponding standard deviation are shown in Table 6.1.

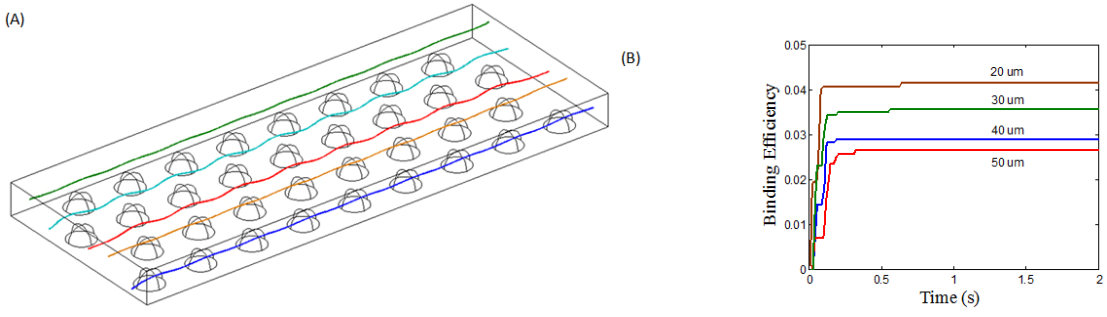

Figure 6.7 A, typical trajectories of cells injected in the device; B, binding efficiency of cells as a function of time for devices with different separation distance. The binding efficiency increased from 1% to 4% when the distance between adjacent GBs decreased from 50 to 20 µm.

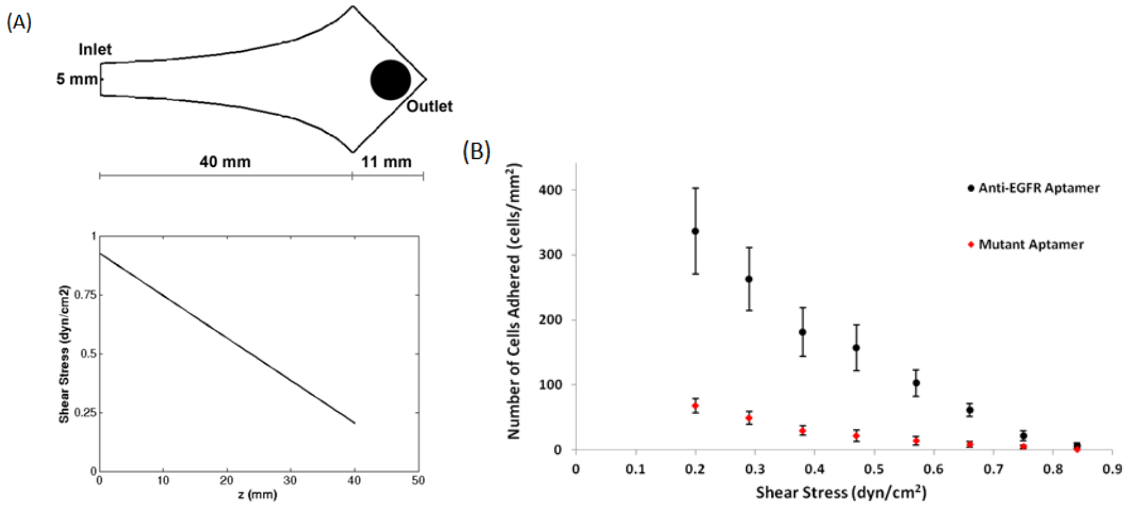

Figure 6.8 A 60 µm thick SU-8 photoresist is used to create the Hele-Shaw device. A shows Hele-Shaw device structure and dimensions; shear stress plot shows gradual decrease along the flow axis. B shows number of cells binding to two different aptamer functionalized glass substrate at increased shear stresses.

6.2.3 Cell Capture with Glass Bead Array

Hele-Shaw device with 25 µm depth pits were fabricated using PDMS molding (Figure 6.9). The diameter of pits were set to be 50 µm for loading GBs, and the equilateral triangle pattern with 20 µm spacing were suggested by simulation results. From the cross-section micrographs, the wall of each pit was vertical, and the depth and diameter conformed to the original design. The aptamer functionalized GBs carried overall negative charges, and they show hydrophilic properties. The repulsion between GBs ensured that these stayed stable and did not form clumps in solution; otherwise strong aggregation could have happened in buffer solution. On the other hand, the methyl groups on PDMS surface make the polymer hydrophobic; as a result when a water droplet is placed on the PDMS surface, it tends to minimize its surface to achieve a spherical shape due to high surface tension (*190*). In this study, the loading efficiency was very low if hydrophilic aptamer functionalized GBs were prepared in PBS. Most of GBs remained in PBS instead of falling into the pits, or these were easily removed from the pits just with gentle shaking. In general, the structure of the surface and the surface tension of the droplet decided the wetting degree of the surface when the liquid

came in contact with surface (*191*). A solution that provides low surface tension as well as kept DNA/aptamer hybridized was preferred. Pure ethanol, which meet both requirements, was thus adopted (*192*). PDMS device was also treated with oxygen plasma to make its surface hydrophilic. The Hele-Shaw device contained an array of 250, 000 pits within 516 mm^2 surface, and 40 mg GBs were prepared to fill up the pits. The GBs were added into the device, and a flat PDMS cover was bonded to the device after steady shaking. The loading efficiency (the ratio of the number of loaded pits to the whole number of pits on the surface) was 98% (S.D.: 0.2). Excessive ethanol was completely removed by PBS rinsing; which also removed unloaded GBs. To determine the cell isolation efficiency, 100 hGBM cells, suspended in PBS, were injected, and the capture efficiency was seen to be 44.3% (S.D.: 2.5). Figure 6.10A shows two hGBM cells captured at the 40 mm position along the axis. PDMS is higher surface energy and hydrophilic surface on PDMS is achieved by oxygen plasma, which facilitates cell attachment (*193*). However, PDMS gradually becomes hydrophobic again; therefore cells rarely adhere to bare PDMA surface. No cells were captured at the top of GBs due to higher shear stress (3.03 dynes per cm^2). The shear stress was much lower at the bottom of GBs, thus it ledto higher chance of cell adhesion. Cell morphology on GBs was significantly different from what it looked like on flat glass surface or nano-textured PDMS surface (*147, 180*). Cells did not change from spherical shape (in suspension) to flat on the aptamer grafted GB surface, but kept semielliptical shapes. Cells are known to resist higher shear stress when flattened. However, the height of cell did not decrease too much on GBs surface due to curved surface, and this might have been one cause for relatively lower capture efficiency. The GBs with captured cells were easily removed from the microfluidic device by simply placing the device upside down. Figure 6.10B shows the collected GBs which carried captured hGBM cells. Thermodynamic releasing, proteolytic enzyme degradation, and electrochemical desorption methods have been used for cell detachment. However, during the eluting or proteolytic enzyme treatment procedure these methods have the potential to harm to the cell integrity. These can also affect

the separation culture o the captured cells, especially the proteolytic enzyme method which can totally digest the receptors on cell membrane. To remove the captured cells from GBs we used an antisense release molecule.

Table 6.1 Mean values ± standard deviation of captured cell number at specific distances from inlet on anti-EGFR and mutant aptamer functionalized substrates.

		Distance from the inlet (mm)							
		5	10	15	20	25	30	35	40
Average number of cells captured for two types of substrates plus S.D.	Anti-EGFR aptamer	6.3 ± 4.1	21.9 ± 7.5	61.2 ± 10.1	102.7 ± 20.3	156.9 ± 35.2	181.3 ± 37.4	262.5 ± 48.6	336.2 ± 66.1
	Mutant Aptamer	0.6 ± 0.8	4.7 ± 2.4	8.5 ± 3.9	14.4 ± 6.6	21.5 ± 8.8	29.7 ± 7.4	49 ± 9.9	67.4 ± 11

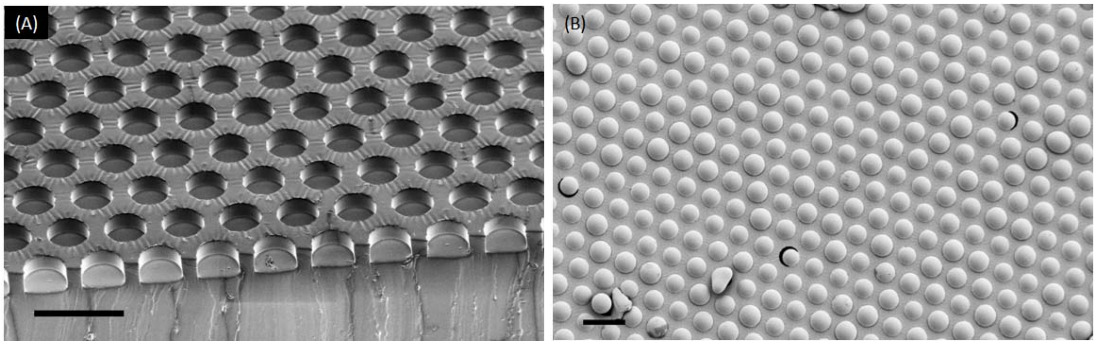

Figure 6.9 SEM micrographs of Hele-Shaw microfluidic device with pits and loaded glass beads. A shows the equilateral triangle array of pits; B shows the loaded beads (diameter: 45 – 53 µm). The scale bars are 100 µm in both micrographs.

6.2.4 Cell Detachment by Release Oligonucleotide

The cell attachment on GB surface was not as stable as it was on flat glass surface or nano-textured PDMS surface. These cells could be eluted from GB surface by resuspending GBs. During the soft resuspending process, the collision between GBs and the higher shear stress removed cells, and cells could be harvested from the supernatant when GBs settled to

the bottom of tube by gravity. However, the releasing efficiency was not satisfactory. On the other hand, vigorous shaking could hurt cell completeness. To retrieve all the cells that were bound to GBs and retrieve these without damaging them, a release RNA molecule was used. The release RNA competitively hybridized with cell-bound anti-EGFR aptamer to release cells from GB surface. The release RNA (REL) and the anti-EGFR aptamer were analyzed using native polyacrylamide gel electrophoresis (PAGE) first, and the results showed that the REL associated with aptamer (Figure 6.11A). Note mobility shift of the anti-EGFR apamter + FACS + REL to a higher weight relative to anti-EGFR aptamer without the REL. Our initial results (data not shown) indicated that complementary DNA was not able to release the aptamer from the cells. I could be that DNA-RNA interactions are insufficiently strong to denature the RNA-RNA interactions. Comparing the results of the anti-EGFR aptamer with control RNA (anti-EGFR aptamer + RNA) to that of anti-EGFR aptamer with REL (anti-EGFR aptamer + REL) we saw a 76% reduction in the median fluorescence (Figure 6.11B). Mutant aptamer (Mutant Apt) or the FACS extension DNA-alone produced fluorescence levels just slightly above background. The fluorescence for complex of anti-EGFR aptamer and REL was slightly above this nonspecific binding level. This did not seem to be due to internalization of the aptamer which could render it resistant to REL. The experiment was also performed with cell incubation done at 4 °C (which should have inhibited internalization) but the results were the same (data not shown).

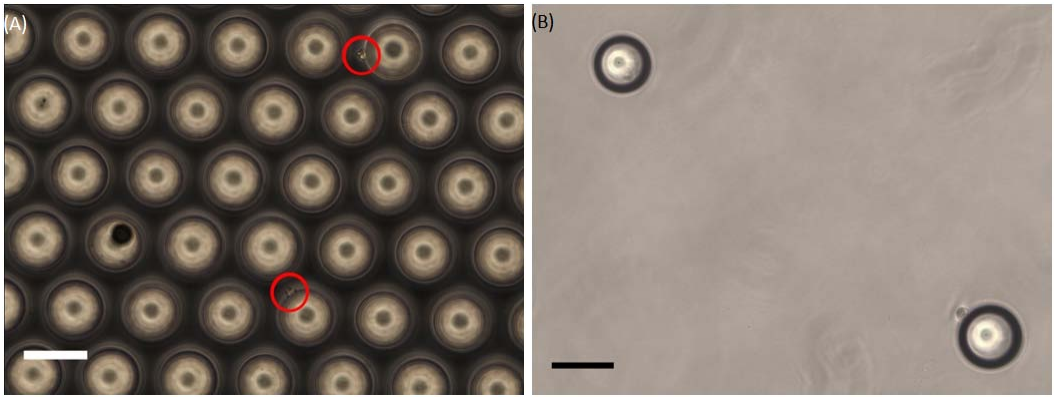

Figure 6.10 hGBM cells captured using GB array. A shows captured cells in red circles; B shows released glass beads with hGBM cells. Flow rate of cell suspension was set as 1 ml/h.

There were on average 73 cells (S.D.:11) adhered to 100 GBs after incubation. In control group which was not further incubated with REL, there were on average 23 cells (S.D.: 6) still attached on 100 GBs after soft resuspending. In other words, sofr suspending could remove around 69% captured cell from GBs surface. However, the GBs which were further treated with REL, only 6 cells (S.D.: 3) could remain on 100 GBs surface. The release efficiency was thus improved to 92%. Deu to the REL which hybridized with anti-EGFR aptamer and completely opened up its hairpin structure, anti-EGFR aptamer no longer could specifically bind to EGFR. The results from flow Cytometry revealed that 76% of anti-EGFR aptamers could be released from the surface. The rest might not have interacted with REL, or these aptamers might have entered into cytoplasma via EGFP mediated endocytosis. Overall, because of REL effect on the hairpin structure of anti-EGFR aptamer, the cell adhesion force significantly decreased. Therefore, cells could be easily detached from GBs during the resuspending process.

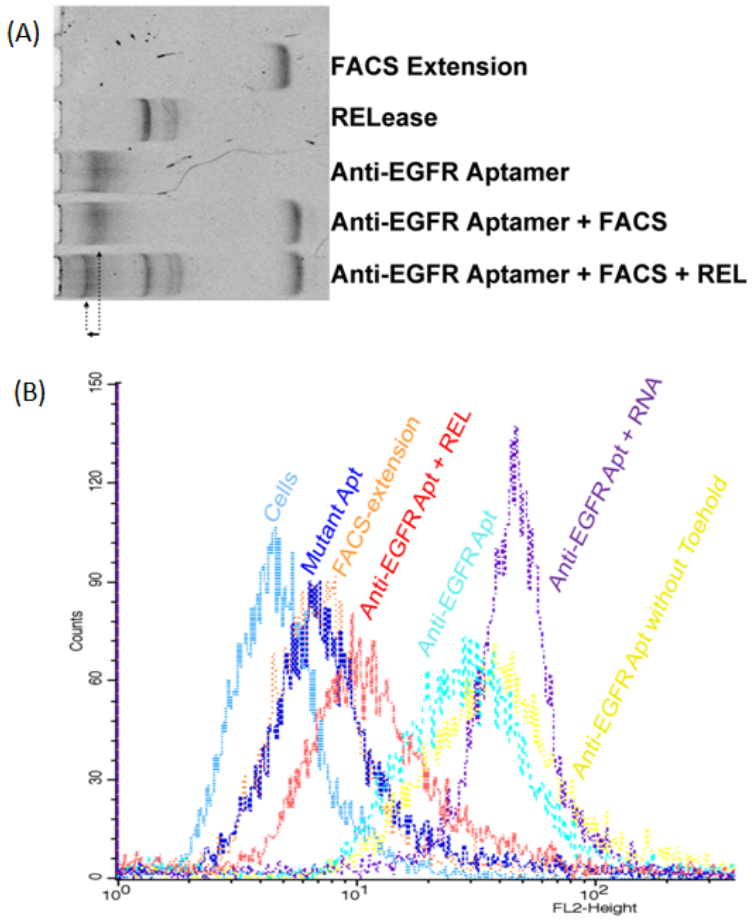

Figure 6.11 A, native PAGE for the molecule complexes showing REL lane with strong band; B, fluorescence intensity of FACS flow cytometer. REL RNA agent can significantly affects the fluorescence intensity before and after adding.

6.3 Conclusion

It has been shown that anti-EGFR aptamer grafted glass bead array can recognize and capture hGBM cells that overexpress EGFR. The device flow through velocity of 1 ml/h gives a single-pass capture efficiency that can reach 44%. The cells are detached from the glass beads for further analysis using an antisense release oligonucleotide which invades the anti-EGFR aptamer structure and decreases cell adhesion. The microfluidic device could be used for isolation of CTCs from peripheral blood and dramatically facilitate cell harvest, intervention and prognosis of metastasis.

CHAPTER 7

ANTI-EGFR APTAMERS INHIBIT HUMAN GLIOBLASTOMA CELLS PROLIFERATION AND MIGRATION

The targeted disruption of specific tumor signaling pathways is a less toxic method with higher therapeutic index in cancer treatment (*107, 194, 195*), as compared to traditional chemotherapies which may lack specificity or efficacy (*108, 196*). One example is EGFR and its downstream tyrosine kinase signaling pathway. A number of strategies have been developed for targeting the extracellular ligand-binding domain of EGFR, the intracellular tyrosine kinase domain, or the substrate-binding region in order to prevent or intercept the signaling pathway (*111*). Such inhibitors that have been applied in clinical therapy include monoclonal antibodies, enzyme inhibitors, antisense oligonucleotides and small-molecule drugs (*196*). The ideal agents should have high affinity and high specificity for their targets and favorable pharmacokinetics (*197*). However, antibodies and drugs have high levels of off-target cross-reactivity and toxic side effects that can affect their efficacy against tumors. We report inhibition of cell proliferation in biomimetic microenvironments with an anti-EGFR aptamer that can block EGF binding to A431 cells (epidermoid carcinoma cell line). Western blot analyses show that this anti-EGFR aptamer can block EGF-induced EGFR phosphorylation (*137, 198*). The anti-EGFR aptamer provides a tangible impact on hGBM cells proliferation and migration *in vitro*. We present a biomimetic cell proliferation and migration assay showing that anti-EGFR aptamer can significantly inhibit hGBM cell proliferation and suggest that it may be possible to prevent their migration *in vivo* and thereby stop metastasis. The hunt for novel therapeutics can benefit from

an assay that clearly demonstrates inhibition of cell motility in a confined, biomimetic environment.

7.1 Materials and Methods

7.1.1 Aptamer Preparation

More details can be found in chapter 3.1.1.

7.1.2 hGBM Cell Culture with EGF and/or Aptamers

The cell culture method follows the formal protocol. Cells were divided into four groups for culture with EGF and/or aptamer: with EGF, without EGF, with EGF/anti-EGFR aptamer, and with EGF/mutant aptamer. The whole culture medium was changed every 24 h (in vitro half-life of aptamer is about 5 to 15 hours). In cell migration study, cell culture followed the same protocol; except that we increased cell seeding density to 60, 000 cells per well in a 24 well plate (diameter: 8 mm).

7.1.3 BrdU Immunostaining for Examing a Cell Proliferation

We added 1 mM BrdU solution into each ml of cell culture media, and incubated with cells at 37 °C for 1 h, then culture media was removed and cells were fixed with 4% paraformaldehyde in 1 × PBS at 4 °C for 1 h (*199*). After removing paraformaldehyde, the samples were washed with 1 × PBS twice. For BrdU immunostaining, the samples were incubated with washing solution (WS, 0.5% triton in 1 × PBS) at room temperature for 30 min. The samples were then treated with ice-cold 1 N HCl for 10 min and 2 N HCl for 30 min at 37 °C respectively. After removing the acidic solution, the samples were washed with PBS three times. The samples were treated with blocking solution (4% goat serum in WS) for 1 h at room temperature. Pre-cold primary BrdU antibody (1:500 mlgG1) was incubated with samples at 4 °C overnight. The samples were washed with WS three times, and incubated with the secondary antibody (Goat anti-mlgG1 Dylight 488, Jackson Immunoresearch) at room temperature for 1 h. After removing the secondary antibody, the samples were washed with WS three times. Finally 4',6-diamidino-2-phenylindole (DAPI) was dissolved in PBS to 1 μg/ml

concentration and incubated with cells at room temperature for 20 min (*200*). Samples were washed with PBS three times and stored in fresh PBS at 4 °C for imaging. For analysis, total 200 representative images (50 pictures of each group × 4 groups) were randomly taken (no overlapping). The DAPI stained cell nuclei were counted with *ImageJ* software, and the cell densities (number of cells per mm^2) were calculated.

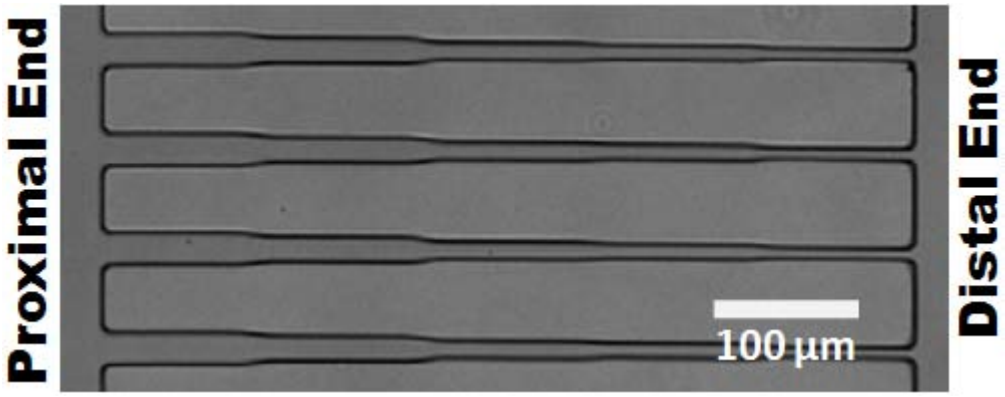

Figrue 7.1 The taper design PDMS channels; the width of channel gradually decreases from 20 to 15, 10, 8 and 5 µm from proximal end to distal end. The scale bar is 100 µm.

7.1.4 Monitoring of hGBM Cells Migration

The taper design PDMS channels (20, 15, 10, 8 and 5 µm) with 15 µm height and 580 µm length were fabricated and used for cell migration study (Figure 7.1). The PDMS devices were punched, sterilized, treated with oxygen plasma for 30 min and then attached on sterilized glass coverslips. The glass surface was coated with 10 µg/ml Laminin which would increase hGBM cell radial migration (*201*). 30, 000 live cells were seeded in proximal side reservoir and allowed to migration toward the taper-design microchannels (20 µm opening). Once hGBM cells entered into the microchannel, they vigorously migrated toward the 5 µm end, and exited to the distal side reservoir. Images were taken every 12 h for 5 days. DIC and fluorescence images were overlapped for quantification. The number of microchannels containing cells and mivrochannels where cells transited were calculated, and the transit time of cell were also measured.

7.2 Results and Discussion

7.2.1 Cell Proliferation and Division

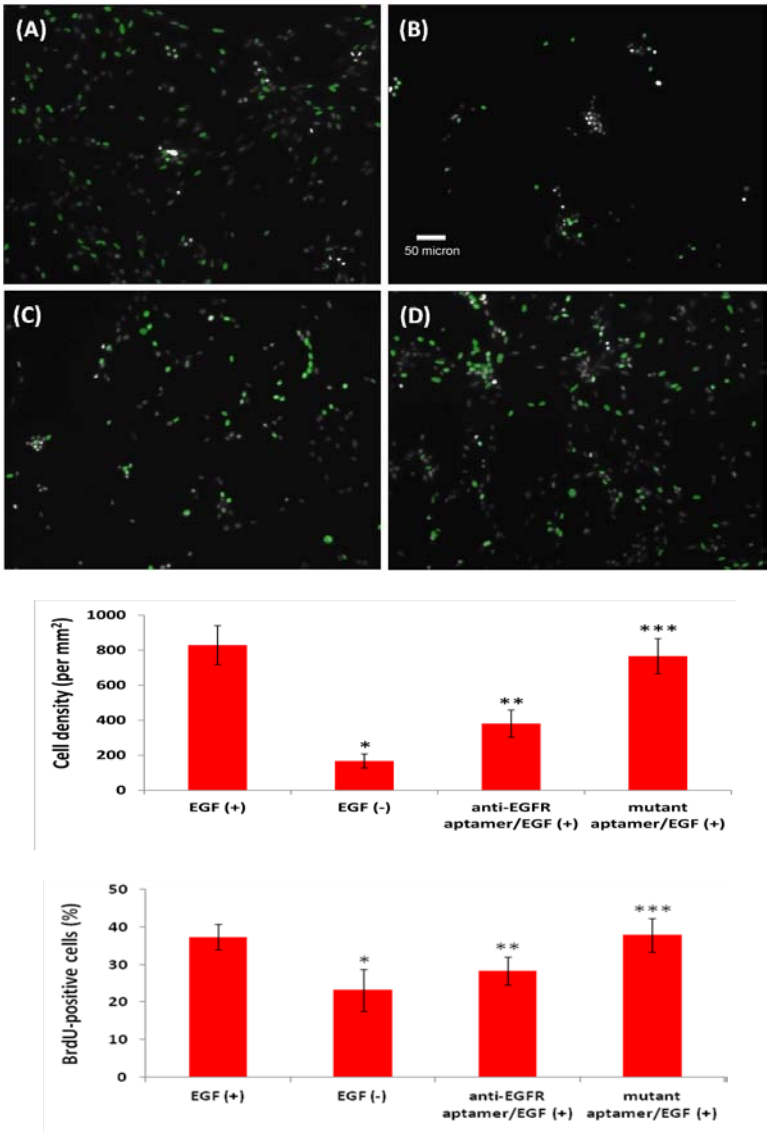

Figure 7.2 The density and division proportion of hGBM cells in each group. Cells were evenly divided into four groups, and incubated with EGF, without EGF, with EGF/anti-EGFR aptamer, and with EGF/mutant aptamer at 37 °C for 72 h. Cells were fixed and treated with BrdU and DAPI staining. (A) to (D) show DAPI stained cell nuclei and green fluorescent nuclei show dividing cells. (E) shows the average cell density (per mm^2) in respective group. * $P < 0.01$ between EGF (-) and the others; ** $P < 0.01$ between anti-EGFR aptamer/EGF(+) and the others; *** not significant between mutant aptamer/EGF(+) and EGF (+). (F) shows proportion of dividing cells: in each group respectively. * $P < 0.05$ between EGF (-) and the others; ** $P < 0.05$ between anti-EGFR aptamer/EGF(+) and the others; *** not significant between mutant aptamer/EGF(+) and EGF (+).

Cells were evenly divided into four groups, and treated with EGF, without EGF, with EGF/anti-EGFR aptamers, and with EGF/mutant aptamers at 37 °C for 72 h. After BrdU and DAPI staining, cell proliferation and division was monitored and imaged (Figure 7.2). Figure 7.2A to 7.2D show DAPI stained nuclei in each group; green fluorescent nuclei show dividing cells. The results show 828.9 (S.D: 111.3), 167.8 (S.D: 40.2), 381.2 (S.D: 77.3), and 766.3 (S.D: 100.1) hGBM cells per mm^2 in each group respectively (Figure 7.2E). Cell density of EGFR/anti-EGFR aptamer treated group was less than that of EGF or EGF/mutant aptamer treated groups, and the later two groups did not show difference in cell density. With EGF/anti-EGFR aptamer treated group as reference, T-tests were run for both EGF and EGF/mutant aptamer treated groups. The P-value was less than 0.01. The cell density of non-EGF group was the lowest. The data indicated cell division rates varied in the four groups. BrdU staining images were used to further characterize cell division status. There were 37.3% (S.D: 3.4), 23.2% (S.D: 5.5), 28.3% (S.D: 3.8), and 37.8% (S.D: 4.5) cells undergoing division in respective groups. Even if we consider varying proliferation rates for different groups, the cells in EGF/mutant aptamer treated group could keep normal division; while cells in the EGF/anti-EGFR aptamer treated group showed inhibited cell division, and the division rate was close to that of the group without EGF, but less than the other two groups ($P < 0.01$). It has been demonstrated that hGBM cell lines with medium and low levels of EGFR grow slowly with EGF. In EGF negative group, cell number was far less than the other three groups; cell division rate was also the lowest. However, when suitable concentration of EGF was present, it stimulated their growth. On the contrary cell division slowed down or ceased in serum-free conditions (*202-204*). As we mentioned before, EGF binding to EGFR can trigger a series of intracellular pathways that can stimulate cell proliferation. EGF also has an anti-apoptotic effect, and it can induce cyclin D_1 for cell cycle progression from G_1 (*205*). As expected, in EGF treated groups, cells number increased significantly during the culture period, and the division rates were higher than that for EGF negative group. Interference in EGF activity with the anti-EGFR aptamer is therefore

expected to inhibit cell growth and division. High concentration of anti-EGFR aptamer showed inhibition of autophosphorylation of EGFR. The cell density and division rate were lower than that for EGF only culture and EGF/mutant aptamer control groups. In EGF/mutant aptamer group, the mutant aptamer without the correct structure could not recognize and bind to EGFR, and the therefore it could not inhibit cell proliferation. No significant difference in cell density was found between EGF and EGF/mutant aptamer groups. It is known that hGBM cells frequently express EGFRvIII, which can phosphorylate without EGF binding. Figure 7.2B shows cells without EGF still have division activities to a certain degree. The same autophosphorylation activities also exist in other three groups. It is possible that the EGFRvIII is responsible for the remaining proliferation under no-EEGF conditions or conditions containing the anti-EGFR aptamer. If we consider 23.2% cell division rate in EGF negative group as reference, anti-EGFR aptamer inhibition effect (5.1%) is only one third of the rest of the groups (14.1% and 14.6% respectively).

7.2.2 Morphology of hGBM Cells

Cell morphology had close relationship to its proliferation and division rate. Although cells were culture on non-natural surface, the morphology of cell in different groups still shows significant difference. We show that the aptamer treated morphology closely resembles the EGF-negative control cells. This is expected as cell spreading, migration and morphology on the surface is mediated by its surrounding extracellular matrix (ECM) (*206*). It has been found that Laminin, fibronectin and type IV collagen can promote cell attachment and migration (*207*), and hGBM cell also express these ECM protein. So the content of these ECM proteins on cell surface might affect cell attachment and migration on Laminin coated surface. In EGF and EGF/mutant aptamer treated groups, cell proliferation rate was faster than the other two groups. With sufficient ECM proteins, cell could easily attach on the surface and migrate. In EGF negative and EGF/anti-EGFR aptamer treated groups, cell proliferation and division were inhibited or interfered, that resulted in a discernable change in their respective morphology. Cell

morphology images were taken after the first 12 h culture and at the end of culture (Figure 7.3). Images were taken randomly, so the images provide an unbiased survey of the population. Figure 7.3A, C, E and G show cells incubated with EGF, without EGF, with EGF/anti-EGFR aptamer, and with EGF/mutant aptamer, respectively, at 37 °C for 12 h. Figure 7.3B, D, F and H show cell morphology after 72 h culture of respective group (cells were fixed first). The substrate surface was coated with Laminin which promoted hGBM cells spreading and migration. In EGF and EGF/mutant aptamer treated groups, hGBM cells show astrocytes-like morphology with multiple long thin processes extending from the cell body. Most of cells can spread well on the Laminin coated surface (Figure 7.3A and G). On the contrary, in EGF negative and EGF/anti-EGFR aptamer treated groups, although long thin processes formed, cell spread less well on the substrate, and cell body still showed rounded shape (Figure 7.3C and E). After 72 h culture, in EGF and EGF/mutant aptamer treated groups, cell further thoroughly spread on the surface; in certain regions, few cells even overlapped each other (Figure 7.3B and H). However, in EGF negative group, cell bodies further shrank and formed hump (Figure 7.3D). Most of the cells showed bipolar morphology, while long thin processes were still observable. In EGF/anti-EGFR aptamer treated group, cell morphology was close in shape to the first two groups but their spreading was limited compared to the two groups (Figure 7.3F).

7.2.3 Cell Migration through Microchannels

Cells were seeded in the proximal side reservoir and cultured with 20 ng/ml mouse EGF until cell migrated into at least 10 channels. It took around 48 hours. Then the original culture medium containing EGF was removed, medium containing EGF, no EGF, EGF/anti-EGFR aptamer and EGF/mutant aptamer were added into respective devices. After 5-days tracking, the number of channels containing cells and the number of channels where cell passed through the distal end were counted. We found in 96.4% (54 of 56) channels containg EGF, 14.1 (9 of 64) channels containing no EGF, 35.2% (25 of 71) channels containing EGF/anti-EGFR aptamer, and 95.1% (58 of 61) channels containing EGF/mutant aptamer, cell passed through

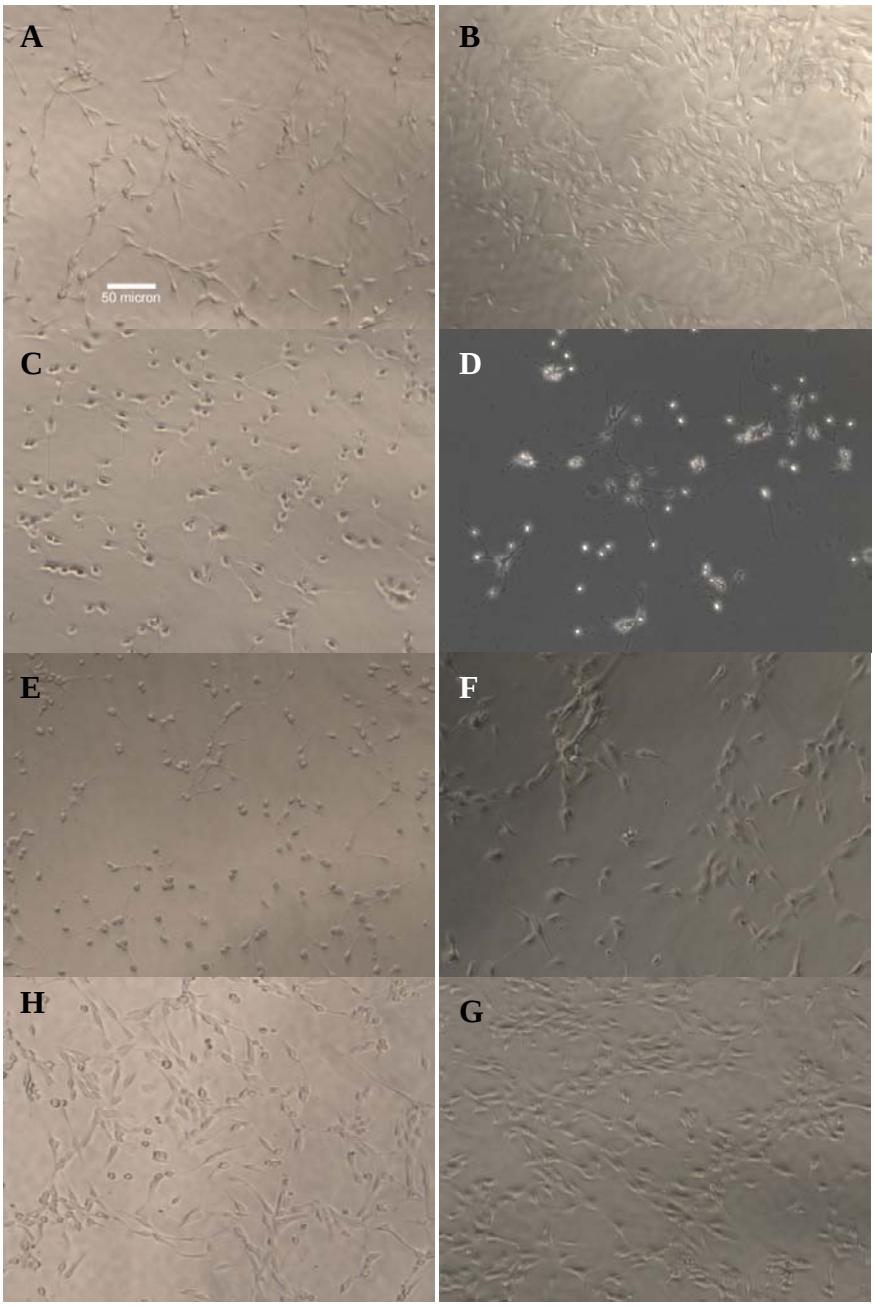

Figure 7.3 Cell morphology after different treatments. (A), (C), (E) and (G) show cells incubated with EGF, without EGF, with EGF/anti-EGFR aptamer, and with EGF/mutant aptamer for 12 h, respetively. (B), (D), (F) and (H) show cell morphology after 72 h culture of respective group.

the whole tapered channel (Figure 7.4). It is noteworthy that the number of cells in channels from different groups also varied. The channels containing EGF or EGF/mutant aptamer from proximal ends to distal ends were full of cells (average: 12.7, S.D: 2.1, and average: 12.5, S.D:

2.7, respectively) (just after only 24 to 36 hours migration), indicating vigorous proliferation and migration of cells (Figure 7.4A and D). It revealed the mutant aptamer had not significant effect on hGBM cell migration. On the contrary, in the channels containing no EGF or EGF/anti-EGFR aptamer, the number of cells was thin (average: 2.8, S.D: 1.1, and average: 4.3, S.D: 1.8, respectively) (After around 100 hours). In these two groups of channels few cells aggregated at the 20 µm wide segment, and very few cells adapted to the 5 µm channel (Figure 7.4B and C). We also found when cells arrived at 15 and 10 µm wide sections, these lacked sufficient morphological flexibility to move forward and enter into narrower 5 µm wide part. Some cells even moved back to the wider region of the channels (Figure 7.5B and C). This indicated that cells without EGF or inhibited with anti-EGFR aptamer lost their normal morphological flexibility. These two kinds of cells could easily adapt to 20 µm channel but very few cells adapted to the smaller size channel (less than 5 µm). In addition, it also took them longer to transit. On the contrary, cells treated with EGF or EGF/mutant aptamers could pass through the whole channel quickly. The channel transit time of cell in each group also affected. Here, the total time was recorded when the first cell pass through the distal end in each groups. In EGF and EGF/mutant aptamer treated groups, cell could traverse the whole channel within 24 to 36 h (Figure 7.5A and D), and 148 cells (56 channels) and 140 cells (61 channels) presented in the distal side. However, cells in distal side reservoir were composed of immigrant cells and their newly divided passage cells that were not discernable. So the exact number of cells which passed through the channel in these two groups was difficult to count. On the other hand, in no EGF and EGF/anti-EGFR aptamer treated groups, only 10 cells (64 channels) and 28 cells (71 channels) respectively passed through the channel in 95 hours or even more. Thus our results are conservative: cell migration rate might have been slower if we had treated cell with no EGF or EGF/anti-EGFR aptamer through the whole experiment. We compared the cell number in the channel, the morphological flexibility, and the transit time among each group. We found cells treated with anti-EGFR aptamer were inhibited from entering, slowed in transit and their

morphological flexibility reduced due to aptamer-mediated inhibition of cell proliferation. ECM proteins and cell adhesion molecules play a key role in cell migration. Laminin, collage type IV, integrins, etc. have been reported to stimulate hGBM cell migration. A great variety of methods aiming to inhibit cell migration on different levels have been studied (*208-212*). It is known that activation of tyrosine kinase can trigger a series of downstream pathways, including phospholipase C-γ (PLC- γ), mitogen-activated protein kinase (MAPK), and factor receptor tyrosine (FAK). These stimulate cell migration via reorganizing actin cytoskeleton, initiating the asymmetric motile phenotype and modulating integrins adhesive function (*213*). Attenuated EGFR signaling can inhibit EGF-dependent migration. The anti-EGFR aptamer inhibits EGF induced autophosphorylation, disturbs EGFR signaling pathways, and inhibits cell migration. In this work, we did not add TGF-α, platelet derived growth factor, or fibroblast growth factor to stimulate cell growth and still observed clear differences in growth and proliferation between EGF and no-EGF cases. We may thus discount the small amount of autocrine growth factors, and assume that hGBM cell proliferation and migration depends primarily on EGF in our experimental system.

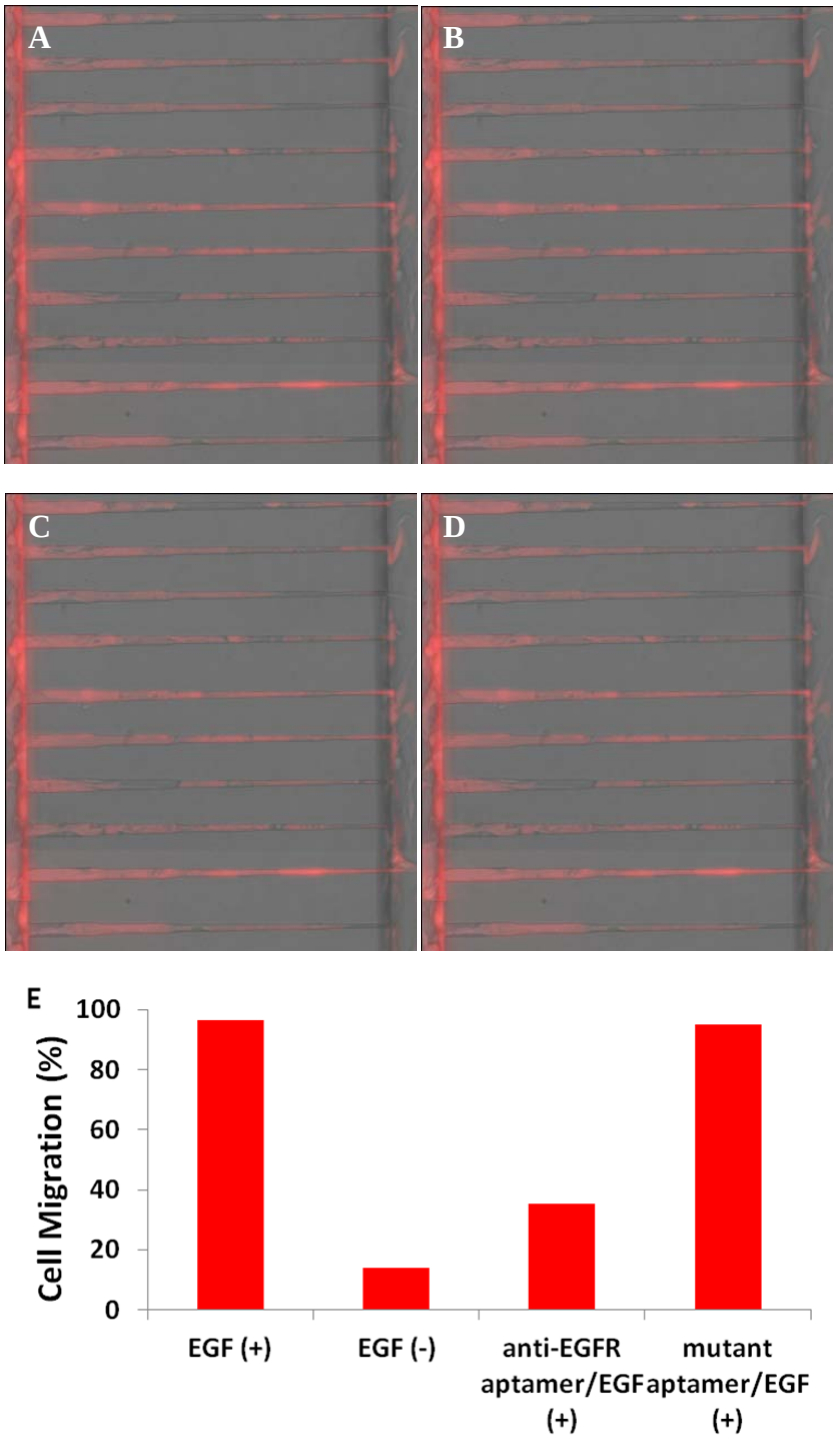

Figure 7.4. Cell migration through the microchannels. (A), (B), (C) and (D) show cell migration in the channels containing EGF, no EGF, EGF/anti-EGFR aptamer, and EGF/mutant aptamer. (E) the percentage of channels in which cells completely passed through in each group.

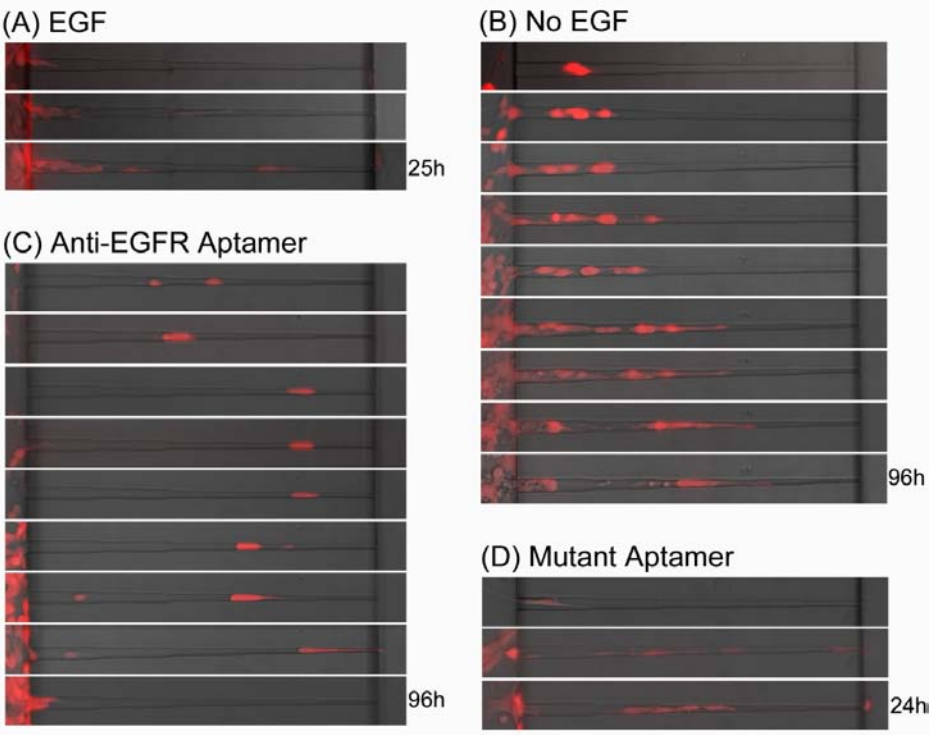

Figure 7.5. Cell migration through the microchannels. (A), (B), (C) and (D) show cells spent different times to pass through the microchannels which contained EGF, no EGF, EGF/anti-EGFR aptamer, and EGF/mutant aptamer respectively.

7.3 Conclusion

Anti-EGFR aptamers can intercept the RTK signal pathway by blocking EGF autophosphorylation effects upon binding to EGFR, and therefore inhibit hGBM cells proliferation to one third of their normal level. Meanwhile, anti-EGFR aptamer treated cells lose their normal transformation and migration ability. Compared to other groups with EGF treatment, these cells spend 2-3 times longer time to completely pass through tapered microchannels, and the low cell number in the channel further demonstrate that these lack the typical EGF induced rates of proliferation and migration. The work clearly shows that the anti-EGFR has *in vitro* inhibition effect on hGBM cell proliferation and migration. We suggest that this assay for cells' ability to invade small spaces is a direct method for probing prospective cancer therapeutics.

REFERENCES

1. M. López-Lázaro, *Mol. Med.* **16**, 144 (2010).

2. J. Yokota, *Carcinogenesis* **21**, 497 (2000).

3. C. Ellerman, O. Bang, *Bakteriol* **46**, 595 (1908).

4. K. Toyoshima, *Uirusu* **31**, 123 (1981).

5. A. Dipple, *Carcinogenesis* **16**, 437 (1995).

6. B. N. Ames, L. S. Gold, *P. Natl Acad. Sci. USA* **87**, 7772 (1990).

7. R. H. Mole, *British J. Radiol.* **48**, 157 (1975).

8. A. G. Knudson, *Nat Rev Cancer* **1**, 157 (2001).

9. I. J. Fidler, *Nat Rev Cancer* **3**, 453 (2003).

10. M. Schnabel *et al.*, *Osteoarthr. Cartilage* **10**, 62 (2002).

11. C. A. Klein, *Science* **321**, 1785 (2008).

12. P. A. Futreal *et al.*, *Nat. Rev. Cancer* **4**, 177 (2004).

13. C. A. Klein *et al.*, *Lancet* **360**, 683 (2002).

14. L. R. Bernstein, L. A. Liotta, *Curr. Opin. Oncol.* **6**, 106 (1994).

15. L. A. Liotta, *Sci. Am.* **266**, 54 (1992).

16. M. Paulsson, *Crit. Rev.Biochem. Mol. Biol.* **27**, 93 (1992).

17. R. Timpl, *Eur. J. Biochem.* **180**, 487 (1989).

18. S. A. Mousa, D. A. Cheresh, *Drug Discov. Today* **2**, 187 (1997).

19. D. Gospodarowicz *et al.*, *et al.*, *Cancer Res.* **38**, 4155 (1978).

20. C. S. Chen *et al.*, *Science* **276**, 1425 (1997).

21. A. R. Mackay *et al.*, *Cancer Res.* **50**, 5997 (1990).

22. R. G. Flemming *et al.*, *Biomater.* **20**, 573 (1999).

23. G. A. Abrams *et al.*, *Cell Tissue Res.* **299**, 39 (2000).

24. G. A. Abrams *et al.*, *IOVS* **38**, 350 (1997).

25. M. Cristofanilli *et al.*, *J. Clin. Oncol.* **23**, 1420 (2005).

26. S. Braun *et al.*, *J. Clin. Oncol.* **18**, 80 (2000).

27. M. Cristofanilli *et al.*, *New Engl. J. Med.* **351**, 781 (2004).

28. G. T. Budd *et al.*, *Clin. Cancer Res.* **12**, 6403 (2006).

29. S. Riethdorf *et al.*, *Clin. Cancer Res.* **13**, 920 (2007).

30. D. F. Hayes *et al.*, *Clin. Cancer Res.* **12**, 4218 (2006).

31. J. Tol *et al.*, *Ann. Oncol.* **21**, 1006 (2010).

32. J. den Toonder, *Lab Chip* **11**, 375 (2011).

33. D. Olmos *et al.*, *Ann. Oncol.* **20**, 27 (2009).

34. S. J. Cohen *et al.*, *J. Clin. Oncol.* **26**, 3213 (2008).

35. K. Yamaguchi *et al.*, *Ann. Surg.* **232**, 58 (2000).

36. H. Patel *et al.*, *Ann. Surg.* **235**, 226 (2002).

37. C. Alix-Panabières *et al.*, *Clin. Cancer Res.* **14**, 5013 (2008).

38. M. Ignatiadis *et al.*, *Clin. Cancer Res.* **14**, 2593 (2008).

39. T. Fehm *et al.*, *Breast Cancer Res* **11**, R59 (2009).

40. S. A. Bustin *et al.*, *Int. J. Surg. Invest.* **2**, 49 (2000).

41. A. G. J. Tibbe *et al.*, *Cytometry* **47**, 163 (2002).

42. X. C. Hu *et al.*, *Oncol.* **64**, 160 (2000).

43. A. Jemal *et al.*, *CA Cancer J Clin.* **53**, 5 (2003).

44. P. Paterlini-Brechot, N. L. Benali, *Cancer Lett.* **253**, 180 (2007).

45. Q. A. Pankhurst *et al.*,*J. Phys. D Appl. Phys.* **36**, R167 (2003).

46. R. Gertler *et al.*, *Recent Results Cancer Res.* **162**, 149 (2003).

47. V. Muller *et al.*, *Clin. Cancer Res.* **11**, 3678 (2005).

48. P. Wufing *et al.*, *Clin. Cancer Res.* **12**, 1715 (2006).

49. T. M. Morgan *et al.*, *Front Biosci* **12**, 3000 (2007).

50. A. A. H. Talasaz *et al.*, *P. Natl. Acad. Sci. USA* **106**, 3970 (2009).

51. A. M. Sieuwerts *et al.*, *J. Natl. Cancer I.* **101**, 61 (2009).

52. A. De la Taille *et al.*, *Prog. Urol.* **7**, 930 (1997).

53. G. Vona *et al.*, *Am. J. Pathol.* **156**, 57 (2000).

54. H. Mohamed *et al.*, *J. Chromatogr. A* **1216**, 8289 (2009).

55. S. J. Tan *et al.*, *Biomed. Microdevices* **11**, 883 (2009).

56. S. Zheng *et al.*, *J. Chromatogr. A* **1162**, 154 (2007).

57. K. Pachmann *et al.*, *Clin. Chem. Lab. Med.* **43**, 617 (2005).

58. W. He *et al.*, *P. Natl. Acad. Sci. USA* **104**, 11760 (2007).

59. E. I. Galanzha *et al.*, *Nat. Nanotechnol.* **4**, 855 (2009).

60. E. I. Galanzha *et al.*, *Cancer Res.* **69**, 7926 (2009).

61. R. M. Weight *et al.*, EMBC **3**, 106 (2009).

62. D. Marrinucci *et al.*, *Hum. Pathol.* **38**, 514 (2007).

63. R. T. Krivacic *et al.*, *P. Natl. Acad. Sci. USA* **101**, 10501 (2004).

64. M. P. MacDonald *et al.*, *J. Biol. Reg. Homeos. Ag.* **18**, 200 (2004).

65. M. P. MacDonald *et al.*, *Nature* **426**, 421 (2003).

66. X. Hu *et al.*, *P. Natl. Acad. Sci. USA* **102**, 15757 (2005).

67. P. R. C. Gascoyne *et al.*, *Electrophoresis* **30**, 1388 (2009).

68. E. G. Cen *et al.*, *J. Microbiol. Meth.* **58**, 387 (2004).

69. L. K. Shawver *et al.*, *Cancer Cell* **1**, 117 (2002).

70. C. H. Kua *et al.*, *Innovat. Manuf. Syst. Technol.* (2005).

71. S. Nagrath *et al.*, *Nature* **450**, 1235 (2007).

72. A. A. Adams *et al.*, *J. Am. Chem. Soc.* **130**, 8633 (2008).

73. J. H. Myung *et al.*, *Langmuir* **26**, 8589.

74. G. Jin *et al.*, *Biosens. Bioelectron.* **22**, 200 (2006).

75. T. Deng *et al.*, *Appl. Phys. Lett.* **80**, 461 (2002).

76. S. K. Sia, G. M. Whitesides, *Electrophoresis* **24**, 3563 (2003).

77. M. Toner, D. Irimia, *Annu. Rev. Biomed. Eng.* **7**, 77 (2005).

78. S. R. Shi *et al.*, *J. Histochem. Cytochem.* **45**, 327 (1997).

79. S. D. Jayasena, *Clin. Chem.* **45**, 1628 (1999).

80. N. Hamaguchi *et al.*, *Anal. Biochem.* **294**, 126 (2001).

81. D. Proske *et al.*, *Appl. Microbiol. Biotechnol.* **69**, 367 (2005).

82. O. C. Farokhzad *et al.*, *Cancer Res.* **64**, 7668 (2004).

83. K. Nagel-Wolfrum *et al.*, *Mol. Cancer Res.* **2**, 170 (2004).

84. J. A. Phillips *et al.*, *Anal. Chem.* **81**, 1033 (2008).

85. C. Tuerk, L. Gold, *Science* **249**, 505 (1990).

86. A. D. Ellington, J. W. Szostak, *Nature* **346**, 818 (1990).

87. F. Jarosch *et al.*, *Nucleic Acids Res.* **34**, e86 (2006).

88. L. Cerchia *et al.*, *PLoS Biol.* **3**, e123 (2005).

89. J. A. Hurt *et al.*, *P. Natl. Acad. Sci. USA* **100**, 12271 (2003).

90. J. K. Joung *et al.*, *P. Natl. Acad. Sci. USA* **97**, 7382 (2000).

91. C. Lorenz *et al.*, *Nat. Protoc.* **1**, 2204 (2006).

92. G. Carpenter, S. Cohen, *J. Biol. Chem.* **265**, 7709 (1990).

93. G. Carpenter, S. Cohen, *Ann. Rev. Biochem.* **48**, 193 (1979).

94. C. Le Roy, J. L. Wrana, *Nat. Rev. Mol. Cell Biol.* **6**, 112 (2005).

95. S. Cohen, *Bioscience Rep.* **6**, 1017 (1986).

96. T. Mitsudomi, Y. Yatabe, *FEBS J.* **277**, 301 (2010).

97. N. E. Hynes, G. MacDonald, *Curr. Opin. Cell Biol.* **21**, 177 (2009).

98. J. Mendelsohn, *Endocr-Relat. Cancer* **8**, 3 (2001).

99. R. I. Nicholson *et al.*, *Eu. J. Cancer* **37**, 9 (2001).

100. R. E. McLendon *et al.*, *J. Histochem. Cytochem.* **48**, 1103 (2000).

101. W. K. Hong, A. Ullrich, *Oncol. Biother* **1** (2000).

102. G. Carpenter, *Mol. Cell. Endocrinol.* **31**, 1 (1983).

103. C. J. Wikstrand *et al.*, *Cancer Res.* **57**, 4130 (1997).

104. J. Baselga, *Eu. J. Cancer* **37**, 16 (2001).

105. S. Maheswaran *et al.*, *New Engl. J. Med.* **359**, 366 (2008).

106. C. T. Kuan *et al.*, *Endocr-Relat. Cancer* **8**, 83 (2001).

107. A. Gschwind *et al.*, *Nat. Rev. Cancer* **4**, 361 (2004).

108. E. K. Rowinsky, *Drugs* **60**, 1 (2000).

109. A. S. Goustin *et al.*, *Cancer Res.* **46**, 1015 (1986).

110. C. Desbois Mouthon *et al.*, *Int. J. Cancer* **119**, 2557 (2006).

111. E. Zwick *et al.*, *Trends Mol. Med.* **8**, 17 (2002).

112. A. Ulman, *Chem. Revi.* **96**, 1533 (1996).

113. M. C. Pirrung, *Angew. Chem. Int. Edit.* **41**, 1276 (2002).

114. M. Fuentes *et al.*, *Biomacromolecules* **5**, 883 (2004).

115. S. Sathornsumetee *et al.*, *Neurol. Clin.* **25**, 1111 (2007).

116. P. Y. Wen, S. Kesari, *New Engl. J. Med.* **359**, 492 (2008).

117. A. P. Stout, *Cancer* **1**, 30 (1948).

118. Y. Xia, G. M. Whitesides, *Ann. Rev. Mater. Sci.* **28**, 153 (1998).

119. R. S. Kane *et al.*, *Biomater.* **20**, 2363 (1999).

120. D. Qin *et al.*, *Nat. Protoc* **5**, 491.

121. J. C. McDonald *et al.*, *Electrophoresis* **21**, 27 (2000).

122. J. N. Lee *et al.*, *Anal. Chem.* **75**, 6544 (2003).

123. M. W. Toepke, D. J. Beebe, *Lab Chip* **6**, 1484 (2006).

124. D. Bodas, C. Khan-Malek, *Sensors Actuat B Chem.* **123**, 368 (2007).

125. R. A. Lawton *et al.*, *Colloid. Surface A* **253**, 213 (2005).

126. G. S. Ferguson *et al.*, *Macromol.* **26**, 5870 (1993).

127. M. Jin *et al.*, *Macromol. Rapid Comm.* **26**, 1805 (2005).

128. Y. C. Jung, B. Bhushan, *Nanotechnol.* **17**, 4970 (2006).

129. H. W. Chen *et al.*, *ChemMedChem* **3**, 991 (2008).

130. N. Usman, L. M. Blatt, *J. Clin. Investig.* **106**, 1197 (2000).

131. J. Charlton *et al.*, *Chem. Biol.* **4**, 809 (1997).

132. P. J. Bates *et al.*, *Exp. Mol. Pathol.* **86**, 151 (2009).

133. K. T. Guo *et al.*, *Stem Cells* **24**, 2220 (2006).

134. J. K. Herr *et al.*, *Anal. Chem.* **78**, 2918 (2006).

135. R. Schäfer *et al., Rofo.* **179**, 1009 (2007)

136. Y. Xu *et al.*, *Anal. Chem.* **81**, 7436 (2009).

137. N. Li *et al.*, *PLoS One* **6**, e20299 (2011).

138. S. M. Iqbal *et al.*, *Nat. Nanotechnol.* **2**, 243 (2007).

139. L. Mezzasoma *et al.*, *Clin. Chem.* **48**, 121 (2002).

140. J. Raj *et al.*, *Biosens. Bioelectron.* **24**, 2654 (2009).

141. R. M. Bachoo *et al.*, *Cancer Cell* **1**, 269 (2002).

142. Y. Kim *et al.*, *Lab Chip* **9**, 2576 (2009).

143. H. Morisaki, *J. Microbiol. Method.* **22**, 69 (1995).

144. K. C. Hazen *et al.*, *Infect. Immun.* **59**, 907 (1991).

145. Y. Tamada, Y. Ikada, *J. Colloid Interf. Sci.* **155**, 334 (1993).

146. E. Kökoğlu *et al.*, *Cancer Biochem. Biophys.* **13**, 57 (1992).

147. S. V. Khadapkar *et al.*, *Cancer Res.* **35**, 1520 (1975).

148. P. Sillanaukee *et al.*, *Eu. J. Clin. Investig.* **29**, 413 (1999).

149. Y. Wan *et al.*, *Cancer Res.* **70**, 9371 (2010).

150. L. A. Liotta *et al.*, *Nature* **284**, 67 (1980).

151. S. Ayad, *The extracellular matrix factsbook* (Academic Pr, 1998).

152. M. Egeblad, Z. Werb, *Nat. Rev. Cancer* **2**, 161 (2002).

153. Y. Itoh, H. Nagase, *Essays Biochem.* **38**, 21 (2002).

154. A. Thapa *et al.*, *Biomater.* **24**, 2915 (2003).

155. D. C. Miller *et al.*, *Biomater.* **25**, 53 (2004).

156. V. Karageorgiou, D. Kaplan, *Biomater.* **26**, 5474 (2005).

157. G. Vozzi *et al.*, *Biomater.* **24**, 2533 (2003).

158. S. Udenfriend *et al.*, *Science* **178**, 871 (1972).

159. S. Stein *et al.*, *Arch. Biochem. Biophys.* **155**, 203 (1973).

160. P. Bohlen *et al.*, *Arch. Biochem. Biophys.* **155**, 213 (1973).

161. C. M. Chan, *Hanser NY.* (1994).

162. M. Nosonovsky, B. Bhushan, *Adv. Funct. Mater.* **18**, 843 (2008).

163. B. Bhushan, *J. Vac. Sci. Technol. B* **21**, 2262 (2003).

164. J. Z. Wang *et al.*, *Nat. Mater.* **3**, 171 (2004).

165. Q. F. Xu *et al.*, *Appl. Phys. Lett.* **93**, 233112 (2008).

166. S. Bhattacharya *et al.*, *Appl. Surf. Sci.* **253**, 4220 (2007).

167. S. Bhattacharya *et al.*, *J. Adhes. Sci. Technol. 24* **15**, 2707.

168. H. Hillborg, U. W. Gedde, *Polymer* **39**, 1991 (1998).

169. S. Bhattacharya *et al.*, *J. Microelectromech. S.* **14**, 590 (2005).

170. Y. Berdichevsky *et al.*, *Sensors Actuat. B Chem.* **97**, 402 (2004).

171. G. A. Diaz-Quijada, D. D. M. Wayner, *Langmuir* **20**, 9607 (2004).

172. A. Chakravarti *et al.*, *Cancer Res.* **62**, 200 (2002).

173. A. Franovic *et al.*, *P. Natl. Acad. Sci. USA* **104**, 13092 (2007).

174. F. Krombach *et al.*, *Environ. Health Persp.* **105**, 1261 (1997).

175. G. I. Bell, *Science* **200**, 618 (1978).

176. S. C. Kuo, D. A. Lauffenburger, *Biophys. J.* **65**, 2191 (1993).

177. K. C. Chang, D. A. Hammer, *Biophys. J.* **76**, 1280 (1999).

178. P. Decuzzi, M. Ferrari, *Biomater.* **27**, 5307 (2006).

179. C. Dong *et al.*, *Ann. Biomed. Eng.* **27**, 298 (1999).

180. Y. Wan *et al.*, *Cancer* **118**, 1145 (2012)

181. M. Fuentes *et al.*, *Biomacromolecules* **5**, 883 (2004).

182. A. W. Peterson *et al.*, *Nucleic Acids Res.* **29**, 5163 (2001).

183. O. Ernst *et al.*, *Lab Chip* **7**, 1322 (2007).

184. H. Lu *et al.*, *Anal. Chem.* **76**, 5257 (2004).

185. L. S. L. Cheung *et al.*, *Lab Chip* **9**, 1721 (2009).

186. H. Zhu *et al.*, *Colloid. Surf. B* **64**, 260 (2008).

187. G. M. Whitesides, *Nature* **442**, 368 (2006).

188. S. Usami *et al.*, *Ann. Biomed. Eng.* **21**, 77 (1993).

189. Y. Wan *et al.*, *J. Phys. Chem. B* **115**, 13891 (2011)

190. A. Mata *et al.*, *Biomed. Microdevices* **7**, 281 (2005).

191. E. Nun *et al.*, *Macromol. Symp.* **187**, 677 (2002).

192. J. A. Dean, *McGraw Hill Book Co., NY.* (1985).

193. D. Fuard *et al.*, *Microelectron. Eng.* **85**, 1289 (2008).

194. J. Downward, *Nat. Rev. Cancer* **3**, 11 (2003).

195. F. Ciardiello, G. Tortora, *Clin. Cancer Res.* **7**, 2958 (2001).

196. J. R. Woodburn, *Pharmacol. Therapeut.* **82**, 241 (1999).

197. L. Cerchia *et al.*, *FEBS Lett.* **528**, 12 (2002).

198. C. L. Esposito *et al.*, *PLoS One* **6**, e24071 (2011).

199. D. Zink *et al.*, *Hum. Genet.* **102**, 241 (1998).

200. S. Hamada, S. Fujita, *Histochem. Cell Biol.* **79**, 219 (1983).

201. T. Demuth, M. E. Berens, *J. Neuro-oncol.* **70**, 217 (2004).

202. M. Westphal *et al.*, *Cancer Lett.* **38**, 283 (1988).

203. O. Engebraaten *et al.*, *Int. J. Cancer* **53**, 209 (1993).

204. M. Lund-Johansen *et al.*, *Cancer Res.* **50**, 6039 (1990).

205. J. E. Perry *et al.*, *Prostate* **35**, 117 (1998).

206. Y. Fukushima *et al.*, *Int. J. Cancer* **76**, 63 (1998).

207. D. R. Friedlander *et al.*, *Cancer Res.* **56**, 1939 (1996).

208. B. B. Tysnes *et al.*, *Int. J. Cancer* **67**, 777 (1996).

209. S. S. Lakka *et al.*, *Oncogene* **23**, 4681 (2004).

210. J. C. Loftus *et al.*, *Mol. Cancer Therapeut.* **8**, 1505 (2009).

211. C. R. Hauck *et al.*, *Cancer Res.* **61**, 7079 (2001).

212. M. Tamura *et al.*, *Cancer Res.* **59**, 442 (1999).

213. R. N. Jorissen *et al.*, *Exp. Cell Res.* **284**, 31 (2003).

BIOGRAPHICAL INFORMATION

Yuan Wan was born on July 31, 1981 in Lianshui, China where he grew up and completed his primary and high school. He moved to Nanjing and graduated from Southeast University Medical School where he got MD degree in 2004. That same year, his Alma Mater awarded him full scholarship for his Master degree of Genetics. From 2004 to 2007, he worked as research assistant with his advisor Dr. Zuhong Lu, director of the State Key Lab of Bioelectronics, and his previous research focused on DNA microarray development and gene diagnosis. After graduation, he worked as a technical leader of Outdo Biotechnology Corporation from 2007 to 2008. He joined University of Texas at Arlington in August 2008 for PhD in Biomedical Engineering. He has been working under supervision of Dr. Samir M. Iqbal.